Active Tectonics and Seismic Hazard Assessment of Afghanistan and Slip-rate Estimation of the Chaman Fault Based on Cosmogonic ^{10}Be Dating

June 10, 2020

Zakeria Shnizai

Graduate School of Science and Engineering

Doshisha University

Acknowledgment

As many willing and helpful hands make work light, there are several people to thank that have made this research possible. I wish to express my appreciations and sincere thanks to these numerous contributors through these acknowledgements.

Foremost, I would like to express my sincere gratitude to my supervisor Prof. Hiroyuki Tsutsumi for the continuous support of my Ph. D. research and for allowing me to come first to Kyoto University and then Doshisha University. His sincere motivation, patience, enthusiasm and immense knowledge enable me to finish my studies. His guidance helped me to research and writes this thesis. I could not have imagined to have a better advisor and mentor for my doctoral study. Under his supervision, I was able to explore various exciting topics in active tectonics of Afghanistan. His willingness to give his time so generously has been very much appreciated. I am very much indebted and would remain as much for life no matter the location.

Thanks are also extended to Associate Prof. Yuki Matsushi at DPRI (Disaster Prevention Research Institute), Kyoto University who patiently supported my research on slip-rate estimation of the Chaman fault using Beryllium-10 surface exposure dating. Dr. Matsushi always encouraged me in my lab work and helped me in geochemical analysis and Beryllium-10 dating. He also suggested me many corrections and helped me improved the dating the samples, particularly about Azadkhail study area.

My profound thanks are given to Prof. Akira Hayashida at Doshisha University, one of the advisory committee members for my Ph. D., and his guidance and continuous help with the project. My sincere thanks and appreciation goes to all the professors who in diverse ways have impacted my life. I also would like to thank Adi Patria for taking the time and effort to review the manuscript.

I am indebted to thank Professor Takashi Nakata and Dr. Yoshio Soeda for their work on anaglyph images interpretation. They helped me to make the anaglyph images from 1-arcsecond SRTM DEM and ALOS PRISM satellite images. I, therefore, was able to map

active and presumed active faults of the whole country based on the 3D anaglyph images interpretation.

I am greatly indebted to Ministry of Education, Culture, Sports, Science and Technology (MEXT) of Japan who supported me for the 1 1/2 year as a research student in Kyoto University and three straight years in Doshisha University. They were generous enough to fund me; without this, it would have been impossible to start my doctoral studies at the Doshisha University. The beryllium-10 TCN exposure dating to calculate the slip rate of the Chaman fault was supported by a Japan Society for the Promotion of Science (JSPS) grant to Hiroyuki Tsutsumi (Grant No. 17H02032). Active and presume active fault mapping project is also supported by a JSPS grant to Takashi Nakata (Grant No. 18H00766).

I am thankful to the laboratories of DPRI, Kyoto University and MALT (Micro Analysis Laboratory, Tandem Accelerator) at the University of Tokyo for analyzing the rock samples and the staff, particularly Akiko Morikawa for the kind cooperation and essential support.

I want to thank the Doshisha University for access to facilities and literature for providing me important literature and materials. Thanks are also extended to Mrs. Yuki Doi for giving me support for the things which I wanted to do in my research work and for always motivating me.

I feel obliged to express my gratitude to all the people, particularly Hamedullah Torabi, Enayat Rahman Mayar, Mohammad Fahim Amini and all others who helped me during my fieldwork. With their help, my research became feasible, otherwise collecting rock samples and geological data is almost impossible from this politically hostile area.

I want to extend my thanks and gratitude to the officials at Kabul Polytechnic University, Ministry of Higher Education, and Ministry of Mines and Petroleum in Afghanistan for their cooperation in collecting data during my research trips. I also would like to acknowledge with thanks the unforgettable hospitality of the entire people of Japan. Lastly, I offer my regards to all of those who have supported me in any respect during the completion of this research work.

Last but not least, I would like to thank my family for the overwhelming support throughout my academic life. Without the endless psychological and social support of my family, I would not have been able to come this far.

To all those who care for a better tomorrow for Afghanistan

Abstract

This dissertation focuses on the active tectonics of Afghanistan, slip-rate estimation of the Chaman fault and assessing seismic hazard in the Kabul basin. Afghanistan is a tectonically complex zone developed as a result of the collision between the Eurasian plate and the Indian plate to the southeast and the Arabian plate to the south. For seismic hazard mitigation, there is no large-scale active fault map in Afghanistan. I, therefore, mapped active and presumed active faults mainly based on interpretation of 1-arcsecond SRTM anaglyph images. The map reveals that there are significant active faults across the country. Based on the available data and geomorphic criteria, twenty-two faults are considered seismically active. The result from the mapping represents that three dominant types of structures (left-lateral strike-slip, right-lateral strike-slip, and thrust faults) characterized the interior of Afghanistan. Then the map was combined with earthquake catalog to interpret the seismic hazard and define earthquake sources based on focal mechanisms and distribution of earthquakes. To better understand seismic hazard, the dissertation outlines regions with similar neotectonic constraints and observations of type and age of faults that generate background seismicity. Four seismic source zones were delineated; 1) east-northeastern; 2) Afghanistan-North Pamir; 3) Northern Afghanistan platform; and 4) middle and south-western Afghanistan. The east-northeastern seismic zone is the most seismically active and has more crustal earthquakes. This zone is cut by large active faults, and Chaman fault is the most significant fault that produced five historical surface ruptures.

I report the first late Quaternary slip rate of the northern Chaman fault in Afghanistan based on ^{10}Be dating of offset alluvial fans surfaces. Field mapping complemented with CORONA and ALOS satellite images, shaded relief and topographic data allows accurate observation of piercing points across the fault zones at two displaced alluvial fans (Ghat Bandakul and Azadkhail). ^{10}Be TCN (Terrestrial Cosmogenic Nuclides) dating of well-embedded sandstone boulders and cobbles are used to constrain the age of the offset fans. At the Ghat Bandakul site, 165 ± 15 m and 235 ± 24 m offset alluvial fans, for which ^{10}Be TCN model ages average 46.9 ± 3.5 kyr and 66.6 ± 4.9 kyr, respectively, yield a slip rate of 3.5 ±

0.4 mm/yr. At the Azadkhail site, the ^{10}Be TCN ages from offset terraces attest to the complex processes involved in sediment transport and deposition. There, two offsets terraces were identified. Based on offset of 500 ± 50 m with 111.2 ± 10.5 kyr age, a slip rate of 4.5 ± 0.6 mm/yr was obtained. Combining the 800 ± 70 m left-lateral offset matching with an average age of 176.8 ± 17.1 kyr for the fan yields the same geomorphic slip-rate of 4.5 ± 0.6 mm/yr. These slip rates are smaller than the geologically, geomorphologically, and short-time defined slip rates along the southern Chaman fault. The result shows a clear trend of decreasing fault slip rate with increasing distance from the southern end to the northeastern end of the fault. The observations suggest that the southern portion of the fault accommodates the majority of the fault-parallel component of relative motion between the Indian and Eurasian plate. The lower slip rate of the fault in Afghanistan may be explained by the transfer of the left-lateral shear onto the Gardez and Mokur faults that splay northward from the Chaman fault.

The northern extension of the Chaman fault is the Paghman fault located in the Kabul basin. The Kabul basin is the home of the economic and political centers of Afghanistan. The basin is bounded by large active faults, which have a high risk of destructive earthquakes. However, little is known for the location, length, and slip rate of these active faults that are essential for seismic hazard analyses. I mapped the active faults in and around the Kabul basin based on the interpretation of high-resolution stereo-paired satellite images and field observations. The left-lateral Paghman fault and northern Chaman fault on the western margin of the basin and the right-lateral Sarobi fault on the northeastern margin of the basin show geomorphic evidence for late Quaternary activity. Based on their lengths, these faults may be capable of producing earthquakes as large as Mw 7.8. Historical earthquake catalogs suggest that the northern Chaman fault last ruptured during the 1505 M 7.3 earthquake. The fault with a slip rate of ~4.5 mm/yr has accumulated enough elastic strain to produce a large inland earthquake close to the densely populated capital city of the country.

Table of Contents

List of Figures

List of Tables

Chapter 1

Introduction

1.1. Background

Active deformation in central Asia is a consequence of the collision between the Indian and Eurasian continents (Fig. 1.1). The collision has produced the Himalayan, Pamir, and Hindu Kush Mountains since 55 Ma (Molnar and Tapponnier, 1975) and the process continues as these mountains are rising at rates as much as 10 mm/yr based on recent GNSS measurements (Dhakal, 2015; Ischuk et al., 2013). The segment of the Alpine-Himalaya orogenic belt extending from Iran to Myanmar is one of the most seismically active intercontinental regions in the world (Gupta, 1993; Koulakov et al., 2002). After the initial collision, the Indian subcontinent has been underthrusting beneath the Eurasian continent along a series of large thrust faults, whose movement causes destructive earthquakes. Hence, plate dynamics and mountain-forming processes exclusively control the occurrence of earthquakes in this area.

Afghanistan is located in a broad deformation belt west of the Himalayas near the southern margin of the Eurasian plate (Fig. 1.1). At the Makran coast, the Indian and Arabian plates subduct northward under the Eurasian plate at a shallow angle (e.g., Gaedicke et al., 2002; Quittmeyer and Jacob, 1979). The convergence rates of the Indian and Arabian plates with respect to the Eurasian plate are ≥39 mm/yr and 23 mm/yr, respectively (Ambraseys and Bilham, 2003a). The Arabian and Eurasian convergence is accommodated in the Zagros Mountains as well as the Kopeh Dagh and Alborz Mountains and the central Caspian area (Fig. 1.1). Relatively aseismic central Iran separates these areas of intense deformation (Walker and Jackson, 2004). The boundary between the Indian and Eurasian plates comprises of the large fold and thrust belt extending from Himalaya, Hazara-Salt, and Sulaiman-Kirthar Mountains (Menon et al., 2004). Quaternary faulting and earthquakes show that most of the

active deformation in central Asia is partitioned between sliding along large strike-slip faults and thrusting in mountainous belts (Tapponnier and Molnar, 1979).

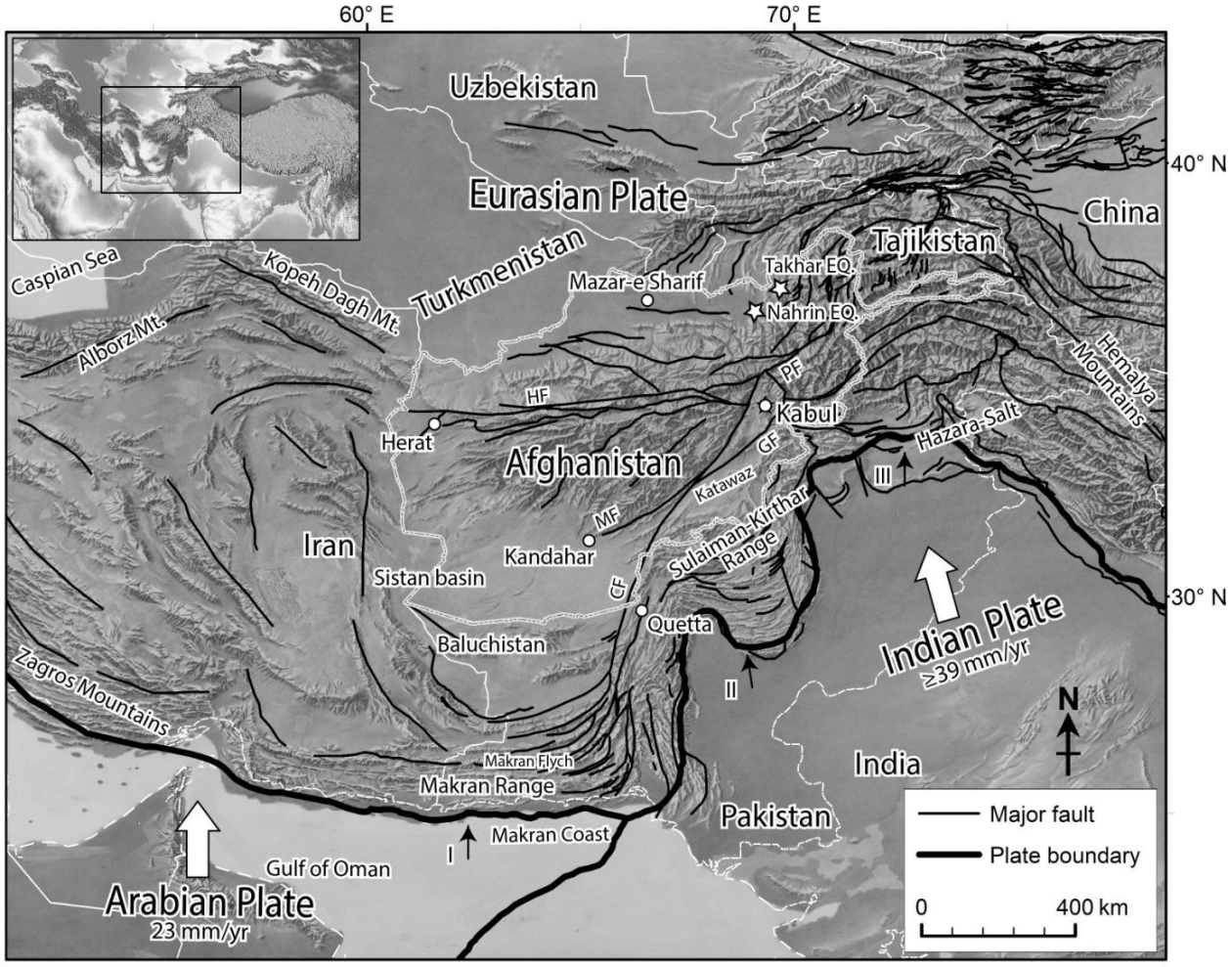

Figure 1.1: Tectonic setting of Afghanistan and surrounding regions. Major active faults are displayed on SRTM elevation data. White arrows show relative plate motion directions of the Arabian and Indian plates with respect to the Eurasian plate (plate velocities from Ambraseys and Bilham 2003). Abbreviations of fault names: CF, Chaman fault; GF, Gardez fault; HF, Herat fault; PF, Panjshir fault. The plate boundaries are marked with numbers: I) Makran subduction zone, II) fold-and-thrust belt east of the Chaman fault, and III) Himalaya collision zone. White stars show the location of the Takhar earthquake (M 6.5) in 1998 and Nahrin earthquake (M 6.1) in 2002. Major faults from Walker and Jackson (2004), Ruleman et al. (2007) and Mohadjer et al., (2016).

Consequently, the country is situated in a zone of significant earthquake hazard. In Afghanistan, records of historical earthquakes exist since 2000 B.C. (Boyd et al., 2007), and

documentation of seismic events had started in the eighth century. Ambraseys and Bilham (2003) estimated locations and surface wave magnitude for damaging earthquakes before 1900 based on narrative accounts. Damaging earthquakes have killed more than 10,000 people in the last two decades. Moderate to large earthquakes such as the Takhar earthquake (Mw 6.5) in 1998 and Nahrin earthquake (Mw 6.1) in 2002 claimed the lives of thousands of people (Fig. 1.1). The 2002 earthquake (Mw 6.1) occurred on a fault that is a southeast-dipping and parallels the linear northeast-trending range front of the Hindu Kush Mountains (Yeats and Madden, 2003). There is no evidence of liquefaction, lateral spreading or ground disturbance by surface rupture. The earthquake is a reminder of the potential for moderate earthquakes near populated areas. Most of the damaging earthquakes have magnitudes 5 or higher. It should be noted that earthquakes are damaging not only because of their magnitude but also because of the period of shaking, energy release, focal depth, and vulnerability of buildings. Regions near the fault rupture and on loose soils may experience strong ground shaking and substantial damage like the 1832 Badakhshan earthquake. The earthquake destroyed most of the villages, killing thousands of people and caused a massive landslide that dammed the Varduj River for eight days. The largest intermediate-depth earthquakes in northeastern Afghanistan have magnitudes more than 7.0. Because of the shallower depth (<40 km), they produce severe shaking than deep earthquakes of similar magnitude.

The country is intersected by many significant faults and folds of various types, ages, and directions. The major faults in Afghanistan have not been studied and characterized in sufficient detail to assess seismic hazards. A number of large faults were identified using aerial and satellite imageries (e.g., Abdullah et al., 2008; Doebrich et al., 2006; Lawrence et al., 1992; Mohadjer et al., 2016; Quittmeyer and Jacob, 1979; Ruleman et al., 2007; Wellman, 1966; Wheeler et al., 2005). However, the extension and type of faults were not well recognized due to the lack of high-resolution imageries and topographic data. Many faults shown by previous work follow a basic geologic framework and topographic lineaments lacking geomorphic evidence of Quaternary activity. Some faults with small-scale Quaternary tectonic landforms were not recognized. Strike-slip faults are densely distributed in

Afghanistan, and the geometry of these faults is the result of their lateral deformation.

The Chaman fault is one of the largest and most active strike-slip faults in the region. The Chaman fault system, which includes a group of parallel to sub-parallel strike-slip faults, is a major left-lateral strike-slip fault that accommodates much of the differential movement between the Indian and Eurasian plates in southwestern Afghanistan and Pakistan. The ~860-km-long fault strikes from N10°E to N35°E (Lawrence et al., 1992) and marks a boundary between the Katawaz basin, ophiolite belt and Kabul block, and central Afghanistan (Fig. 1.1). Left-lateral slip rate of the Chaman fault has been estimated by several studies (Fig. 1.2). InSAR data yielded a slip rate of 8 mm/yr along the fault at latitude 31.0°N and 31.96°N, respectively (Crupa et al., 2017; Furuya and Satyabala, 2008). On the time scale of 7 years, GPS-based measurements yielded a slip rate of 18 ± 1.0 mm/yr (Mohadjer et al., 2010). Matching four geologic features at 25-20 Ma displaced along the fault indicates a slip rate of 19-24 mm/yr (Lawrence et al., 1992). About 1150 m displaced alluvial fan with a ^{10}Be exposure age of ~35 kyr in the border region of Afghanistan and Pakistan yields a slip rate of 33.3 ± 3.0 mm/yr (Ul-Hadi et al., 2013) (Fig. 1.2). There is also a report of volcanic rocks with ~60-80 km offset along the Chaman fault in Afghanistan, for which model age 2 Ma yielded a slip rate of 25-35 mm/yr (Beun et al., 1979).

The northern extension of the Chaman fault is called the Paghman fault, which exhibits an intricate pattern of fault strands. The primarily left-lateral strike-slip motion on the Chaman fault changes into left-lateral oblique-thrust motion on the Paghman fault. The Chaman and Paghman faults bound the western margin of the Kabul basin. The Kabul basin is located in east-central Afghanistan, within the terrane called the Kabul block (Fig. 1.2). The region is tectonically active because large active tectonic structures bound it. The Sarobi fault is located in the eastern margin of the basin, while the Hindu Kush suture is located in the north.

1.2. Motivation

For the evaluation of the seismic hazard of the country, it is needed to integrate data on modern seismicity, historical earthquakes, and active faults. However, due mainly to unstable political conditions in the past several decades, there are limited studies of active tectonics of Afghanistan. Tectonic studies in Afghanistan began in the 1970s, but the studies were purely geological, and the relations between active tectonic features and seismicity were not evaluated. From 2005 to 2007, the United States Geological Survey (USGS) conducted detailed studies of Quaternary faults and historical earthquake records since AD 734. The previous studies focused on plate boundary processes, geologic structures, and distribution of earthquakes, and provided a basic geologic framework that is used as a guide to identify, describe, and characterize active faults.

Kabul metropolitan area is located in the northeastern part of the tectonically active Kabul block and has a high risk of damaging earthquakes and related hazards. Kabul, with a population of more than 4 million, is the capital city of the country. It is one of the most rapidly growing cities on earth due to the influx of refugees and people from the countryside. However, many people live in houses and buildings that have been heavily damaged by war or constructed without adequate seismic enforcements. The slip rate of the active faults around the Kabul basin, particularly the Chaman and Paghman faults, is high and these faults pose a high seismic risk to the area. A massive earthquake in the Kabul Province would cause hundreds to thousands of casualties and substantial damages. Although various strategies and actions can substantially reduce the seismic hazards, little work has been done for Kabul and surrounding regions.

To better mitigate seismic hazards in Afghanistan and particularly in the Kabul metropolitan area, a detailed map of active faults, source of the destructive inland earthquakes, is needed. This dissertation, therefore, summarizes the tectonic and geologic setting of Afghanistan and interprets the Bouguer and free-air gravity anomaly data obtained since 1966 to better understand active tectonic processes in Afghanistan. Then active faults were mapped using three-dimensional anaglyph images of shaded relief maps constructed

from digital elevation data of 1-arcsecond Shutter Radar Topography Mission (SRTM) together with the Environmental Systems Research Institute (ESRI) base map. Active faults are identified that have deformed alluvial plains and terraces. The geomorphic surfaces associated with active faults within the Kabul basin were classified based on morphology and degree of dissection. Then seismicity and destructive historical earthquakes are analyzed based on the summary catalog of Afghanistan earthquakes since AD 734. This study also provides the first detailed description of active faults in the Kabul basin based on the interpretation of topographic anaglyph images produced from high resolution Advanced Land Observing Satellite (ALOS) Panchromatic Remote-sensing Instrument for Stereo Mapping (PRISM) satellite images, and field observation using geomorphic criteria.

Along the Chaman fault in Afghanistan, there is some information about the relative ages of some deposits and landforms (e.g., Doebrich et al., 2006), but their absolute ages are unknown, making it impossible to determine the slip rate of the fault. Determining the slip rate is usually difficult in desert areas because of the lack of ^{14}C dating materials. I, therefore, employ cosmogenic dating as was done in the Pakistan side (e.g., Ul-Hadi et al., 2013), on two alluvial fans (Ghat Bandakul and Azadkhail), which show clear left-lateral offsets of terraces and stream channels (Fig. 1.2).

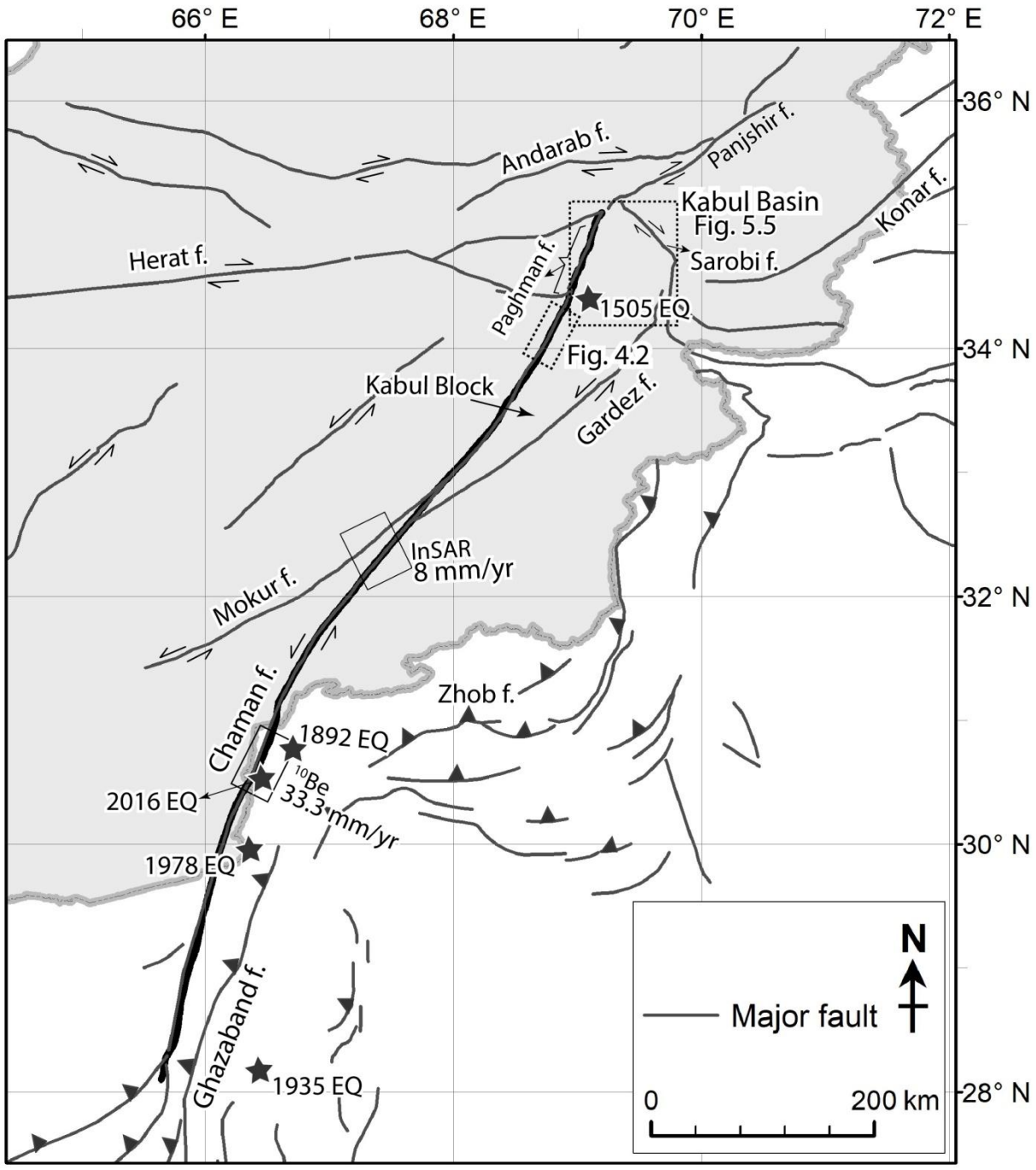

Figure 1.2: The Chaman fault in Afghanistan-Pakistan. The black boxes are the position of InSAR data (Furuya and Satyabala, 2008) and ^{10}Be cosmogenic exposure dating method (Ul-Hadi et al., 2013) used for the slip rate determination. The rectangle with a dotted line shows the position of our study area (Fig. 4.2). The black stars are the location of the Kabul earthquake in 1505 (Mw 7.3), Chaman earthquake in 1892 (Mw 7.0), Baluchistan earthquake (M 7.7) in 1935, an earthquake of Mw 6.4 in 1978, and earthquake (~Mw 5.5) occurred in 2016.

1.3. Purpose and objectives of the study

The overall purpose of this dissertation is to map active and presumed active faults, identify the sources of destructive earthquakes, improve understanding of seismic hazard in the country, calculate the slip rate of the Chaman fault near Kabul, and investigate the active tectonics and seismic hazard of the Kabul basin. To deal with the above goal, the following main objectives of this dissertation need to be achieved:

(1) To summarize and interpret previously published data and provide new insight into active tectonics and earthquake hazard of Afghanistan.

(2) To analyze gravity anomaly to better understand active tectonic processes.

(3) To map active and presumed active faults, and briefly describe their geometry and tectonic geomorphology using anaglyph images.

(4) To use data from the catalogs of Afghanistan earthquakes and International Seismological Center (ISC) as primary data in this study to evaluate seismic hazards and define earthquake sources in the country.

(5) To analyze the active fault map in conjunction with seismicity data to identify the main seismic source zones of the country.

(6) To describe the geomorphology of offset surfaces in detail based on CORONA and ALOS PRISM satellite images interpretation, and for which ^{10}Be dating of the offset surfaces allows determination of the geomorphic slip rate of the Chaman fault near Kabul.

(7) To compare the obtained result with previously reported slip rates along the Chaman fault to discuss fault behavior for a better seismic hazard assessment.

(8) To map active and presumed active faults by interpreting stereo 3D anaglyph images and field observation in the Kabul basin.

(9) To show the detailed location and length of the active faults that are essential to seismic hazard analyses and estimate the magnitude of maximum credible earthquakes from the active faults around the Kabul basin.

1.4. Dissertation outline

This dissertation consists of the following chapters.

Chapter 1: Provides an introduction about the background research, motivation, the purposes and outlines of the dissertation.

Chapter 2: Summarizes tectonic setting of Afghanistan, bedrock geology, Quaternary geology and geomorphology. This chapter also includes information about the interpretation of gravity anomalies since 1964.

Chapter 3: Introduces active fault map in Afghanistan to better understand the distribution and level of seismic hazard. Then, the active fault map was combined with crustal seismicity to interpret the seismic hazard and define earthquake source zones.

Chapter 4: Describes the slip rate of the Chaman fault using ^{10}Be terrestrial cosmogenic nuclides (TCN) dating, in Afghanistan. The result shows the fault slip rate is decreasing to the northeast. The detailed map of the Chaman fault was prepared using CORONA satellite images analysis.

Chapter 5: Describes active tectonics and seismic hazard in the Kabul basin, which has a long history of damaging earthquakes.

Chapter 6: Discusses slip rate discrepancies along the Chaman fault. Slip rates based on various methods, such as geology, geomorphology and geodesy, are generally inconsistent with the slip rate that have been found based on ^{10}Be TCN.

Chapter 7: Summarizes the main findings of this study. In addition, this chapter provides recommendations for conducting further research in the whole country, and particularly along the Chaman fault and Kabul basin.

Chapter 2

Regional geology and tectonic setting of Afghanistan

2.1. Plate tectonics

The tectonic history of Afghanistan is related to successive accretion of Gondwana and Laurasia since the end of the Paleozoic (Wheeler et al., 2005). At about 200 Ma, there were two supercontinents, Gondwana and Laurasia in the south and north, respectively, were separated by the Tethys Ocean. The Indian continent was rifted from Gondwana at about 100 Ma and moved northward and collided with Eurasia at 55-60 Ma (Molnar and Tapponnier, 1975; Wheeler et al., 2005). The first collision was possibly in the early Mesozoic along the Hindu Kush and Kunlun faults in Tibet (Dhakal, 2015; Tapponnier et al., 1982). In Afghanistan, the initial margin between India and Eurasia lies along the Panjshir and Herat faults south of the Hindu Kush Mountains (Tapponnier et al., 1982) (Fig. 1.1).

The convergence of the Gondwana-derived continental blocks and Eurasia resulted in orogenic segments in Afghanistan. The orogenic segments extend in an east-west direction from the Pamir syntaxis to the Kopeh Dagh Mountains over a length of approximately 1300 km (Fig. 1.1). These segments also extend in a north-south direction from the Amu Darya and Afghan-Tajik basins southward to the Baluchistan and Indus basin over a width of 1100 km (Figs. 2.1, 2.2). The segments can be divided into: 1) the late Varsican or Hercynian domain (late Palaeozoic) of northern Afghanistan; 2) the Cimmerian suture zone (late Triassic-early Cretaceous) of middle Afghanistan, central Afghan Block and the northern Pamir Mountains; and (3) the Himalayan domain (Cenozoic) along the Chaman fault in the west and Konar fault in the north (Boulin, 1990; Siehl, 2017) (Fig. 2.1).

In the vicinity of the Herat fault and along the northern border of Hindu Kush, deformation of upper Tertiary rocks is characterized by large folds, particularly in the Afghan-Tajik basin (Fig. 2.2). The platform was uplifted out of the former Tethys Ocean due

to the collisions of suspect terranes during late early Carboniferous to Triassic time (Shroder, 2014; Wheeler et al., 2005), to become mountains, high plateaus, and plains. East of the basin in the foreland of the Pamir Mountains, Pliocene molasses are folded and tilted eastward (Tapponnier et al., 1981). During the late Triassic, grabens and horsts were developed on the platform basement (Brookfield and Hashmat, 2001; Siehl, 2017). This platform is subdivided into the Shabarghan, Badghis-Mimana, and Qala-e Naw blocks and Herat trough by NW-trending, right-lateral strike-slip faults (Fig. 2.1). There are more faults near the eastern and southern edges of the platform than its interior.

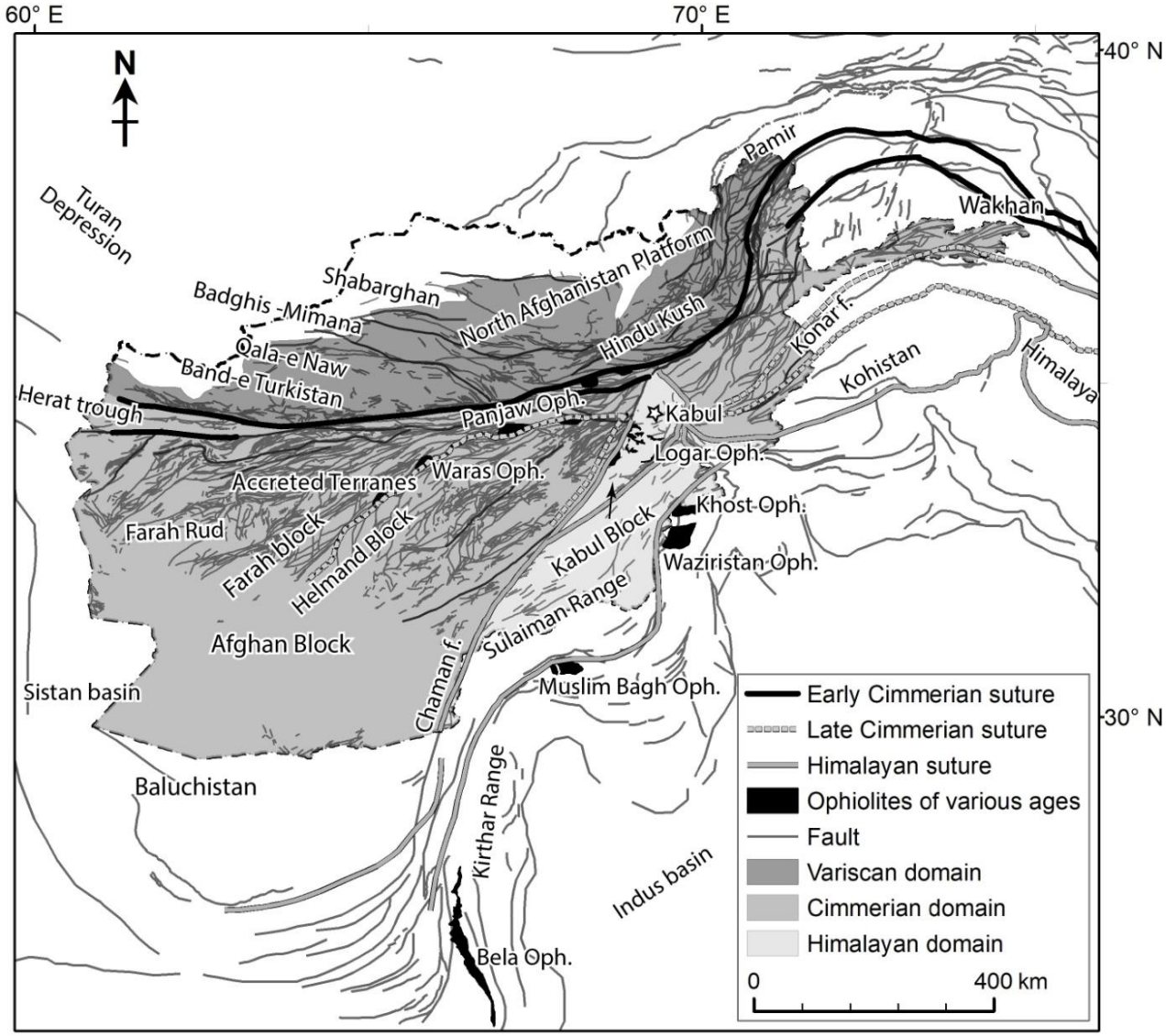

Figure 2.1: Tectonic sketch map of the Afghanistan orogenic segments. The map is modified from Boulin (1990), Abdullah et al. (2008) and Siehl (2017).

Strike-slip faulting and compressional and extrusion deformation characterize tectonics of middle Afghanistan. In accreted terranes south of the Qarghanaw and Bande Bayan faults, Tertiary tectonics has been dominated by strike-slip faulting. The deformation gradually decreases to the southwest toward the Sistan basin (Fig. 2.1). Mountain ranges in southwestern Afghanistan consist of diverse rocks with different ages that are extensively faulted. Shroder (2014) suggested that these rocks have been formed elsewhere and then moved to their current location as accreted terranes. These rocks docked against the Eurasian plate and sutured on it. Based on Shareq (1981), igneous rocks south of the Herat fault are ophiolites (Fig. 2.1). The presence of ophiolites in central Afghanistan is evidence for another suturing event in the upper Jurassic and lower Cretaceous (Dhakal, 2015). Thus, the Tethys Ocean had subducted in early Carboniferous to Triassic time (Sengor, 1984) during Cimmerian orogeny. The ophiolite belt divides central Afghanistan into two blocks; the Helmand block to the east and the Farah block to the west (Fig. 2.1).

Himalayan orogenic events in northeastern Afghanistan started with the collision of the Indian plate with the Eurasian plate at approximately 55 Ma (Quittmeyer and Jacob, 1979). Northeast Afghanistan contains several north-northeast-trending shear zones and faults, particularly along the boundary between the Cimmerian and Veriscan domains (Fig. 2.1). The subduction caused a contractional deformation of a large part of the Eurasian promontory, including the plate boundary at the southeast corner of Afghanistan (Fig. 1.1). The deformation is divided into thrust faults at and around the plate boundary, and northeast-trending strike-slip faults such as the Chaman fault that is one of the most significant continental strike-slip faults in the region (Fig. 2.1). Southeast Afghanistan includes the Kabul block, ophiolite belt, and Katawaz basin, which developed during the Himalayan orogeny (Figs. 2.1, 2.2). The Kabul block is bounded by the Chaman, Gardez, and Sarobi faults (Fig. 2.2). East of the Chaman fault, several tectonics units have been overthrust to the south along the margin of the Indian plate. In this region, the Khost and Kabul-Altimur ophiolites can be separated.

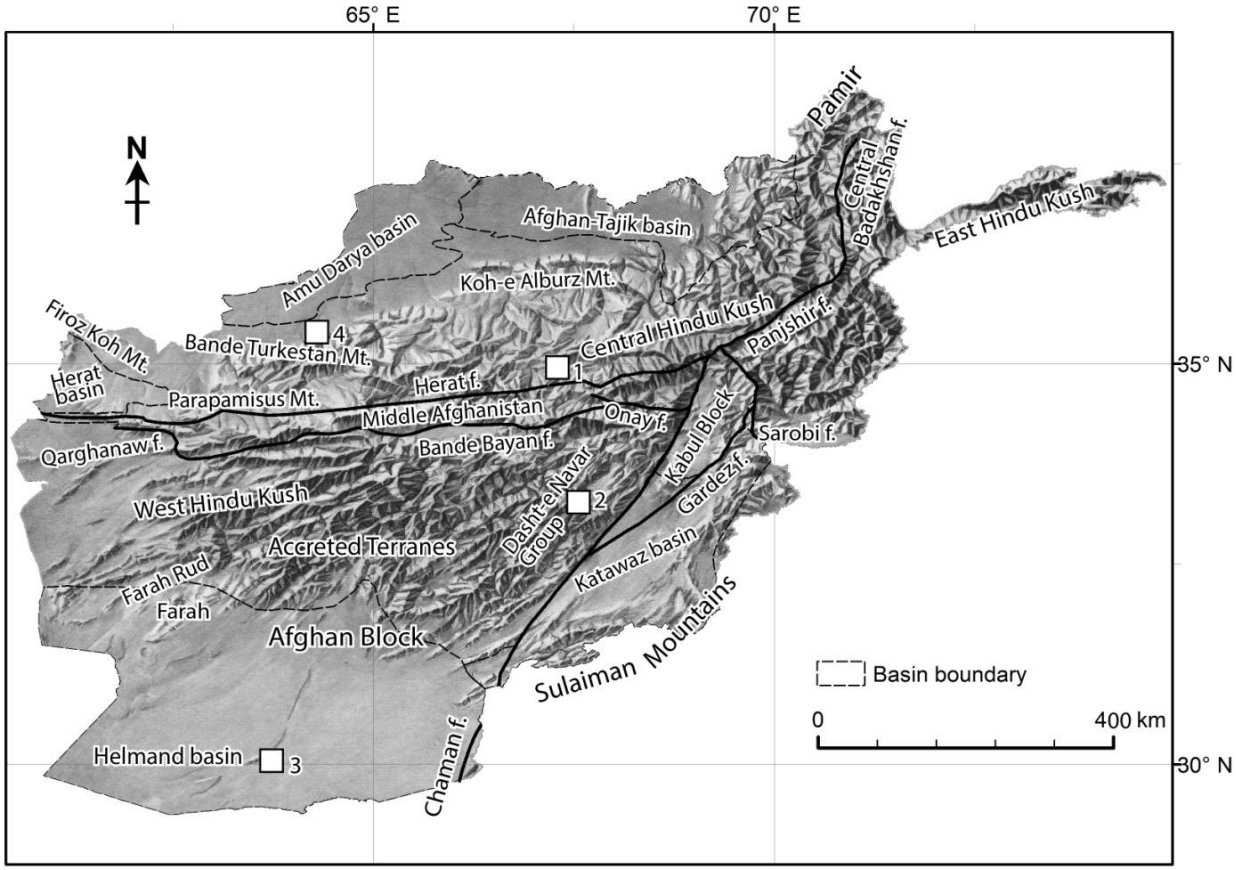

Figure 2.2: Geomorphology of Afghanistan. The dashed lines show the boundary of each drainage basin. Based on mountains, passes and valleys, the Hindu Kush Mountains are divided into the eastern, central and western mountains. White-filled rectangles marked with numbers show young magmatism and volcanism products: 1) Share-Arman complex, 2) Dasht-e Nawar complex, 3) Khanneshin complex, and 4) Sarlogh complex.

2.2. Bedrock geology

Geology of Afghanistan is very complex resulting from continental fragments moved across the ancient Tethys Ocean over millions of years. Most of the orogenic structures in Afghanistan have been subjected to tectonic and magmatic activation from Miocene to the present (Boulin, 1990). According to Chmyriov et al. (1978), three types of young magmatism and volcanism products have been recognized in this country; 1) Miocene alkaline granite intrusions like the Share-Arman complex; 2) Middle Paleogene-early Quaternary volcanism such as Dasht-e Nawar complex; and 3) Early-middle Quaternary volcanism in central

regions, alkaline carbonatitic like the Khanneshin complex and trachy basalt such as the Sarlogh complex (Fig. 2.2). Products of middle Quaternary volcanism are restricted to regions of major faults that are currently active such as in Afghan block (Fig. 2.1).

Northern Afghanistan is part of the continental shelf of the southern Eurasian plate, including the Afghan-Tajik and Amu Darya basins (Fig. 2.2). Northern Afghanistan is relatively low relief region flanked by the major orogenic belt of the Hindu Kush and Pamir Mountains. North of the Herat fault and west of the Central Badakhshan fault is the north Afghan platform where the basement consists of metamorphic and igneous rocks (Fig. 2.1). The basement developed during the Carboniferous-Permian Variscan orogeny, and since then, the platform has been stable (Shareq, 1981; Tapponnier et al., 1981). It is overlain by a sequence of Mesozoic to Tertiary sedimentary strata (Brookfield and Hashmat, 2001), and crops out in the West Hindu Kush, Parapamisus and Firoz Koh Mountains (Figs. 2.2, 2.3). The Hindu Kush Mountains structures disappear to the west and north under thick layers of shallow marine limestone of Paleocene age. Further north, limestones are in turn covered by continental Tertiary deposits (Fig. 2.3).

In middle Afghanistan, several discreet fault blocks are composed of folded and uplifted blocks of sedimentary rocks ranging from Precambrian to Jurassic in age (Koulakov et al., 2002; Peters et al., 2011). The sedimentary rocks are overlain by post-Neogene and surficial deposits (Fig. 2.3). The Herat fault in the north, and the Qarghanaw, Bande Bayan and Onay faults in the south bound east-trending lens-shaped rock masses (Shareq, 1981; Wheeler et al., 2005), approximately 30-60 km wide and 800 km long (Fig. 2.2). The Farah Rud trough and Band-e Bayan zone are intruded to spars Cretaceous and Eocene-Oligocene intermediate to granitic intrusive rocks (Debon et al., 1987). Active deformations and elevations decrease to the southwest towards the Helmand basin. Lower Tertiary granites are present west of the Chaman fault.

In southeastern Afghanistan, four prominent ophiolites are present: 1) the Kabul-Altimur or Logar, 2) Waziristan-Khost, 3) Muslim Bagh, and 4) Bela. The ages of these ophiolites are between the Late Cretaceous to Paleocene and the early Eocene (Gaina et al.,

2015). Paleontological evidence suggest the sediments were deposited in a deep ocean, and have moved to the southeast as a thrust sheet on top of the ophiolites (Siehl, 2017, Abdullah et al., 2008) (Fig. 2.1). From the Paleocene to lower Eocene, subsequent deformation involved further thrusting and folding, and strike-slip faulting (Tapponnier et al., 1981). The Katawaz basin is located west of the Khost ophiolites, where upper Paleocene to Eocene sediments lie unconformably on top of the metamorphosed autochthonous basement (Doebrich et al., 2006; Robinson et al., 2000; Tapponnier et al., 1981). The basin is bounded on the east along the ophiolite belt by the Indian subcontinent and on the west by accreted terranes (Fig. 2.2). It is a transtensional basin developed as an elongate trough where clastic sediments were transported northeast due to left-lateral shearing along the Chaman fault.

2.3. Quaternary geology and geomorphology

The geomorphology of Afghanistan is strongly influenced by regional and local tectonic activities, as well as surface processes. The highly rugged mountains such as the Hindu Kush form a backbone across the country trending from northeast to southwest. Quaternary deposits are widespread throughout the country, and fill fault-bounded structural basins such as Amu Darya, Afghan-Tajik, Kabul, Katawaz and Herat basins (Fig. 2.1). The ranges are composed of uplifted crystalline and sedimentary rocks. In some places, Quaternary deposits are offset by folds, which are likely related to active faulting such as in the Afghan-Tajik depression (McNab et al., 2019; Nikolaev, 2002; Ruleman et al., 2007). The central plains are local depositional centers for sediments derived from the surrounding bedrock and surficial deposits.

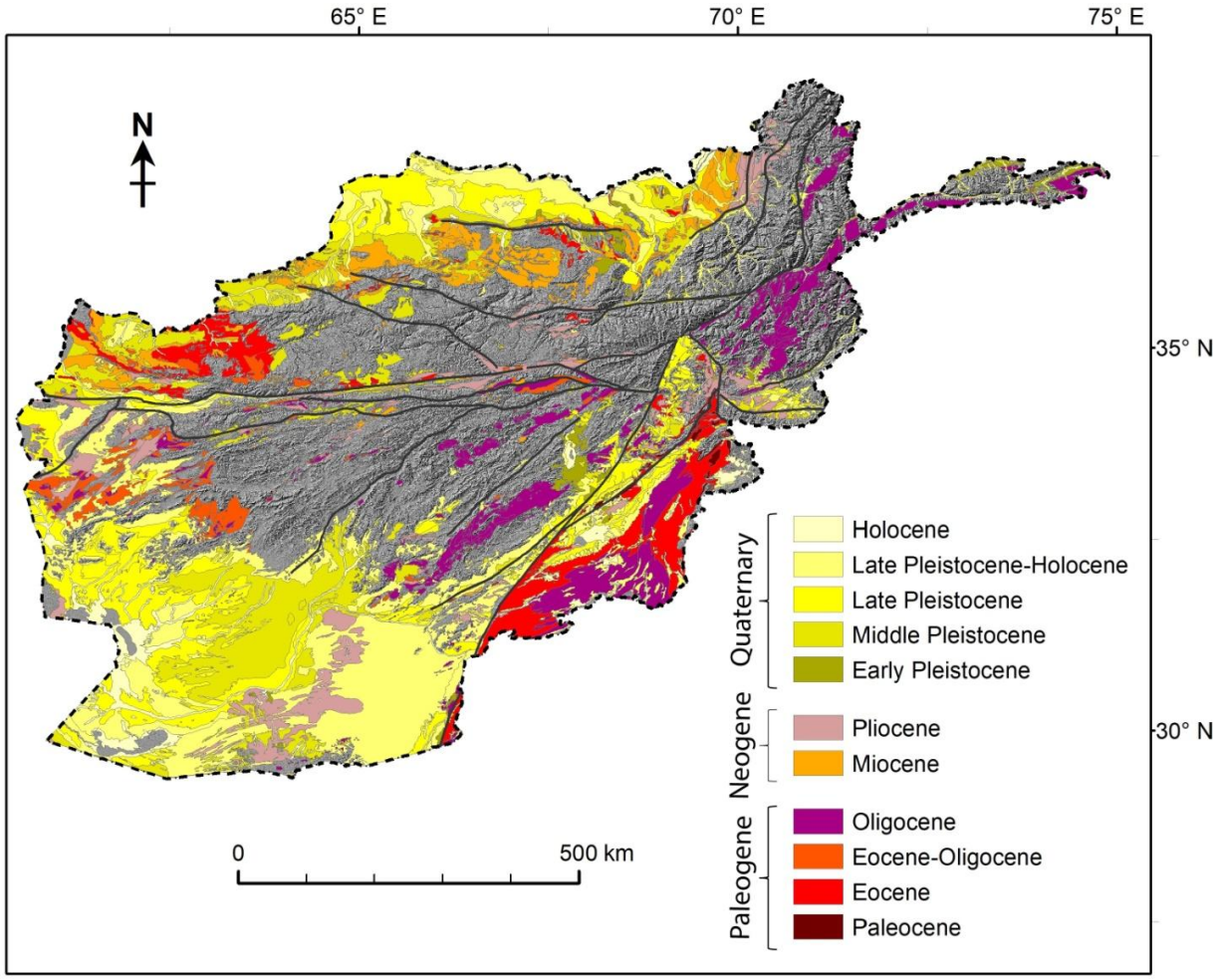

Figure 2.3: Cenozoic geologic map of Afghanistan. The map is modified from Doebrich et al. (2006). Cenozoic rocks cover approximately half of the country.

Surficial deposits in Afghanistan refer to geological deposits typically of Quaternary age, which are differentiated by level of dissection. Two divisions of alluvial deposits (young and old) can be differentiated throughout the country based on the height above currently active streambeds (e.g., Bohannon 2010). The oldest alluvial landform is deeply dissected remnant of thick fan deposits and located at least several meters above the young units. Young alluvial deposits are actively deposited at the bottom of the modern valleys. In addition, the deposits from old alluvial fans have been offset considerable distances from their sources particularly along strike-slip faults such as the Chaman, Darvaz, Herat and others faults (e.g., Ruleman et al., 2007). The alluvial fans compose of high terraces and extensive aggradational plains in the north, west and southeast of Afghanistan. Colluvium, eolian and loess deposits show different types of surficial deposits, which are commonly present on steep

mountain slopes, ridges, flat area and valleys. The surficial deposits in Afghanistan are related to glacial history in the Quaternary time. The deposits have carved out valleys and formed landform features. Geomorphic evidence such as offset landforms and deposits shows that the majority of the faults have been active throughout the Quaternary time.

In northern Afghanistan, some major faults were formed during Neogene-Quaternary and offset the sedimentary cover (Brookfield and Hashmat, 2001) (Fig. 2.3). Also, a prominent east-west trending fold is formed by the Alburz Marmul fault that offsets recent alluvial fan close to Mazar-e Sharif. The western end of the fault is cut by a drainage network. Based on the 1-arcsecond SRTM shaded relief map and ESRI base map, in northern Afghanistan the dominant features are a series of arcuate, north to south trending anticlines. In Afghan-Tajik Basin, anticlines are consistent with activity on blind thrust faults operating above a detachment (McNab et al., 2019). Many smaller faults in central Afghanistan are recognized as strike-slip faults. The Helmand Basin shows a long tectonic history, which is located inside the Afghan Block formed from the collision of several microplates (Siehl, 2017).

In northeastern Afghanistan, younger structures have a southeast convex along the Sulaiman fold-and-thrust belt. This suggests that the first contraction was accommodated by north-verging thrust faults (Ruleman et al., 2007). The recent Quaternary deformation is accommodated by southeast verging thrust faults as well as the strike-slip faults such as the Chaman fault. On the Quaternary alluvial deposits, the faults show evidence of horizontal and vertical displacement. Geomorphic development of piedmont deposits has been influenced by fault activity.

2.4. Gravity

One of the first geophysical investigations carried out in the systematic study of tectonics in Afghanistan, was the interpretation of the gravity anomalies (e.g., Desio and Poretti, 1991). Both the country's rugged terrain and political situation have prohibited an extensive and complete geophysical observation in the study area. Exploration has been done

mostly by small teams or individual people who with their accurate measurements that are still in need of refinement and of being extended (e.g., Desio and Poretti, 1991; McGinnis, 1971). The geophysical survey using gravimeters was carried out since 1964 (Desio and Poretti, 1991; McGinnis, 1971). The observed gravity data has been reduced and corrected using Bouguer and free-air corrections by differential topographic or bathymetric loads above or below the ellipsoid assumes the crust to be 30 km thick (Desio and Poretti, 1991; Hinze et al., 2005) with an average density of 2.67 g/cm3. The density of sediments varies from 2.17 - 2.77 g/cm3. The lithological descriptions and density provide estimates for subsurface densities used in the gravity corrections. Topographical corrections have been calculated from the mean elevations using a digital elevation model (DEM). To quantify the interpretations of the Bouguer and free-air anomalies, the gravity model is constructed using ArcGIS to generate contour lines from corrected point data (Figs. 2.4, 2.5).

The Bouguer and free-air gravity field

The Bouguer anomalies map shows strong trends related to significant reliefs (Fig. 2.4). The contours interval of the gravity anomalies is 25 mGal, which is too coarse to represent any anomalies pertaining to shallow geologic structures. However, the maps illustrate the area of Bouguer and free-air anomalies along the eastern and western Hindu Kush as well as Sulaiman mountains (Fig. 2.2). The highest Bouguer and free-air anomalies are associated with the ophiolites belt, which trends southwest from capital Kabul (Fig. 2.1). The ophiolites belt represents high-density zone (~3.1 g/cm^3) of transition between northwestern (Afghan Block) and southeastern plate boundary zone. The belt consists of Kabul-Alitimur (Logar), Khost, Waziristan and Muslim Bagh ophiolites with different ages (Fig. 2.1). The Bouguer gravity anomalies generally decrease toward west to the Chaman fault with a low value over the Katawaz basin and high over the eastern Sulaiman foreland. The Bouguer anomalies also decrease northwestward from zero mGal in the Sulaiman foredeep (Katawaz basin) to about -190 mGal along the Chaman fault and about -300 mGal in central Afghanistan.

Besides the Bouguer anomalies, free-air gravity anomalies (Fig. 2.5) are presented for the hypothetical models to correct the decrease in gravity with height for the actual mountain ranges (Lillie, 1991). In eastern and western Afghanistan, the gravity profiles (Fig. 2.6) crossing the western and central Hindu Kush Mountains illustrate the major differences in values. The free-air gravity anomalies along profile A-A' from Badghis Murghab, through Parapamis ranges, over Herat and Farah provinces to Helmand basin southwestern Afghanistan has a mean free-air anomaly of +5 mGal (Fig. 2.6a). Along the Sulaiman Mountains, the highest free-air gravity values (around +100 mGal) are observed in areas of high elevation in the fold belt. Profile B-B' from Kunduz (Afghan-Tajik basin), through the central Hindu Kush (Salang Pass), and over Kabul and Jalalabad cities to Turkham has a mean value of -148 mGal (Fig. 2.6b). This mean value was determined along 10 km increments of the profile by averaging free-air anomalies. For isostatic equilibrium to be attained, the Pamir and Hindu Kush complex would have to undergo epierogenic uplift (McGinnis, 1971).

Gravity data shows gross structure across the Sulaiman fold belt and Chaman fault zone (Figs. 2.4, 2.5). In this region, the Bouguer anomalies trend NE-SW along the boundary zone. Negative and near to zero Bouguer anomaly values become more negative toward the Indian plate in the Sulaiman foredeep. The linear trends of the gravity anomalies reflect tectonic features like the Chaman and Herat faults. The gravity anomaly is generally oblique to the structures and parallel to the plate convergence vector between the Indian and Eurasian plates. Based on the gravity data interpretation, the Sulaiman fold belt thickens northward because of sediments thrust over transitional crust (Jadoon and Khurshid, 1996; McGinnis, 1971). Thus, the western convergence of the Indian plate represent the development of the Sulaiman fold belt and enormous thickness of the molasse sediments (Waheed and Wells, 1990).

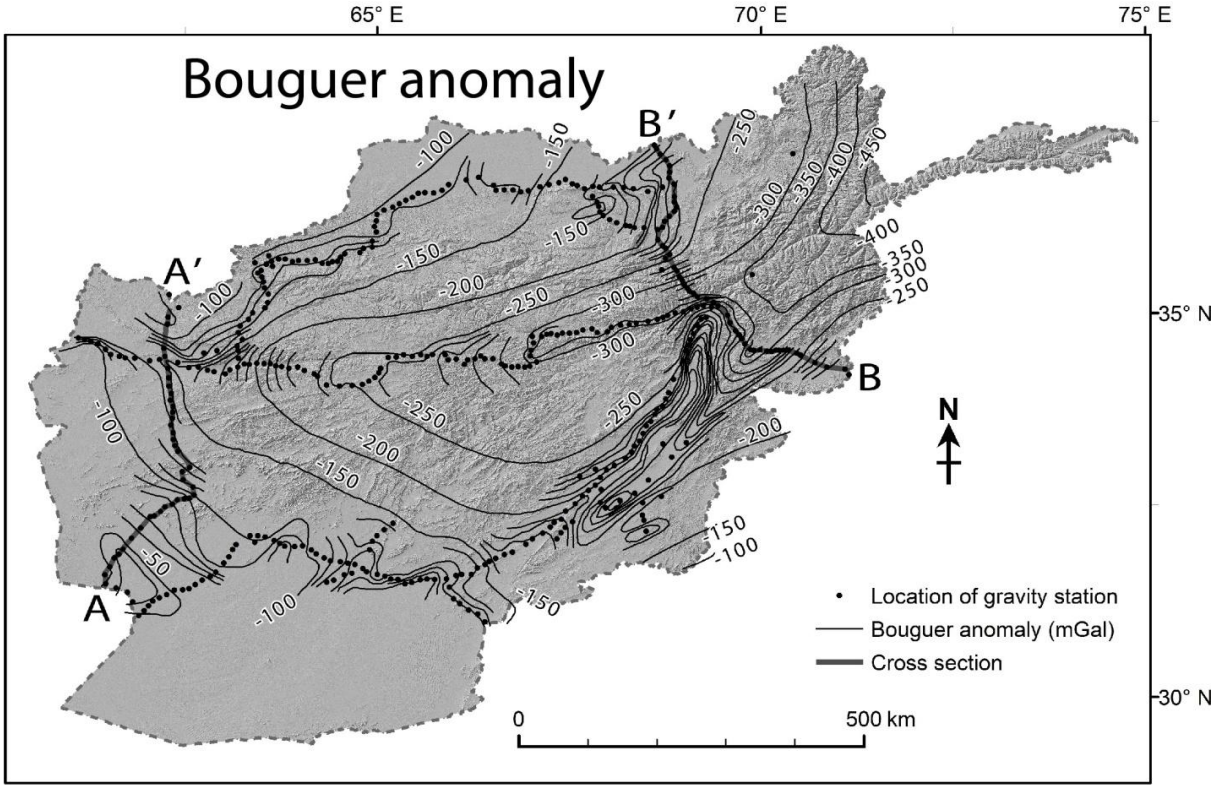

Figure 2.4: Bouguer gravity anomaly map of Afghanistan. Gravity anomaly map is made by contouring gravity data from McGinnis (1971). Gray lines AA′ to BB′ are the Bouguer gravity anomaly, and elevation profile lines in Figures 2.6.

The gravitational field in central and eastern Hindu Kush is characterized by large negative mean free-air anomalies, while in the western Hindu Kush is characterized by zero anomalies (Figs. 2.4-2.6). According to McGinnis (1971), the western Hindu Kush is in isostatic equilibrium, while the central and eastern Hindu Kush Mountains are not in isostatic equilibrium. Therefore, the western Hindu Kush is tectonically stable, but central and eastern Hindu Kush is not, because they are the vulnerable zones for seismic activity due to the development of large shear stress within the crust. If the central and eastern Hindu Kush were allowed to adjust isostatic equilibrium, the region would experience epierogenic uplift for the entire area. Hence the region is far to move rapidly toward equilibrium. In central and eastern Hindu Kush negative free-air anomaly also shows the region where an underthrust slab is postulated from seismic evidence. This is consistent with continental thickening and underthrusting because low-density crust is being pulled down in mantle that has a high density (McGinnis, 1971).

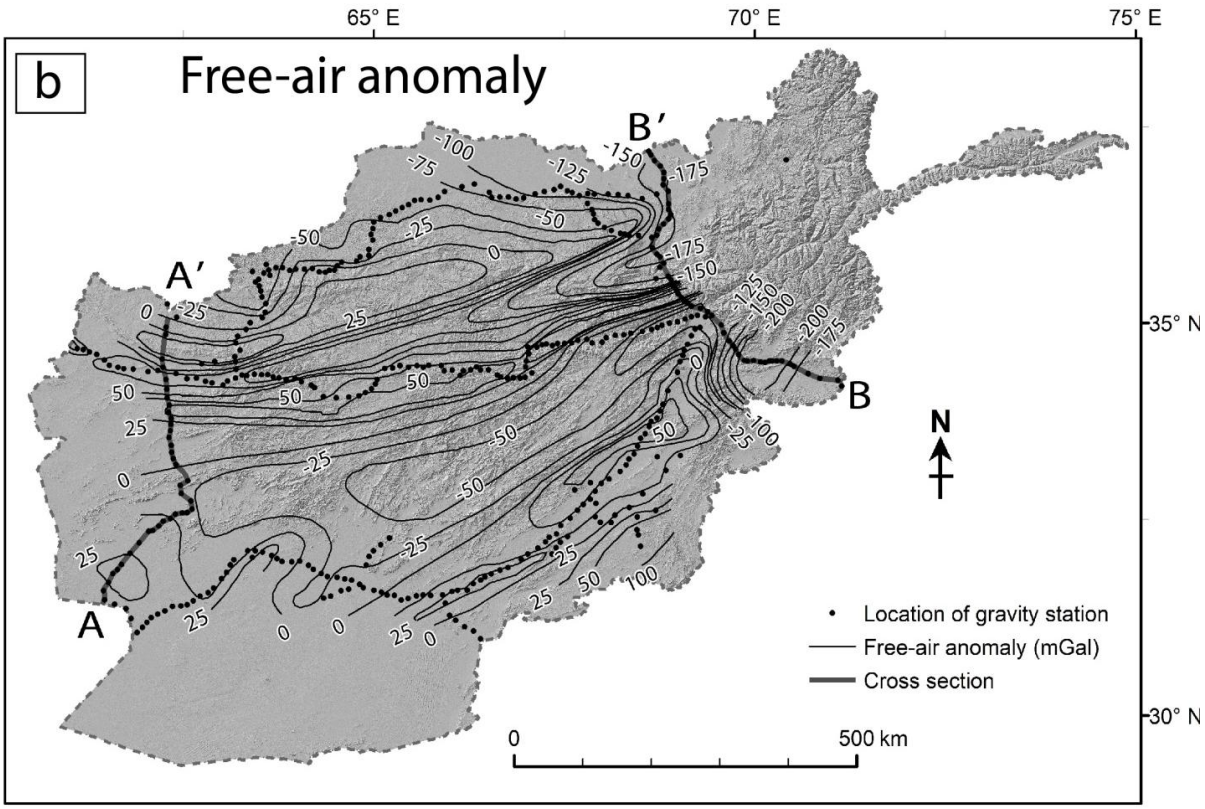

Figure 2.5: Free-air gravity anomaly map of Afghanistan. The highest Bouguer and free-air anomalies are associated with the ophiolites belt representing the northwest border of the Indian plate. The AA′ to BB′ lines are the free-air anomaly, and elevation profile lines in Figure 2.6.

As the east-northeast Afghanistan has experienced more intense deformation and shortening, the crust is thicker than west. Based on gravity data, the crust in the eastern Hindu Kush is about 65 km thick, whereas it is around 53 km thick in western Hindu Kush (McGinnis, 1971). The free-air anomaly in western Afghanistan is zero and negative in eastern Afghanistan (Figs. 2.5, 2.6). Sedimentary cover thickness in high valleys is less than 1 km, whereas it is more than 5 km in the areas located in the north of the Hindu Kush. The sediment thickness in western Afghanistan Helmand basin is approximately 22 km, which appears to be thicker than the north Afghan platform (Jung et al., 2013).

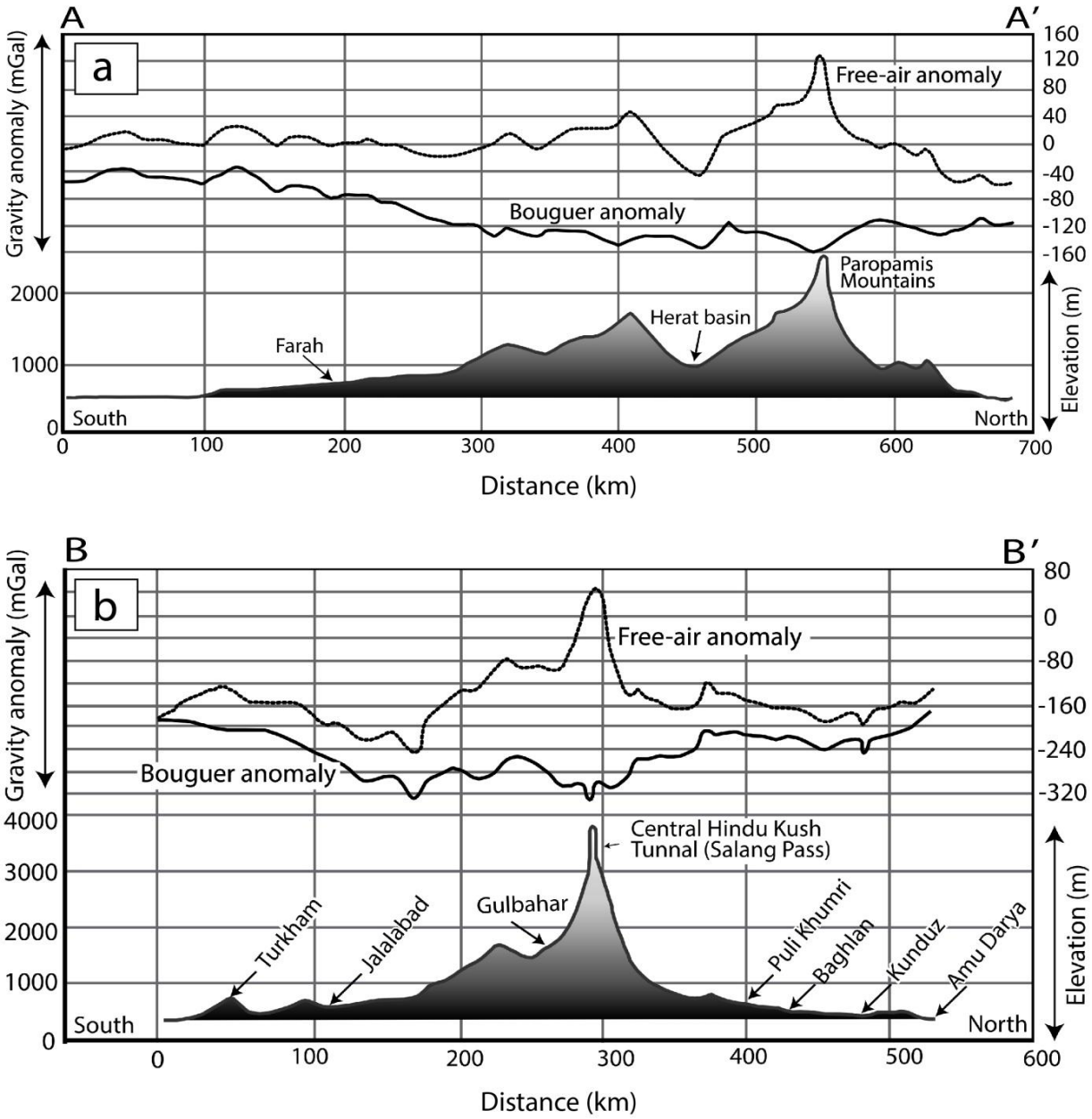

Figure 2.6: Gravity profile AA’ and BB’ (location Figs. 2.4, 2.5) presenting Bouguer anomaly, free-air anomaly, and elevation. The North-south profiles were drawn across (a) the western Hindu Kush (Paropamis and Firoz Koh Mountains) and (b) central Hindu Kush Mountains (from Amu Darya basin through Salang Pass to Jalalabad Turkham). The data is from McGinnis (1971).

Chapter 3

Active fault mapping and crustal seismicity in Afghanistan

3.1. Resources and methods

In this study, I interpreted three-dimensional anaglyph images of shaded relief maps constructed from digital elevation data of 1-arcsecond SRTM together with the ESRI base map (Fig. 3.1a). I first imported the SRTM DEM to Simple DEM Viewer software (Katayanagi, 2019) to produce anaglyph images (Fig. 3.1b). The images were then imported into ArcMap software for geo-referencing into a global framework and mapping individual features. I also created shaded relief maps to facilitate the identification of active faults. The anaglyph images bear sufficient resolutions for interpreting larger-scale tectonic geomorphology. I then digitally mapped active faults using ArcMap software based on geomorphic criteria that are commonly used in Japan for active fault mapping (Iwahashi, 2010; The Research Group for Active Faults of Japan, 1992; Tsutsumi and Perez, 2013). The first criterion for the classification of an active fault is evidence of activity in recent geological time corresponding to the Quaternary period (Fig. 2.3). These kinds of faults displace Quaternary landform or deposits with a progressive amount of offset. Active faults that moved recently preserve more clearly offset surfaces than those faults which moved in earlier geologic times. The landforms that are formed by faulting are called displaced landforms.

Fault classification is based on the presence of displaced young landforms and deposits which are generally located in valleys and along mountain fronts. I noted that the active faults cut all materials except alluvial fans in modern stream channels. Two categories of active faults were employed: active faults and presumed active faults. Active faults offset late Quaternary deposits and landforms. Presumed active faults show no clear evidence of late Quaternary displacement. The presumed active faults have the potential to be active but have

not moved in the late Quaternary. For example, a fault is classified as a presumed active fault while traversing bedrock terrain with no late Quaternary geomorphic surfaces or strata (Tsutsumi and Perez 2013). It is also uncertain whether there will be repeated activity along these faults in future. In the map, faults that marked by thick black color are regarded here as active faults with displaced topography, and those faults marked with light black color are regarded as presumed active faults. The active faults include information such as geologic setting, sense of motion, type and the time of the recent surface rupture.

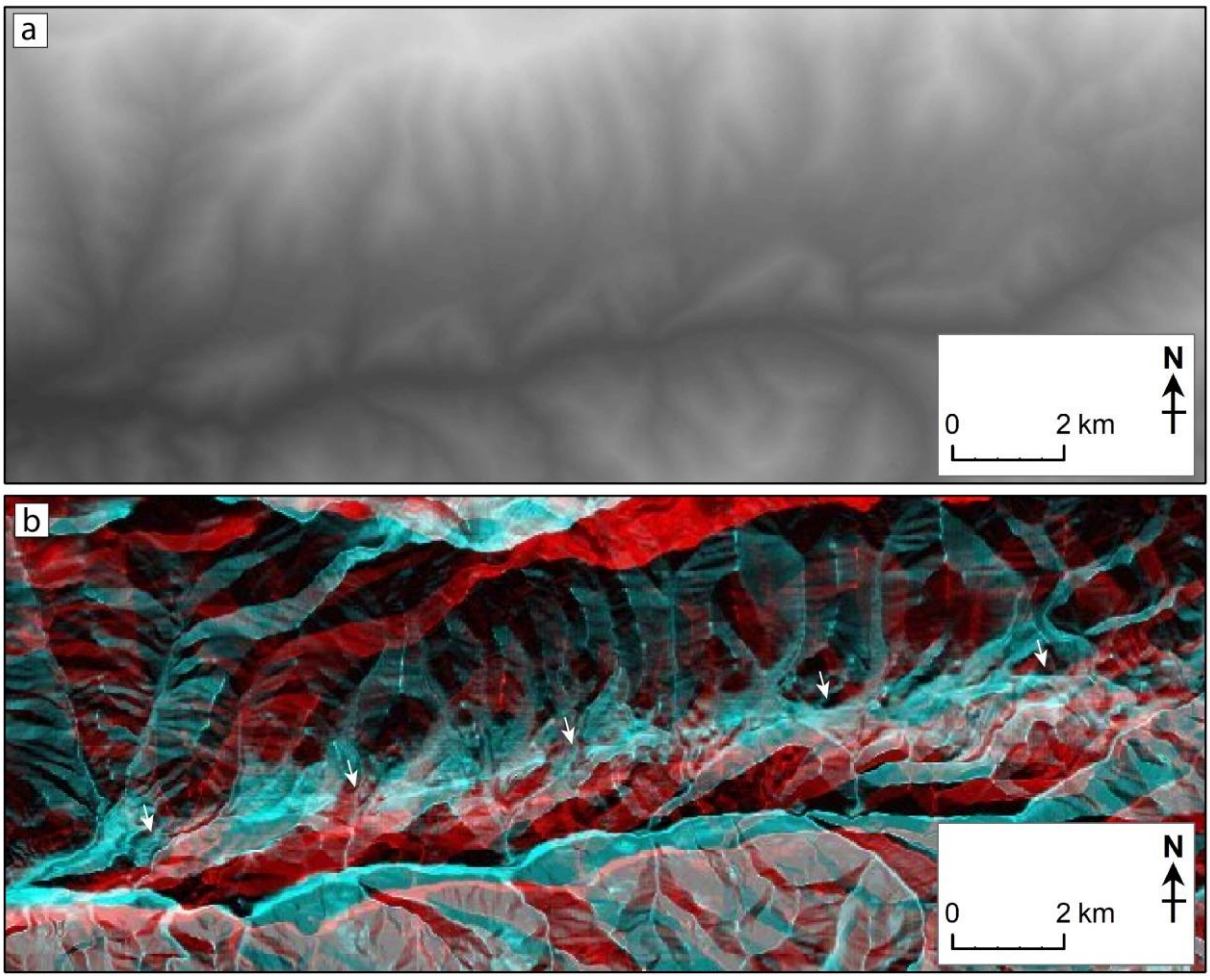

Figure 3.1: Example of grayscale images along the Andarab fault. a) DEM (Digital Elevation Model) of 1-arcsecond SRTM. b) Anaglyph image of the same area created from the 1-arcsecond DEM.

Based on this, an effort was made to measure offset of small- and large-scale tectonic geomorphic features along a fault trace. The most common geomorphic features such as fault scarps, fault saddles, linear depressions, and systemic stream offsets, beheaded channels, offset and tilted alluvial fans, shutter ridges, bulges and grabens were observed along the

strike-slip faults. The SRTM anaglyph images were also used to consider the degree of faults activity and determine their orientation. In bedrock terrane across the Hindu Kush and Pamir, strike-slip faults may be evident from their offset of geological units, but current activity is hard to identify unless the fault cuts through young landforms and/or stream offsets are consistent.

The active fault map was combined with earthquake catalog data prepared by Dewey (2006). The earthquake catalog was also used to interpret the seismic hazard and define earthquake sources based on focal mechanisms and distribution of earthquakes. He compiled the record from 26 preexisting source catalogs (e.g., Abe, 1981, 1984; Abe and Noguchi, 1983; Ambrasyes and Bilham 2003, Ambraseys and Melviller, 1982; Engdahl and Villasenor, 2002; China catalog, 2005; Engdal and others, 1998; Gutenberg and Richter, 1954; India catalog, 2005; International Seismological Centre, 2005; International Seismological Summary, 2002, NOAA-Dunbar and others, 1992; Preliminary determination of Epicenters by USGS; ROTH, 1969, USSR catalog, Kondorskaya and Shebalin, 1982; EB, EBS). The catalog is presented in three formats: 1) summary catalog of Afghanistan earthquakes, 2) master catalog of Afghanistan earthquakes, and 3) summary of macroseismic effects reported for Afghanistan earthquakes. I use the summary catalog of Afghanistan earthquakes, which is the most detailed data set available for the country and the surrounding region. The catalog includes the best estimation of the location and magnitude of earthquakes between M 4.0-8.3 that covers the area 23-45°N and 53-80°E from AD 800 to 2004 with 12,728 earthquake events. The catalog was compiled in three parts: 1) historical documented earthquakes before 1900, 2) earthquakes of magnitude ≥ 5.5 between 1900 -1963, and 3) earthquakes of magnitude ≥ 4 since 1964.

I also used the more recent seismicity (2005-2016) from ISC-EHB catalog to provide a deep understanding of the seismotectonic setting of the study area. The ISC-EHB earthquake catalog is a groomed version of ISC Bulletin, and are relocated using the EHB algorithm (Engdahl et al., 1998). The ISC-EHB catalog contains seismic events from 1964 to 2016. After 2016, USGS data was used for large (M > 6) earthquakes.

3.2. Active fault mapping

I prepared the active fault map to better understand the distribution and level of seismic hazard throughout the country (Table. 1; Fig. 3.2). Many thrust faults are mapped nearby and east of the north Afghanistan platform, and south of the Afghan block, consistent with crustal shortening and thickening (Figs. 3.4a, 3.7c). Similar shortening in the Hindu Kush extends into the southern Afghan-Tajik basin. Strike-slip faults are predominated in the south and northeast parts of the country (Fig. 3.2). The well-defined geomorphic features characteristics of strike-slip faults mark fault trace, which includes numerous discontinuities such as steps as large as several kilometers. The discontinuities may have a strong influence on coseismic behavior of the fault.

Based on the published literature and the criteria (e.g., Iwahashi, 2010; The Research Group for Active Faults of Japan, 1992; Tsutsumi and Perez, 2013), twenty-two significant faults in Afghanistan are identified as seismically active (Table 3.1; Fig. 3.2). Among the faults, the Chaman, Paghman, Darvaz, Herat, Central Badakhshan, Panjshir, Andarab, Sarobi, and Konar faults have evidence for Quaternary movement (Lawrence et al., 1992; Mohadjer et al., 2016; Ruleman et al., 2007; Wellman, 1966; Yeats et al., 1979). Based on tectonic geomorphic interpretations, I divided the country into six regions having different styles of Quaternary deformation (Fig. 3.2): 1) the Chaman fault system, 2) northeastern Afghanistan, 3) Hindu Kush-Pamir, 4) northern Afghanistan, 5) the Herat fault system, and 6) southwestern Afghanistan.

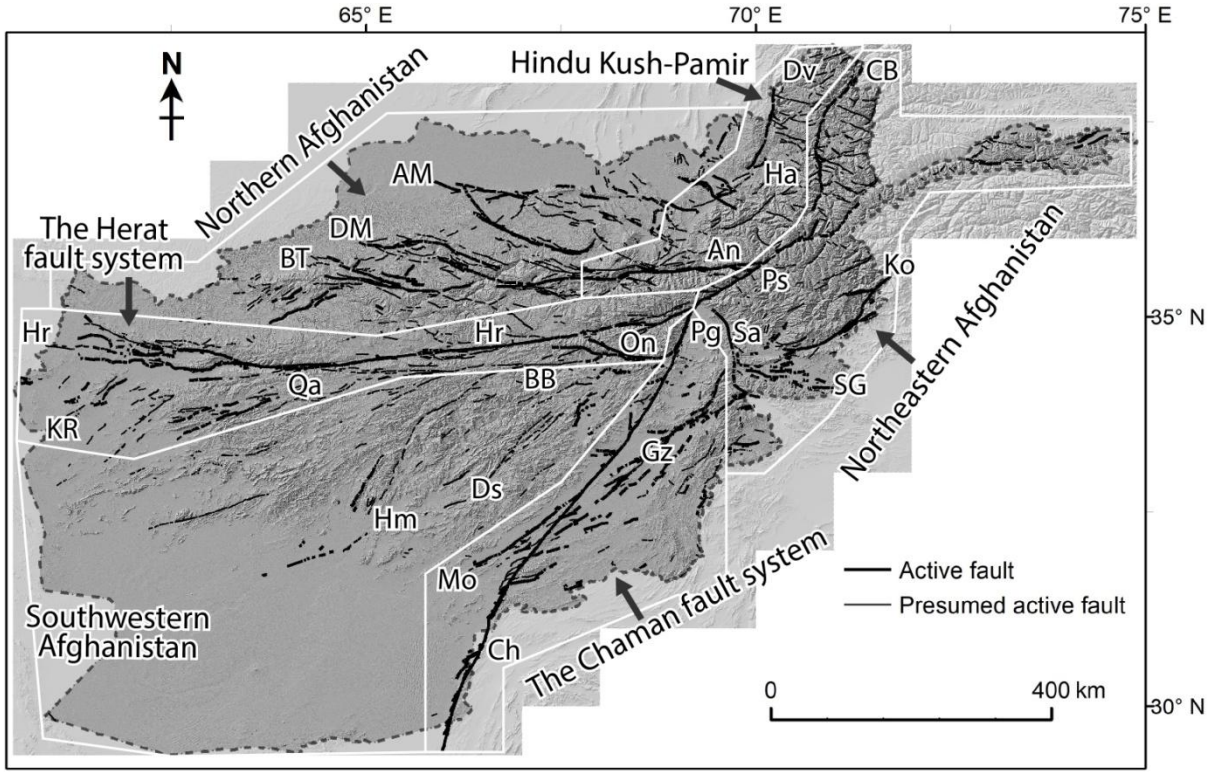

Figure 3.2: Active and presumed active faults of Afghanistan based on this study and six tectonic regions shown by white boundaries. Abbreviations of faults: AM, Alburz Mormul; An, Andarab; BB, Bande Bayan; BT, Band-e Turkestan; Ch, Chaman; CB, Central Badakhshan; Ds, Darafshan; Dv, Darvaz; Dm, Dosi Mirza-Valang; Gz, Gardez; Ha, Henjvan; Hr, Herat; Hm, Helmand; KR, Kaj Rod; Ko, Konar; Mo, Mokur; On, Onay; Pg, Paghman; Ps, Panjshir; Qa, Qarghanaw; Sa, Sarobi; SG, Spin Ghar.

Table 3.1: Summary of the faults considered as active in Afghanistan.

Name	Length and orienta-tion	Fault type	Slip rate	Geomorphic expression	Associated seismicity	Region
1. Chaman fault	~800 km long; SW-NE	Left-lateral strike-slip	8 -35 mm/yr (Beun et al., 1979; Furuya and Satyabala, 2008; Mohadjer et al., 2010; Ul-Hadi et al., 2013; Yeats et al., 1979)	Cut all geologic deposits and bedrock. Alluvial terraces recently offset. The oldest fan is offset for ~1 km, while young surfaces offset for less than 50 m. Much of the fault trace is linear and shows evidence for young activity.	1505 (M 7.3); 1892 (M 7.0); 1935 (M 7.7); 1978 (M 6.4); 2016 (M 5.5)	Northeastern Afghanistan -Baluchistan
2. Mokur fault	~200 km long; SW-NE	Left-lateral strike-slip	Geodetic ~5.4 mm/yr (Mohadjer et al., 2010)	Fault shows Quaternary activity, and has linear and continues scarps on alluvium.		Southern Afghanistan
3. Gardez fault	~300 km long; SW-NE	Left-lateral strike-slip	Geodetic ~5.4 mm/yr (Mohadjer et al., 2010)	Cut Quaternary deposits. The fault has linear and discontinuous scarps on piedmont alluvium and bedrock.		Southern Afghanistan

4. Paghman fault	~80 km long; SW-NE	Left-lateral strike-slip; LL oblique thrust	>10 mm/yr (Ruleman et al., 2007)	Alluvial terraces recently offset for ~200 m. It has discontinuous and arcuate scarps on Quaternary deposits, and contains multiple strands.	1505 (M 7.3)	Central Afghanistan
5. Sarobi fault	~150 km long; N-S	Right-lateral strike-slip		Cut Quaternary landforms. It has continuous, linear scarps on range-front deposits. Late Pleistocene deposits are mapped along piedmont of Kohi-e Safi.	Associated Micro-earthquakes	Northeastern Afghanistan
6. Konar fault	~200 km long; NE-trending	Left-lateral strike-slip	1-10 mm/yr (Ruleman et al., 2007)	It has clear expression on satellite images. I mapped offsets in young deposits of active alluvial fans.	Associated Micro-earthquakes	Eastern Afghanistan
7. Spin Ghar fault	~140 km long; W-E	Right-lateral SS; Reverse		Cut late Pleistocene deposits. South-verging thrusts within the hanging wall of Spin Ghar Mountains.	Associated Micro-earthquakes	Southeastern Afghanistan
8. Panjshir fault	~160 km long; SW-NE	Right-lateral strike-slip		The fault is marked by linear, discontinuous and arcuate scarps on range-front alluviums.	Associated Micro-earthquakes	Northeastern Afghanistan
9. Central Badakhshan fault	~280 km long; N-NE-trending	Left-lateral oblique thrust		The geomorphic expression is unclear along some of its traces. In central Badakhshan, Quaternary deformation is partitioned between SE thrust faults and NW right-lateral faults.	Associated Micro-earthquakes	Northeastern Afghanistan /Hindu Kush
10. Darvaz fault	~300 km long; S-N	Left-lateral strike-slip	Geodetic 11.4 mm/yr (Mohadjer et al., 2010)	The fault rate is based on displaced landforms of probable Holocene and late Pleistocene age. Schurr et al., (2014) located three earthquakes affiliated with the Darvaz fault zone.	Three earthquakes (Schurr et al., 2014)	Northern Afghanistan Pamir
11. Andarab fault	~290 km long; W-E	Right-lateral strike-slip	1-10 mm/yr (Ruleman et al., 2007)	The fault has linear, continuous scarps on Quaternary alluvium and bedrocks. The 1956 EQ appears to have occurred between the Herat and Andarab faults.	1956 (M 7.4)? Associated Micro-earthquakes	Northern Afghanistan / Central Hindu Kush
12. Henjvan fault	SW to NE-N	Strike-slip and SE-verging Reverse		Geomorphic expression of the fault is unclear along much of its length. the scarp is discontinuous, arcuate bounding rnage fronts in large valleys and bedrock terrain.		Northeastern Afghanistan Pamir
13. Alburz-Marmul fault	~220 km long; W-E	Right-lateral strike-slip		It has clear geomorphic expression and bounds E-trending ridges. The deformation is portioned vertically. The fault zone consists of north- and south-verging thrust faults and associated folds.	Associated Micro-earthquakes	Northern Afghanistan Platform
14. Dosi Mirza-Valang fault	~200 km long; NW to E-SE	Right-lateral strike-slip		The fault is composed of a series of fault strands. Different offset stream channels are present along the fault.		Northern Afghanistan
15. Band-e Turkestan fault	~210 km long; NW-SE	Right-lateral strike-slip		The fault has discontinuous scarps forming lineaments across alluvium deposits, bedrock upland terrain. Narrow valleys in rugged terrain contain few Quaternary deposits.		Northern Afghanistan
16. Herat fault	~1100 km	Right-lateral	Geodetic < 2 mm/yr	Most of the fault is in bedrock. Near to Herat the fault is cover by	849 (M 7.0)?;	Middle Afghanistan

	long; W-E	strike-slip	(Mohadjer et al., 2016)	Quaternary deposits. Tectonic features are mainly defined by linear valleys or by alignment of escarpments in bedrock.	1874 (M 7.0); 1956 (M 7.4)?	
17. Kaj Rod fault	~100 km long; SW-NE	Strike slip		The fault separates Pliocene deposits from late Pleistocene-Holocene deposits.		Western Afghanistan
18. Qarghanaw fault	>300 km long; W-E	Left-lateral strike-slip		Most of the fault is in bedrock and offset stream channels.	Associated Micro-earthquakes	Central Afghanistan
19. Onay fault	~110 km long; SE-NW	Left-lateral strike-slip		Most of the fault is in bedrock and offset some stream channels.		Central Afghanistan
20. Bande Bayan fault	>200 km long; W-E	Strike-slip		The fault is marked by linear, discontinuous scarps on bedrock.		Middle Afghanistan
21. Helmand fault	>300 km long; SW-NE	Left-lateral strike-slip		The fault offset geomorphic features on middle Pleistocene deposits. Along southwestern end of the fault, the features bound prominent range fronts		Southwestern Afghanistan
22. Darafshan fault	>200 km long; SW-NE	Left-lateral strike-slip		The fault has a clear geomorphic expression in bedrock, and Quateranry deposits in Dasht-e Nawur.	Associated Micro-earthquakes	Southwestern -central Afghanistan

Active faults are identified that have deformed recent alluvial landforms and deposits. I characterized geomorphic features based on their continuity and geomorphic expression on the surface. Based on the geological map of Afghanistan prepared by Doebrich et al. (2006), the active faults displace Quaternary deposits. The geologic map provides general information about the relative ages of deposits (Fig. 2.3). The active faults have a subtle morphologic expression marked by a scarp whose height ranges from few meters to tens of meters depending on the age of offset fans. Some active faults have geomorphic expression less continuous in the Quaternary landform. They have lower activity rates, part of their scarps may be eroded or buried by younger deposits, and therefore have a discontinuous trace. Active and presumed active faults with different orientations cut each region. In the following sections, I briefly describe the geometry and geomorphology of the Afghanistan faults and fault-related geomorphic features.

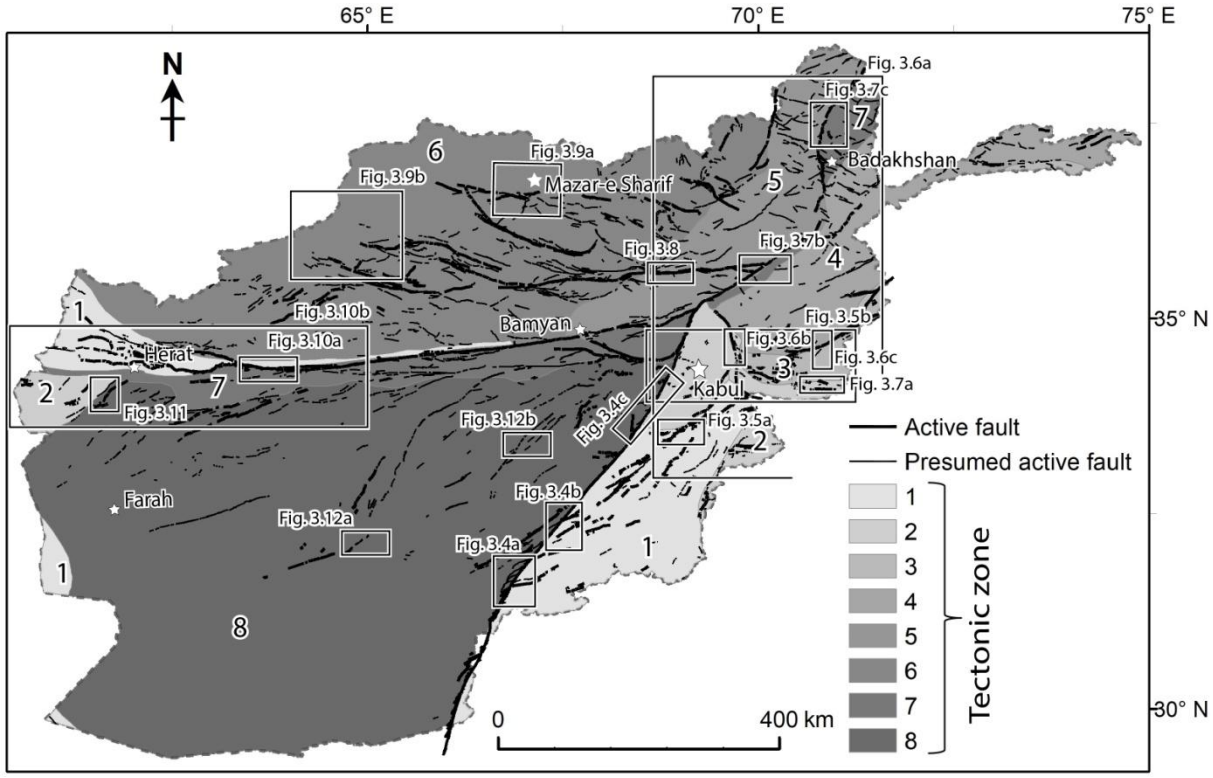

Figure 3.3: Tectonic zones of Afghanistan. Block boxes show location of Figs. 3.4-3.12. The numbers show: 1) Relatively subsided areas; 2) Relatively uplifted areas; 3) Henduraj-Hazar; 4) Nuristan-Pamir; 5) Afghanistan North Pamir; 6) North Afghanistan Platform; 7) Region of Middle Kimmerian Folding, Median Masses; and 8) South Afghanistan, Regions of Alpine Folding. The Afghanistan tectonic zones modified from Abdullah et al. (2008).

3.2.1. The Chaman fault system

The Chaman fault is a major left-lateral strike-slip fault that accommodates much of the oblique motion between the Indian and Eurasian plates in southeastern Afghanistan (Figs. 1.1, 3.2). The fault strikes from N10°E to N35°E (Lawrence et al., 1992) and is the most extensive continental strike-slip faults in the region. The total length of the fault is ~860 km (Fig. 1.2). It is ~650 km long in Afghanistan and terminates near the northern margin of the Kabul block (Fig. 2.1). The Chaman fault marks a boundary between the Katawaz Basin, ophiolite belt and Kabul Block to the northeast, and central Afghanistan to the northwest (Figs. 2.1, 2.2). Along the fault, tectonic geomorphic features such as offset and beheaded stream channels, offset alluvial fans, shutter ridges, fault scarps, and tilted alluvial surfaces

are commonly observed (Fig. 3.4b). The fault offsets late Pleistocene and Holocene deposits. The left-lateral slip rate of the fault has been estimated at 8-35 mm/yr by several studies (Beun et al., 1979; Furuya and Satyabala, 2008; Mohadjer et al., 2010; Ul-Hadi et al., 2013; Yeats et al., 1979).

The Chaman fault trace is remarkably straight (Figs. 3.4a, b). For a distance of ~75 km between 32°58'N and 33°31'N, it is difficult to trace the fault continuously across the flat, heavily vegetated and urban area. The east side of the fault in the vicinity of Ghazni City, where the alluvial fan borders the rocks of the mountains, the Chaman fault traverses the main body of the alluvial fan and displaces it left-laterally. North of Ghazni, west-facing scarps 1 to 40 m high and 65 km long are identified across the alluvial plain of the Sayed Abad valley (Fig. 3.4c). In this area, the Chaman fault is evident and has continuous fault scarp in piedmont alluvium at the bottom of the two massifs' eastern flank. The fault offsets a series of alluvial fans deposited along the western margin of the mountains. In this area, I measured different offset alluvial fans and stream channels from tens of meter to approximately 1 km. On average this part of the alluvial fan lies almost at the same topographic level ~2420-2480 m asl. In Kabul, the northern extension of the Chaman fault exhibits an intricate pattern of fault strands. Southwest of the Kabul City, I identified less than 3 m high east-facing scarps across alluvial lowlands that may be associated with the 1505 M 7.3 earthquake.

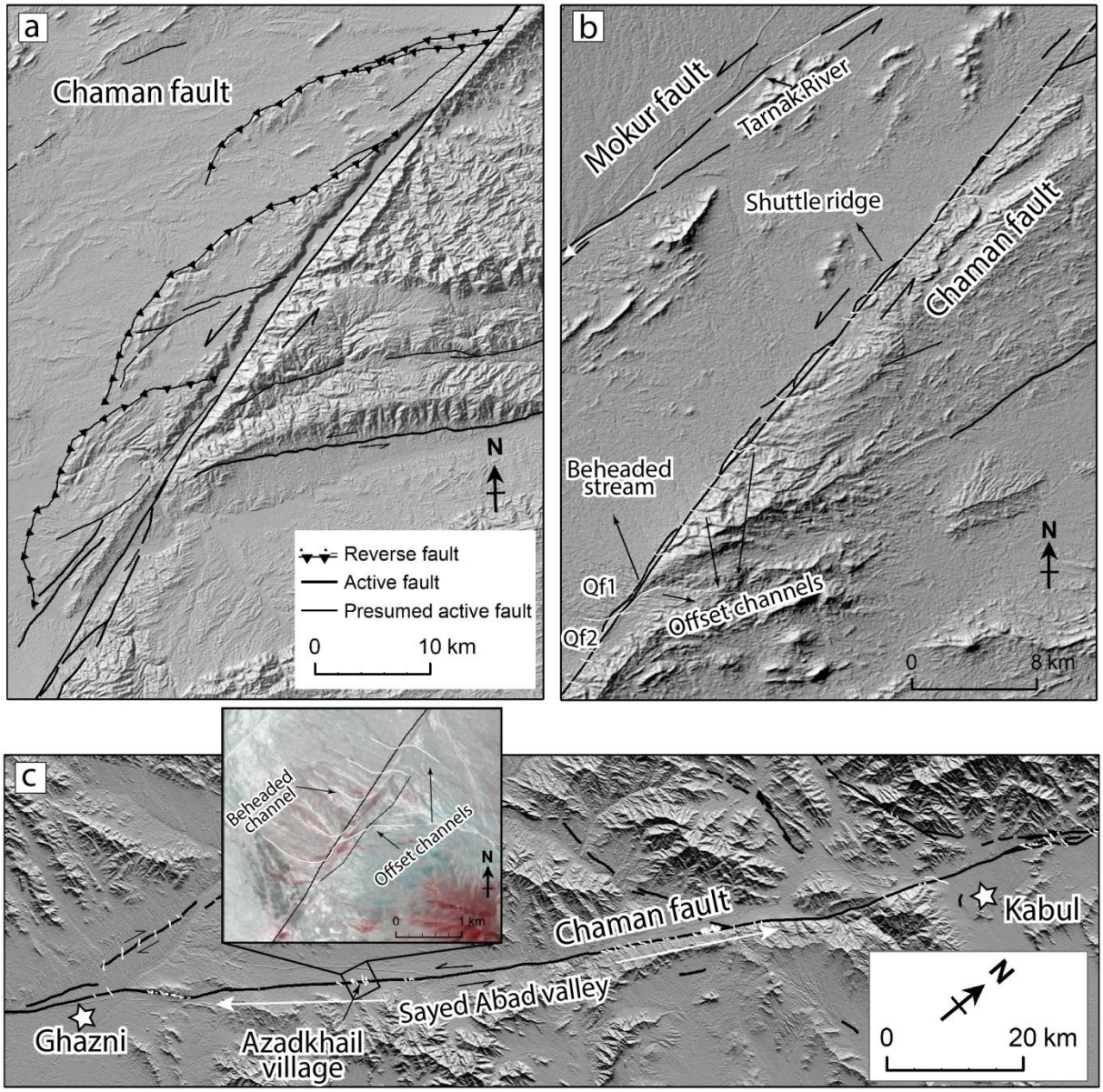

Figure 3.4: Location maps of the Chaman and Makur faults. a) Thrust faults along the western margin of the Chaman fault. b) The Chaman fault cuts through the range front and offset steam channels left-laterally. c) North of Ghazni at Sayed Abad district, the Chaman fault is evident and has continuous fault scarp in piedmont alluvium at the mountains front.

The northeast-trending left-lateral Mokur fault splays southwest from the Chaman fault. The fault has linear fault scarps on alluvium deposits along the Tarnak River valley in Zabul (Fig. 3.4b). The fault zone is linear, and bounds bedrock particularly in the north. The Mokur fault shows evidence for young activity and cuts most geologic deposits and bedrock (Fig. 2.3). The fault extends for about 150 km into the northeast margin of the Helmand basin.

The Gardez fault is a left-lateral strike-slip fault that extends from the Chaman fault to the Sarobi fault east of Kabul (Figs. 3.1, 3.5b). The total length of the fault is approximately 290 km, and the general strike is east-northeast. Along the fault, many offset channels and displaced landforms and deposits were observed (Fig. 3.5a). I measured several steams offset (150-450 m) along the northern side of the Gardez in the mountain front (Fig. 5a). The fault separates the Kabul block from the Katawaz basin (Figs. 2.2, 3.6a).

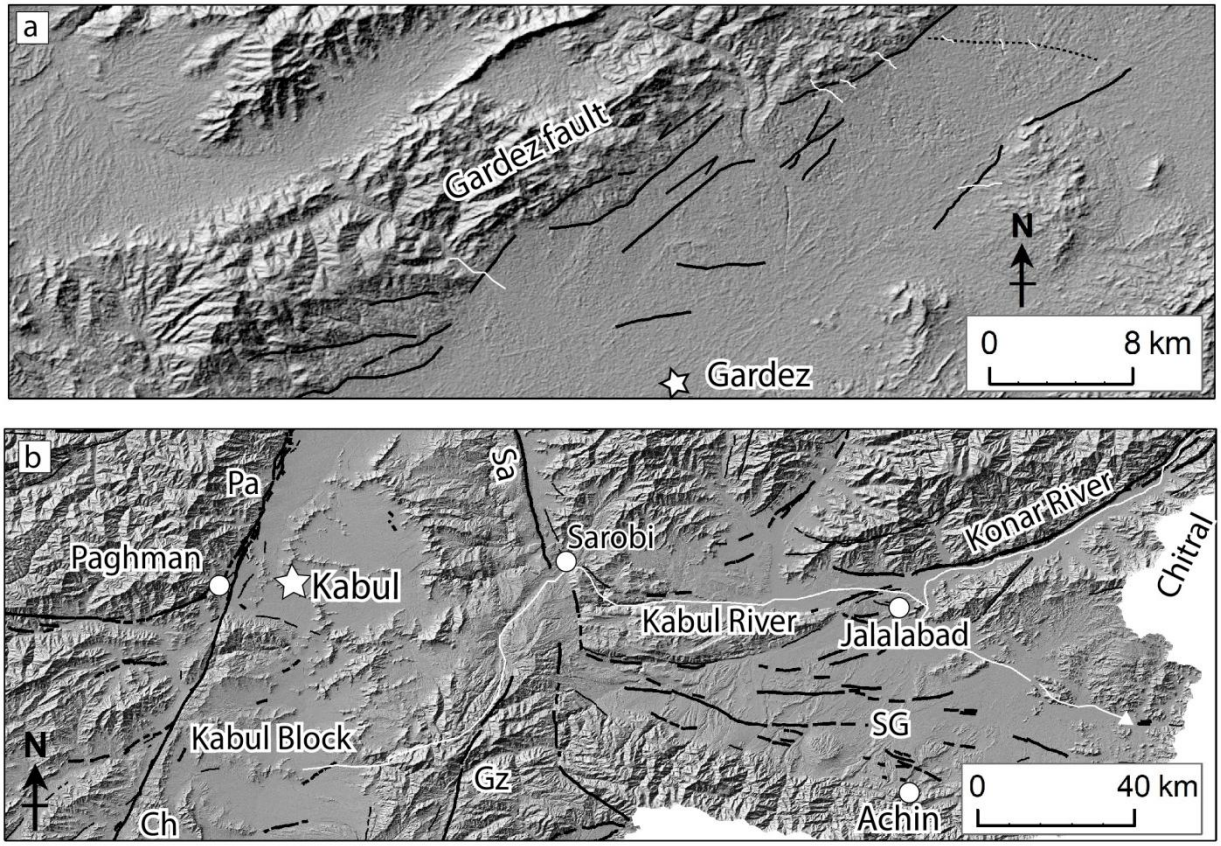

Figure 3.5: Map of geomorphic features in central and eastern Afghanistan. a) The Gardez fault, which has formed southwest-facing scarps. b) Location of geomorphic features associated with active tectonics in the study area.

The ~80-km-long Paghman fault, the northern extension of the Chaman fault, starts from Arghandi Paghman district immediately west of the Kabul City and extends northeastward to the northern margin of the Kabul block (Fig. 3.5b). The fault strike ranges from N16°E to N35°E. The fault is marked by continuous, linear, and arcuate fault scarps on Quaternary deposits and landforms. The Paghman fault also contains multiple strands that offset stream channels by differing amounts. Based on the anaglyph images interpretation, I

measured left-lateral displacement of alluvial fan and active stream channels, which shows very young movement on some fault strands. The alluvial fan stream channels have been moved northward from tens to approximately 300 m along the fault relative to its source drainage. However, there are no age data to estimate the left-lateral slip rate of the fault.

3.2.2. Northeastern Afghanistan

The Sarobi fault is approximately 150 km long, separating the northeast part of the Kabul Block from the Nuristan fault block (Figs. 3.2, 3.6a). The fault scarps on range-front proximal deposits are continuous and linear. The geomorphic expression of the fault is well defined along the whole length of the fault (Fig. 3.6b). However, there is no evidence for recent faulting in the northern end of the Kabul Block. Based on the anaglyph images interpretation, the fault plane dips steeply to almost vertical, particularly in the Sarobi district (Fig. 3.5b).

The Konar fault in eastern Afghanistan is a left-lateral strike-slip fault separating the Konar zone from the Nuristan Pamir tectonic zone to the southeast (Fig. 3.6a). The fault extends from the Sarobi settlement and along the left bank of the Kabul River to the Konar River valley. It further extends northeastward to the Chitral region of Pakhtunkhwa. The fault has continuous east-northeast-trending arcuate scarps on piedmont landforms of various ages (Fig. 3.6c). The Konar fault offsets some small gullies and stream channels along the Konar River left-laterally (Fig. 3.5b). Ruleman et al. (2007) compared the Konar fault to faults in the US and estimated the slip rate to be 1-10 mm/yr.

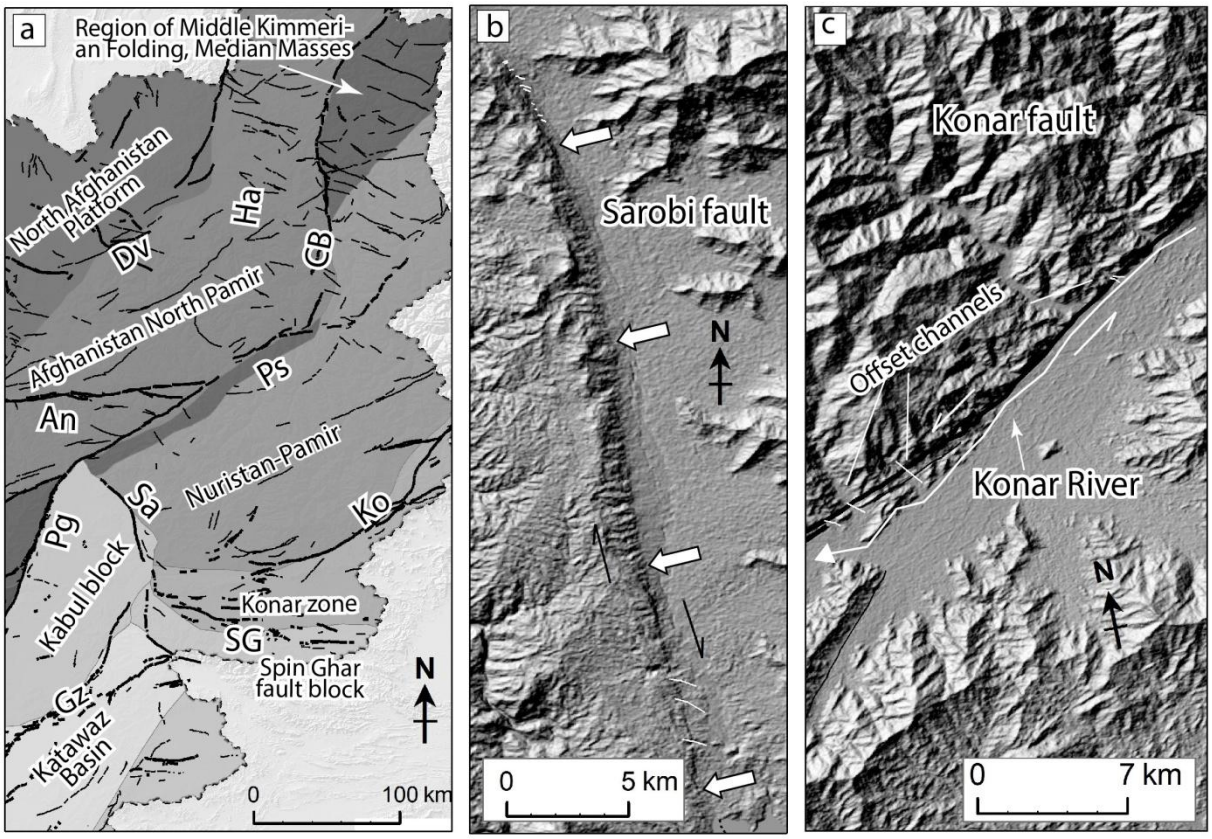

Figure 3.6: Map of active and presumed active faults in northeastern Afghanistan. a) Location of tectonic blocks separated by major active faults in central-northeastern Afghanistan. b) The white arrows denote the Sarobi fault trace. c) The northeast-trending Konar fault shows evidence of left-lateral offset. Locations of the images are shown in Figure 3.3.

The Spin Ghar fault is located in the eastern part of the country, separating the Spin Ghar fault block from the Konar zone's structures to the north (Fig. 3.6a). The fault trace is linear but discontinuous with arcuate scarps (Fig. 3.7a). However, further east between Jalalabad and Achin, there are drastic changes in structural and geomorphic expressions of the fault, where middle and late Pleistocene deposits have been affected by the fault (Fig. 3.5b). The total length of the fault is at least 140 km (Table 3.1).

The northeast-tending Panjshir fault is a right-lateral strike-slip fault with discontinuous linear and arcuate scarps. The fault is located in the narrow Panjshir valley and is convex to south-southeast. The fault extends northeast from the northern end of the Paghman fault (Fig. 3.2). Tectonic geomorphic expression of the fault is evident along the

range front. I identified 3.5 km of right-lateral stream offset in the midstream of the Panjshir River at Hesa-e-Awal Panjshir, where the Andarab fault extends to the west (Fig. 3.7b).

The Central Badakhshan fault is a left-lateral strike-slip fault that extends from the eastern end of the Panjshir fault to the Tajikistan border (Fig. 3.2). The fault's geomorphic expression is unclear along some of its traces. The central Badakhshan fault trends north-northeast and associated with active oblique-thrust faults (Fig. 3.7c). The Central Badakhshan and Panshir faults separate the Afghanistan North Pamir from the region of middle Kimmerian folding (Figs. 3.6a).

3.2.3. Hindu Kush-Pamir region

The Darvaz fault, a left-lateral strike-slip fault, is located in the western part of the Pamir (Fig. 3.2). The northeast-trending fault is less than 300 km long (Table 3.1). The fault extends along the boundary between the Pamir-Badakhshan region and the Afghan-Tajik basin (Figs. 2.2, 3.3). It is located mostly in Afghanistan, but the northern part is located in Tajikistan. The Darvaz fault has continuous, range bounding, north to northeast-trending fault scarps on piedmont and mountain ranges. The fault offsets late Pleistocene and Holocene deposits at the Pamir Mountains front. Kuchai and Trifonov (1977) and Trifonov (1978) noted 20 m left-lateral slip during the late Holocene, about 120 m during the whole Holocene, and 300 m during the late Pleistocene at the north-striking part of the fault in Tajikistan close to Afghanistan border. Mohadjer et al., (2016) reported an 11 mm/yr geodetic slip rate based on GPS observation for the Darvaz fault.

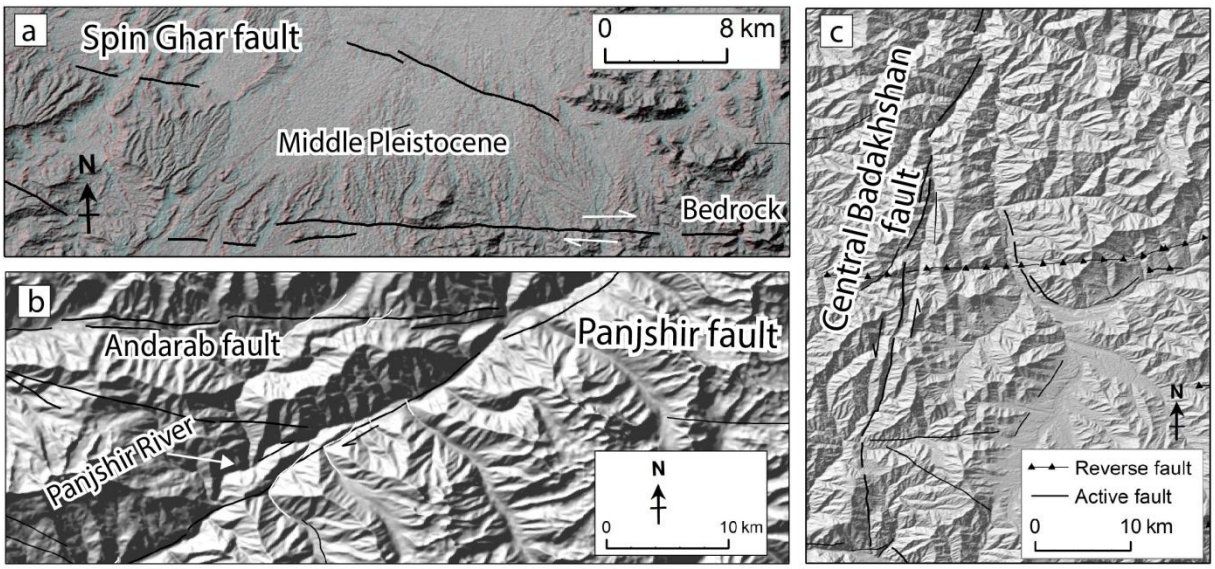

Figure 3.7: Map of the Spin Ghar, Panjshir and Central Badakhshan active faults. a) The Spin Ghar fault offsets middle Pleistocene deposits right-laterally. b) Panjshir fault with 3.5 km of right-lateral stream offset in the midstream of the Panjshir River. c) The left-lateral central Badakhshan fault.

The right-lateral strike-slip Andarab fault is one of the most significant faults in northern Afghanistan and nearly parallel to the Herat fault (Fig. 3.2). The fault runs mostly along the Andarab River valley (Fig. 3.8) and terminates in the northwest-trending fault zone close to the Mirza-Wolang fault system. The fault has continuous and sub-linear scarps on middle and late Pleistocene alluvial deposits and bedrock (Fig. 2.3). The Andarab fault trace appears to be concealed beneath the course of the major rivers along the western part. Based on the images interpretation, I identified two stream offsets greater than 1 km along the southern part of the Andarab valley.

The Henjvan fault is located in the Afghanistan North Pamir tectonic zone (Figs. 3.2, 3.6a). The Henjvan fault is a SE-verging reverse fault approximately parallel to the Central Badakhshan and Darvaz faults. The geomorphic expression of the fault is unclear along much of its length (Fig. 3.2). The Henjvan fault extends through bedrock up to where it merges with the Pamir faults systems.

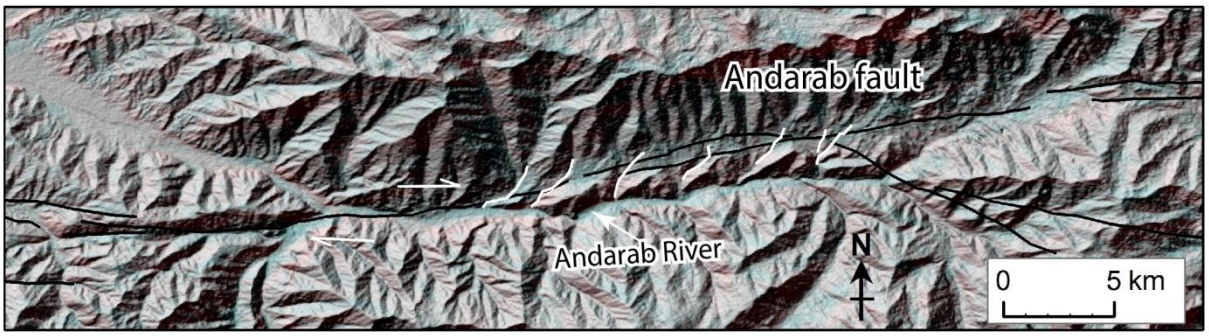

Figure 3.8: Right-lateral offset of river channels along the Andarab strike-slip fault.

3.2.4. Northern Afghanistan

The east-trending, right-lateral Alburz-Marmul fault is about 220 km long (Fig. 3.2). This fault separates the Tajikistan basin from the Parapamiz Bande-Turkistan Mountains (Fig. 2.2). The fault bounds east-trending ridges that are composed of steeply north dipping Cretaceous and Miocene rocks (Ruleman et al., 2007) (Fig. 2.3). Near Mazar-e Sharif, a massive alluvial fan is filling a basin in front of an active fault propagation fold (e.g., Ruleman et al., 2007) (Fig. 3.9a). In northern Afghanistan, both north-south (Alburz-Marmul) and east-striking reverse faults are active (McNab et al., 2019). McNab et al. (2019) argue that both sets of structures are active, and the deformation is partitioned vertically. The result confirms that the east-west compression is accommodated by north trending arcuate folds, and north-south compression is accommodated on east trending thrust faults.

The Dosi Mirza-Valang fault is parallel to the Band-e Turkestan fault. The fault is composed of a series of fault strands, which merge gradually to form a single fault line to the east. The Dosi Mirza-Valang fault is approximately 200 km long and separates the Maymana fault block from the Shebergan fault block to the north (Fig. 3.9b). It is a right-lateral strike-slip fault trending east-southeast. The Band-e Turkestan fault extends through the Bande-Turkestan Mountains, a vast northwest-trending plateau that gradually decreases its elevation northwest (Figs. 2.1, 2.2). The fault runs between the Murghab valley in the south and the Saripul River basin in the north (Fig. 3.9b). According to Shroder (2014), the Band-e

Turkestan fault is a relatively new shear zone as the Herat fault steps out to the northwest to relieve stress as it extends west toward the Herat basin.

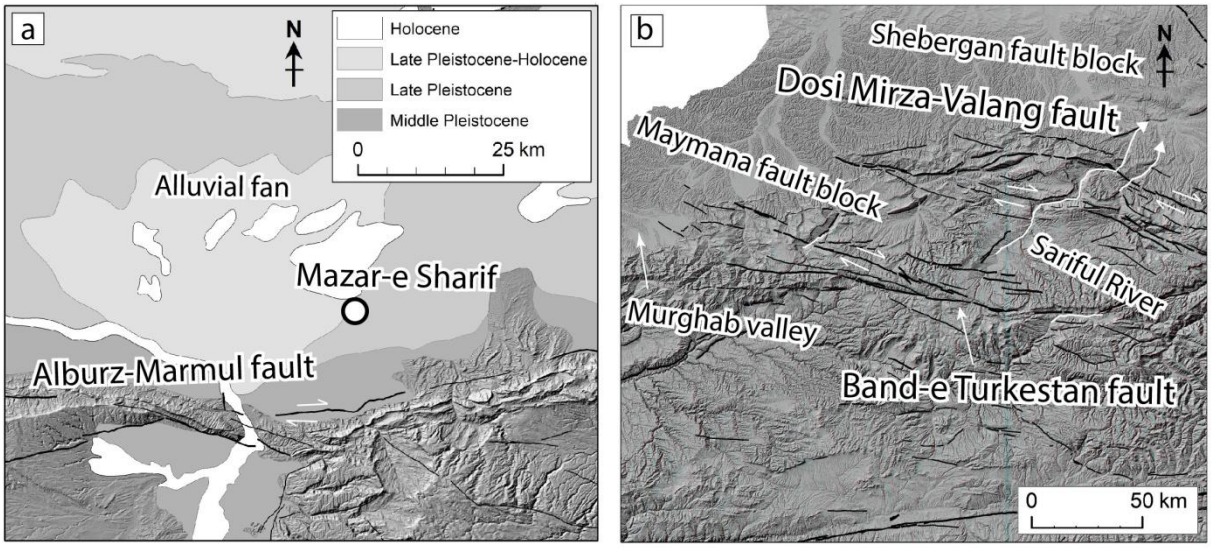

Figure 3.9: Location of geomorphic features in northern Afghanistan platform. a) Large alluvial fan located in front of the right-lateral Alburz-Marmul fault near the City of Mazar-e Sharif. b) Map of features associated with Dosi Mirza-Valang and Band-e Turkestan faults in northern Afghanistan.

3.2.5. The Herat fault system

The Herat (also known as Hari Rud) fault is a right-lateral strike-slip fault trending roughly east to west. The Herat fault exhibits explicit geomorphic expressions (Fig. 3.10a). The fault is one of the most prominent strike-slip faults in middle Afghanistan and separates the northern Afghan platform from central Afghanistan. It also separates the uplifted and subsided areas at the western end (Figs. 3.3, 3.10b). The fault systematically offsets stream channels in the bedrock terrain (Fig. 3.10a). The fault extends from the Panjshir fault westward, running through historical cities of Bamyan and Herat, and terminates at the border region with Iran (Fig. 3.3). The total length of the fault is more than 1100 km. Right-lateral offset streams are observed along the entire fault length. Based on anaglyph interpretation, I measured ~5.5 km offset along the southern part of the Hari Rud River (Fig. 3.10a). Near the northern end of the Kabul block, the fault is flanked to the south by an active anticline uplifting the middle Hindu Kush Range (Fig. 2.2). There are numerous faults south and east

of the Herat fault (Figs. 3.2, 3.10b). I mapped most of these as active faults except in the southwestern part between the Herat and Farah that is covered by young Quaternary deposits (Figs. 2.3, 3.2).

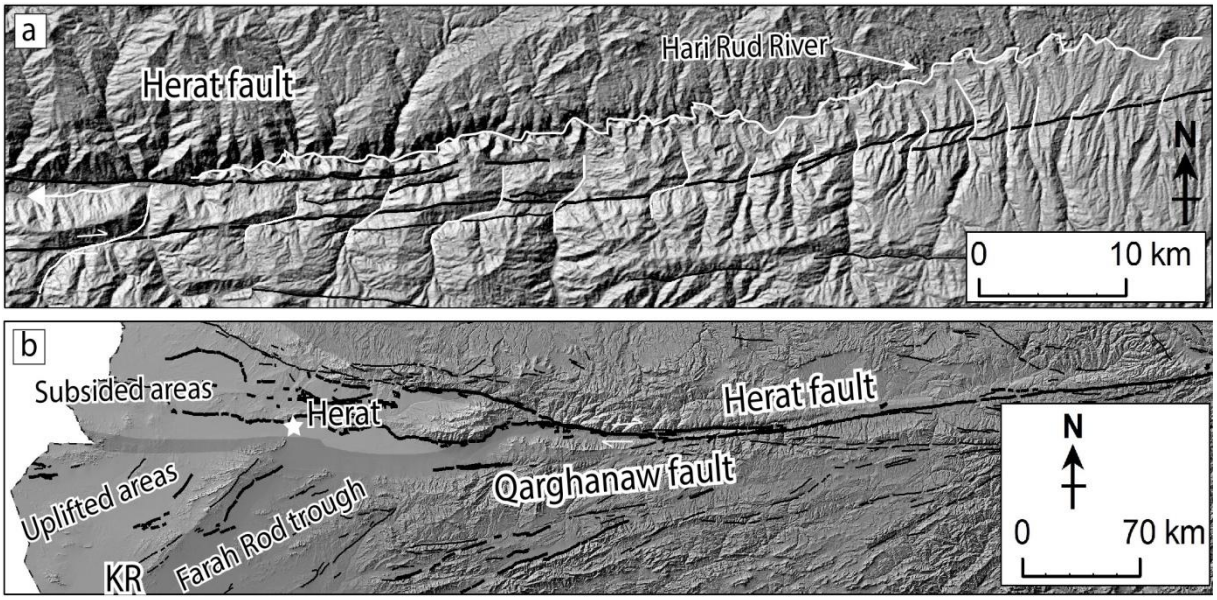

Figure 3.10: Geomorphic features of the Herat fault system. a) The Herat fault shows clear geomorphic expressions on the surface, and offset streams right-laterally along the entire fault length. b) Map of features associated with the active Herat fault system.

The northeast-trending Kaj Rod fault is located south of the Herat basin. The fault separates the Pliocene deposits from late Pleistocene-Holocene deposits (Fig. 3.11). The fault runs between the uplift areas and the Farah Rod trough (Figs. 3.3, 3.10b). This fault trends southwest and has linear and discontinuous scarps. To the northeast, the fault bounds bedrock ranges. The total length of the Kaj Rod fault is approximately 130 km. The Qarghanaw fault is located within central Afghanistan accreted terranes. The east-trending Qarghanaw fault is a right-lateral strike-slip fault extending from east to west (Fig. 3.2). Abdullah et al. (2008) interpreted that the Qarghanaw fault is the extension of the Panjshir fault. The fault extends from the Paghman Mountains Range up to the Herat and merged with Kaj Rod fault (Fig. 3.10b).

The Onay fault has northwest-trending discontinuous scarps and forms a prominent lineament across bedrock terrain. The total length of the fault is more than 100 km (Fig. 3.2).

The east-trending Bande Bayan fault is also a strike-slip fault that extends from the Onay fault. The fault is located in middle Afghanistan and separates middle Afghanistan from the accreted terrane.

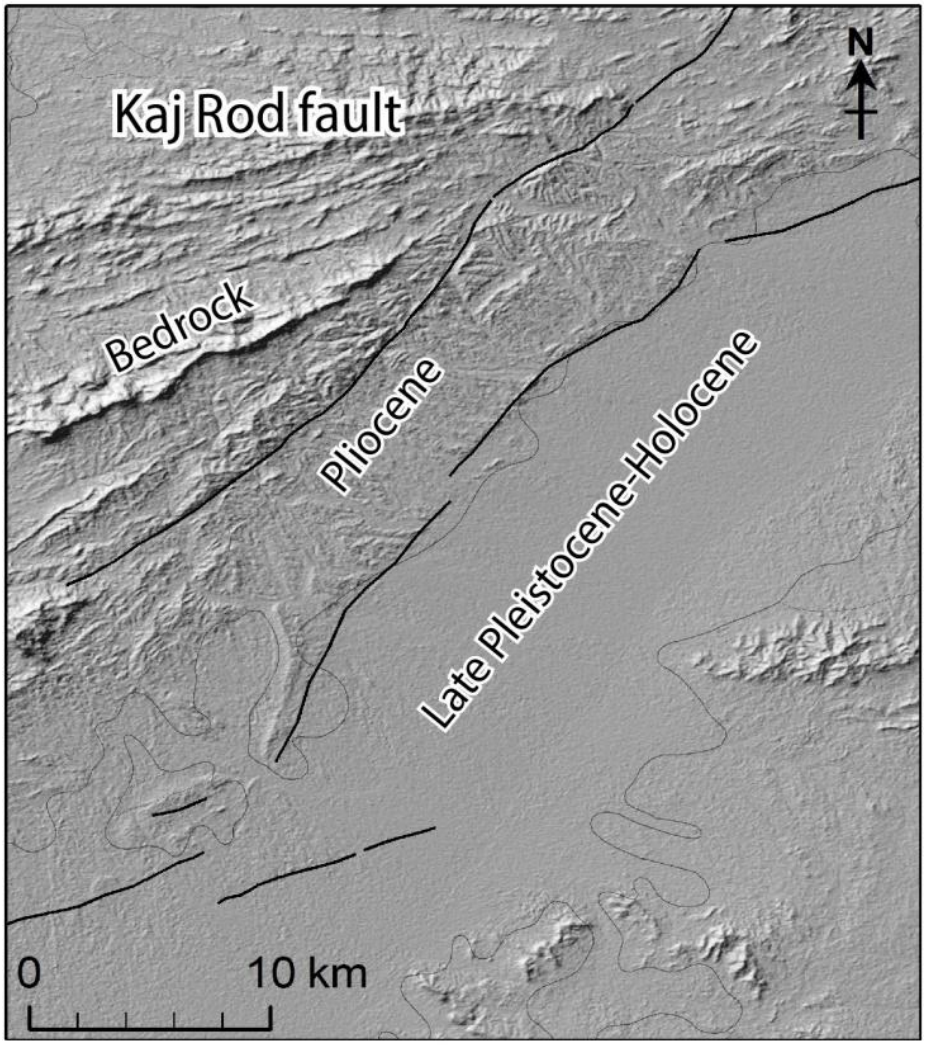

Figure 3.11: The Kaj Rod fault, which separates the Pliocene deposits from late Pleistocene-Holocene deposits.

3.2.6. Southwestern Afghanistan

The Helmand fault is a left-lateral strike-slip fault that is well expressed in central Afghanistan accreted terranes. The northeast-trending fault separates the Farah Block from the Helmand Block (Fig. 2.1). The Helmand fault might be longer than shown on the map because it is mostly covered by sediments to the south in the Helmand basin (Fig. 2.2). There

is some evidence for Quaternary activity of the fault. Offset geomorphic features on middle Pleistocene (Qf1) deposits indicate active deformation along the Helmand fault (Fig. 3.12a). I identified middle Pleistocene fan and loess cut by the Helmand fault at the mouth of Kajaki Dam along the Helmand River (Fig. 3.12a).

The northeast-trending Darafshan fault is a left-lateral strike-slip fault located in the accreted terrane (Figs. 2.1, 3.2). This fault has sub-linear discontinuous scarps in bedrock terrain and along the range fronts. The northern portion of the fault forms a prominent northeast-facing fault scarp. The stream channels bend sharply to the left where they cross the Darafshan fault (Fig. 3.12b).

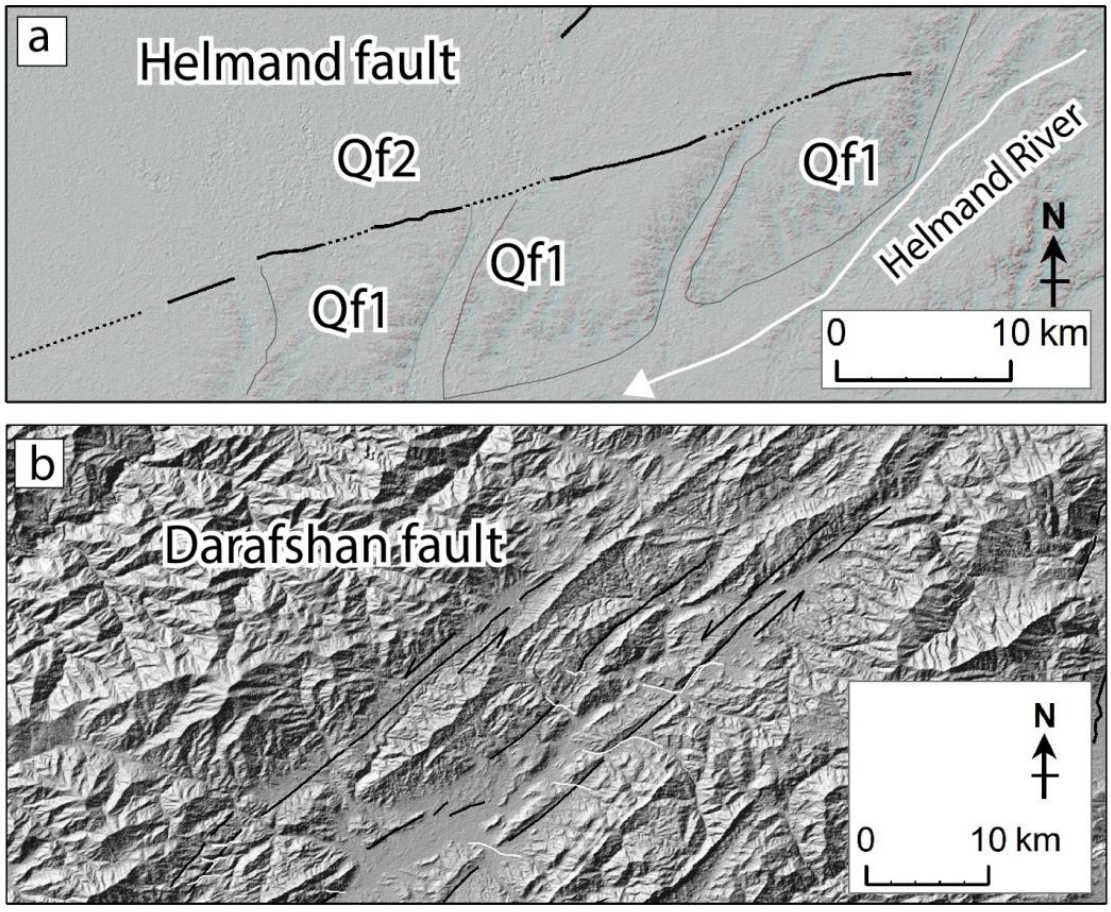

Figure 3.12: Map of the Helmand and Darafshan faults. a) The Helmand fault runs between the middle Pleistocene (Qf1) and late Pleistocene-Holocene (Qf2) alluvial fan deposits along the Helmand River. b) Geomorphic expression of the Darafshan fault that offsets stream channels left-laterally.

3.3. Seismicity

3.3.1. Crustal Seismicity

I plotted the epicenters of crustal earthquakes of magnitude greater than 4 in Afghanistan and the surrounding region (Fig. 3.13). I then plotted only the earthquakes shallower than 40 km based on the information in the summary catalog and ISC-EHB catalog. The summary catalog is one of the three formats of Afghanistan earthquakes designed by Dewey (2006) (Fig. 3.14). Based on the crustal earthquakes and mapped active faults, the greater part of the interior of Afghanistan is interpreted to be seismically less active, while areas near or north and east of Kabul experience significant earthquakes (Figs. 3.13-3.16). The regions with lots of recent earthquakes and with major active faults are likely to have higher rates of seismicity than other regions. Northeastern Afghanistan is characterized by the occurrence of both shallow (<40 km) and deep (>70 km) earthquakes. This seismicity is related to the northward motion of the Indian plate. This area has more seismicity than any other regions in the country due to its proximity to active faults (Fig. 3.2). Deformation along this region is shown by earthquakes during historical and recent times. According to Ambraseys and Bilham (2003), cumulative moment magnitude in eastern Afghanistan is 50% higher than in western Afghanistan. Mapped faults are more numerous near eastern Afghanistan, and therefore it has abundant seismicity (Fig. 3.3).

The plate boundary orientation to the plate motion may also cause shallow-focused earthquakes. On the margin of the Indian plate, several tectonic units have been overthrust to the south, and thus the shallow deformation is in the form of both left-lateral strike-slip and reverse faulting. In southeastern Afghanistan and adjacent Pakistan, seismicity is not limited to the Chaman or any other faults, but distributed across a belt hundreds of kilometers wide (Fig. 3.13). For example, earthquakes distributed in a broad zone in the Sulaiman Range show considerable thrusting in the region that is not on a plate boundary (e.g., Ambraseys and Bilham 2003) (Figs. 1.1, 1.2). The crustal earthquakes occur more frequently throughout northeastern Afghanistan. Beneath the Hindu Kush, the zone of seismicity dips northward while the zone of seismicity dips southward beneath the Pamir (Yeats, 2012). The north-

dipping seismicity zone represents the subduction of the Indian plate, and the south-dipping seismicity zone delineates the Eurasian plate subduction (Pegler and Das, 1998). Generally, the depth and magnitude of crustal earthquakes decrease from east to west or from northeast to southwest (Figs. 3.13, 3.14). Central and western parts, including the Helmand basin, stable blocks, and accreted terranes, are characterized by low seismic activity.

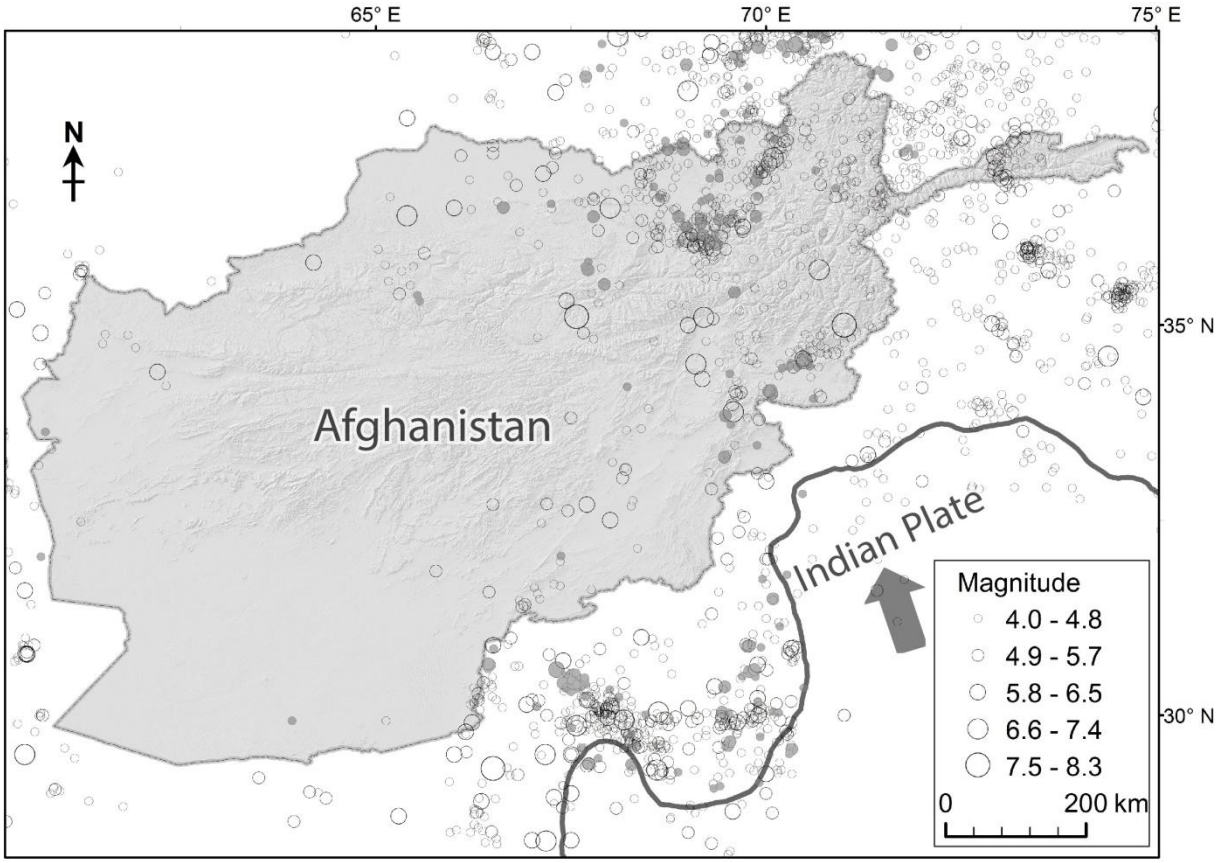

Figure 3.13: Seismicity map of Afghanistan. The map shows the location of crustal earthquakes (M ≥ 4.0). This map was constructed using earthquakes catalog prepared by Dewey (2006), which includes documented earthquakes before 1900, earthquakes with M ≥ 5.5 from 1900 to 1963, and events of M ≥ 4 since 1964. The gray filled circles are locations of instrumentally recorded earthquakes from 2005 to 2017 prepared by International Seismological Centre (ISC-EHB) (http://www.isc.ac.uk/iscgem/).

Many faults in Afghanistan are strike-slip faults and thought to be active, either from direct observation of surface rupture or from geologic expression and spatial association with earthquakes. The surface rupture of an individual historical or prehistorical earthquake is the most robust evidence that the fault is seismically active. Hence, active faults such as the

Chaman fault that have repeatedly ruptured in the recent past have the potential to generate large earthquakes in the future. Some crustal earthquakes had occurred on individual known faults (e.g., Quittmeyer and Jacob 1979; Yeats et al., 1979; Prevot et al. 1980; Shareq 1981) that produces surface ruptures. Several microearthquake surveys were conducted by Prevot et al. (1980) near Kabul but did not find any earthquake associated with the individual fault. The earthquakes were diffusely distributed throughout the area, where five significant faults (Chaman, Sarobi, Darvaz, Konar, and Paghman) are present (Fig. 3.15). The microearthquake studies support some lateral motion of these faults. Also, several microearthquake surveys were conducted on Pnjshir, Central Badakhshan, Alburz-Mormul, Andarab, Qarghanaw, Spin Ghar, Darafshan, and other faults, but no evidence has been given about epicenter location.

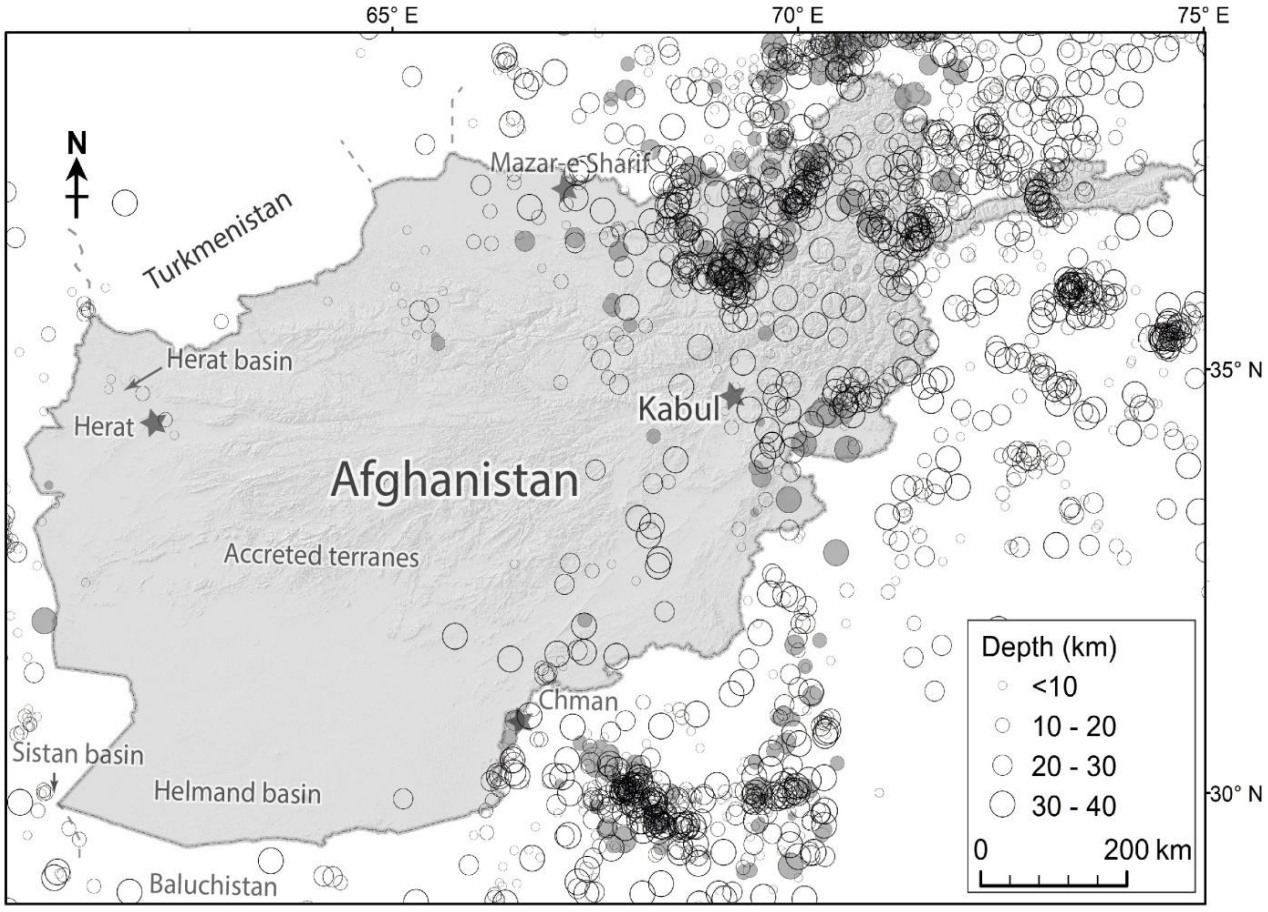

Figure 3.14: Map showing crustal seismicity of the country at depths less than 40 km.

3.3.2. Damaging historical earthquakes

Distribution of historical earthquakes provides useful information on where future earthquakes may occur. The significant historical earthquakes with magnitude 6 or higher are listed in Table 3.2. The historical record of earthquakes in eastern Afghanistan is sparser than in the western country, and the region near Kabul has a long history of damaging earthquakes (Figs. 3.15, 3.16).

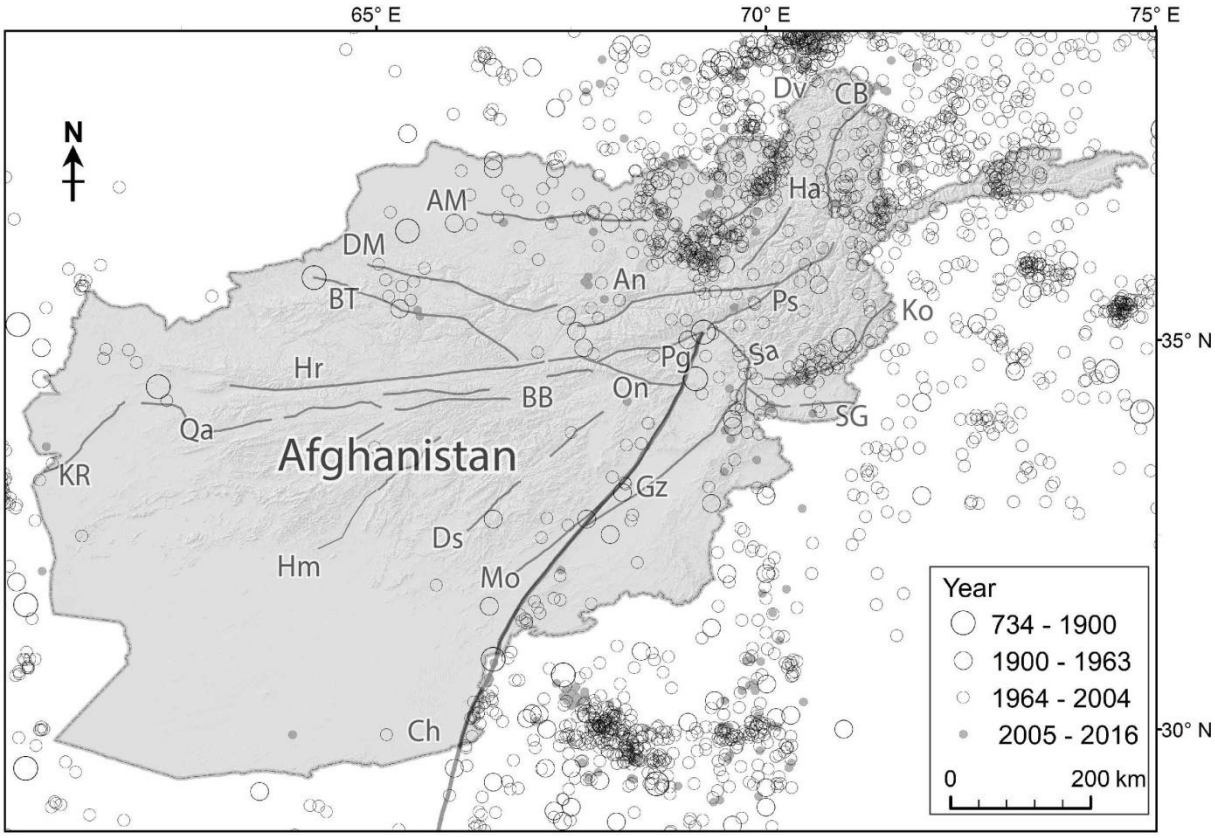

Figure 3.15: Map representing location of all crustal earthquakes occurring between 734 and 2016 with magnitudes between 4.0 and 8.3.

Northern Afghanistan platform has had moderately high levels of seismicity since 1900. The most significant earthquakes in the southwest of Mazar-e Sharif and Kabul occurred before the twentieth century (Fig. 3.15). Earthquakes activity near Herat basin, north of the Herat fault in the vicinity of Turkmenistan, might be related to a significant north-south seismic zone in eastern Iran (Figs. 1.1, 3.14). This represents the northward motion of interior Iran with respect to the Afghan Block (Ambraseys and Bilham, 2003a; Dewey, 2006).

The map reveals damaging earthquakes along the northern mountains of Band-e Turkistan, fronting the Turan depression (Figs. 2.1, 3.13). This suggests some convergence is occurring between the Eurasian plate and the Afghan block. Central Afghanistan appears to have relatively few earthquakes since 1964 (Fig. 3.15). Based on the earthquakes catalog, no recent event (M > 6) has occurred since the 9th century in western Afghanistan. From 734-1900, merely three earthquakes have been recorded in the Sistan basin southwestern Afghanistan. Recent earthquakes along the accreted terranes have occurred with decreasing frequency and magnitude toward the west. On the other hand, some intermediate-depth (40-70 km) earthquakes also occur in southernmost of Afghanistan, possibly as a result of the subduction of the Arabian plate.

Table 3.2: Damaging historical earthquakes of magnitude (M) 6.0 or higher in Afghanistan since 819. The data are compiled from Ambraseys and Bilham (2003), Dewey (2006), Boyd et al. (2007), ISC (2020) and USGS (2020).

Date	Lat (°)	Log (°)	M	Description
819	36.4	65.4	7.4	Balkh Province. Destroyed one-quarter of the Balkh city. Many houses destroyed and caused heavy casualties in Balkh, Faryab, Taliqan and Juzjan provinces.
1428	35.8	64.2	6.5	Taliqan, Takhar. Many people killed and destroyed majority of houses. Shocks continued 10 days.
7/6/1505	34.5	69.1	7.3	Kabul. Destroyed all houses in Paghman district, and ruined ramparts of fort and walls of gardens in Kabul. The earthquake killed ~80 people in Paghman and nearby villages. Vertical offset along the fault ~3. Many aftershocks lasted for 1 month.
1/15/1832	36.5	71	7.4	Badakhshan Province. Destroyed most of the villages in districts, killing thousands. In nearby towns about one-half of the people were killed. A large landslide occurred and dammed the Varduj River for 8 days. A series of aftershocks followed.
2/19/1842	35	71	7.5	Kunar Province. The Chaharbag and Tigri villages were ruined, and killed hundreds of people. At Jalalabad the Kabul gate collapsed, 2.4 km of parapets were damaged and breaches were made in the east face. In the Kunar valley landslides were triggered and two forts were completely destroyed.
10/18/1874	35.1	69.2	7	Kohestan, Afghanistan. The Kohestan, Golbahar and Japal-saraj regions were almost destroyed and had many casualties. Near JaBal-saraj city, the ground opened up possibly due to liquefaction.
7/7/1909	36.5	70.5	7.6	Badakhshan, Porvince. The earthquake caused few deaths and little damage for its magnitude. Maximum effects occurred along the Kunar valley. In Kabul several houses collapsed and ~10 were killed.
1/1/1911	36.5	66.5	6.8	Northern Afghanistan. At Feyzabad, Khanabad, Kalan, and Kabul many houses collapsed, killing 460 people. Effects of two earthquakes about 4 hours apart cannot be separated.
7/4/1911	36	70.5	7.4	Badakhshan Province
11/15/1921	36.204	70.676	7.6	Badakhshan Province
8/27/1931	29.503	67.176	7.2	Mach, in the vicinity of Kandahar. Damaged all buildings and killed only 120 people. Most to all of the houses collapsed in the towns between Mushkaf and Khari, Pakistan. West of these towns, rockfalls occurred and killed flocks of sheep and raised big dust of clouds.

5/30/1935	29.329	66.506	7.6	Quetta, Baluchistan. The Quetta city completely destroyed, and killed >35,000 people, only 15,000 in Quetta. The earthquake damaged rural housed in Kandahar as well. Movement on the Chaman fault resulted in an earthquake, which lasted for three minutes with continuous aftershocks.
6/30/1936	33.6	60	6	Bamrud, Iran. Close to the western border of Afghanistan
3/4/1949	36	70.5	7.4	Badakhshan Province
7/10/1949	39	70.5	7.5	Badakhshan Province
7/9/1950	36.7	70.5	7.5	Badakhshan Province
6/9/1951	36.3	71	7.5	Badakhshan Province
6/9/1956	35.111	67.576	7.5	Bamyan Province. About 70 people were killed and few small villages were destroyed. A big landslide dammed a river for four days, and caused a flood that swept away villages in the valley and drowned ~350 people. Many other landslides block also occurred.
9/16/1956	33.899	69.583	6.7	Zazi (Jaji), Paktia Province. In the epicenter area some houses collapsed and a few people were killed. Snow avalanches and landslides
3/14/1965	36.377	70.72	7.5	Badakhshan Province
6/24/1972	36.268	69.709	6.1	Takhar, Province. A few hundred houses collapsed and about 20 people were killed.
3/11/1975	30.2	66.3	6.8	Apparent co-seismic slip on the Chaman fault
2/4/1982	37.1	69	6.5	About 175 km north of Kabul. Approximately 450 people were killed and 7,000 got homeless
7/29/1985	36.163	70.9	7.4	Badakhshan, Province
2/4/1998	37.1	70.1	6	About 300 km north of Kabul. Approximately 4000 people were killed and 15,000 homeless. Aftershocks continued for the next seven days. Dozens of villages were destroyed. Nearly 15,000 houses were destroyed primarily due to the landslides. Approximately 818 people were injured and 6,725 livestock were killed.
5/30/1998	37.1	70.1	6.5	Takhar Province. This earthquake killed between 4,000-5,000 people. Nearly 7,000 families were affected and estimated 16,000 houses were destroyed or damaged. About 45,000 people became homeless, and several thousand animals were killed. Crops and infrastructure were destroyed.
3/5/2002	36.5	70.48	7.4	Hindu Kush an area 65 km south of Feyzabad, Afghanistan. Around 166 people killed, several injured. About 150 people were killed, and 400 houses damaged or destroyed by a landslide that dammed and flood Surkundara valley, Samangan Province. A 45 m wide fissure opened in Xikjian, China.
3/25/2002	36.1	69.1	6.1	Nahrin, Baghalan Province. At least 2,000 people were killed, several hundred injured and several thousand homeless in Baghlan Province. The earthquake caused enormous damage to infrastructure and water resources. More damage was brought to Nahrin city and several additional villages.
11/15/2015	36.44	70.72	7.5	Hindu Kush, Afghanistan. At least 399 people were killed in Afghanistan and Pakistan, and destroyed many infrastructures.
3/3/2020	36.50	70.48	7.4	Hindu Kush, Afghanistan. Damaged houses in northeastern Afghanistan. Large landslide in the Surkundara River valley killed at least 100 people, damaged over 3000 dwellings and dammed the rivers.

Most of the damaging earthquakes have magnitudes 5 or higher (Figs. 3.13, 3.16). Regions near the fault rupture and on loose soils may experience strong ground motion and the enormous damage like the Badakhshan earthquake in 1832 (Fig. 3.16). In general, seismicity is scattered throughout the east-northeastern seismic source zone, and some of the tectonic activity is due to the movements of these active faults. In 2015 an earthquake (Mw 7.5) occurred in the northeastern Afghanistan (Hindu Kush) with its epicenter approximately 82 km southeast of Fayzabad, Badakhshan (ISC, 2020). According to the Afghan government (ARG, 2015), the earthquake caused 115 causalities, 535 injuries and damage to ~7630

homes. The earthquake resulted due to reverse faulting at a depth of 212 km within the northeast-trending tabular zone beneath the Hindu Kush (Hayes et al., 2017). Another recent earthquake (Mw 7.4) occurred as the result of reverse faulting at intermediate depth in northeastern Afghanistan below the Hindu Kush (USGS, 2020) (Fig. 3.16). The largest of the intermediate-depth earthquakes in northeastern Afghanistan have magnitudes more than 7.0 (Table 3.1). Because of the shallower depth, they produce severe shaking than deep earthquakes of similar magnitude.

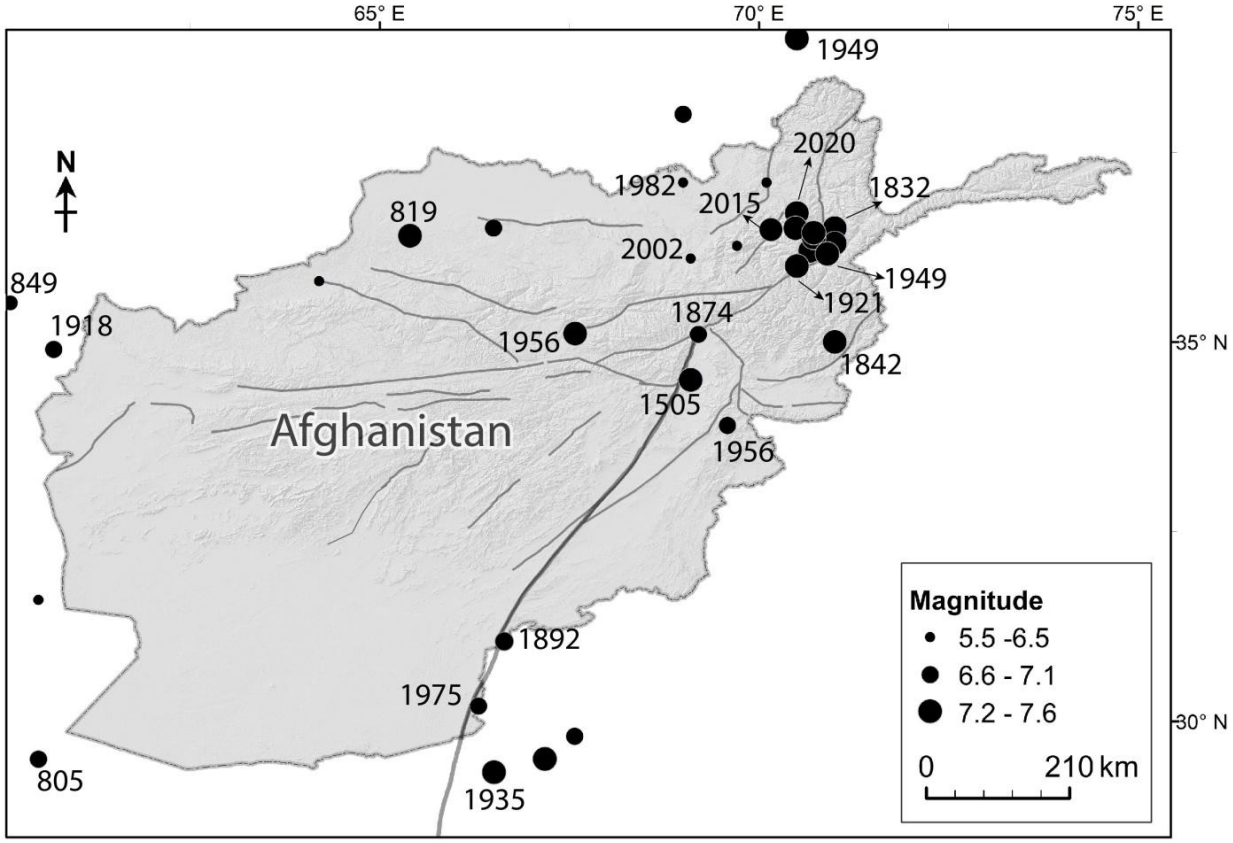

Figure 3.16: Damaging historical earthquakes of magnitude M ≥ 6.0. The map is constructed using earthquakes catalog prepared by Ambraseys and Bilham (2003), Dewey (2006), Boyd et al. (2007), ISC (2020) and USGS (2020).

The Chaman fault earthquake of 1505 took place along the northern end of the fault 3 km south of Kabul (Fig. 3.16). The earthquake produced approximately 60-km-long surface rupture with vertical offset as much as 3 m (Quittmeyer and Jacob, 1979). The earthquake destroyed all houses in Paghman district and killed about 80 people in Paghaman and many more in nearby villages. A landslide occurred in the valley just north of Paghman (Fig. 3.5b).

3.4. Seismic source zones

For contributing to the hazard assessment of Afghanistan, I classified four seismic source zones based on available geologic, active tectonics, and seismicity data (Fig. 3.17). The delineated four seismic source zones are; 1) east-northeastern Afghanistan, 2) Afghanistan-North Pamir, 3) Northern Afghanistan platform, and 4) middle and south-western Afghanistan.

The east-northeastern seismic source zone is the most seismically active region. The zone generates more crustal earthquakes than the rest of the country. This region is cut by major left-lateral strike-slip faults that are approximately parallel to the plate boundary (Figs. 1.1, 3.2). In this zone, large active or potentially active faults are located; the Chaman, Paghman, Panjshir, Central Badakhshan, Konar, Sarobi, and Spin Ghar faults (Fig. 3.17). The Chaman fault produced five historical surface ruptures. Large and destructive earthquakes occurred in the Kabul region in 1505, in the Chaman area in 1892 and Baluchistan in 1935 (Mw 7.7) (Quittmeyer and Jacob 1979; Yeats et al. 1979) (Fig. 3.16). Each earthquake produced several-kilometers-long surface rupture with a few centimeters to several meters of left-lateral and vertical offset. The slip rate of the Chaman fault is between 8-35 mm/yr (Furuya and Satyabala, 2008; Lawrence et al., 1992; Mohadjer et al., 2010; Ul-Hadi et al., 2013). Almost half of the earthquakes recorded in this seismic source zone occurred beneath the northeastern half of the Hindu Kush. Roecker et al. (1980) recorded microearthquakes along the Kabul block that show a high level of seismicity over a broad deformation area. Even though most earthquakes are diffusely distributed in the region, the seismicity along the Chaman and Sarobi faults are apparent. An array of portable seismographs recorded microearthquakes aligned or clustered on the Sarobi and Konar faults (Prevot et al., 1980; Quittmeyer and Jacob, 1979). In general, seismicity is scattered throughout the east-northeastern seismic source zone, and some of the tectonic activity is due to the movements of these active faults.

The Afghanistan-North Pamir seismic zone is seismically less active than east-northeastern Afghanistan, but more active than the Northern Afghanistan platform. In this zone, the Darvaz fault has clear evidence for recent slip (e.g., Boyd et al., 2007; Mohadjer et al., 2016; Trifonov, 1978; Wheeler et al., 2005). The Andarab fault is the second-longest fault in the Afghanistan-North Pamir seismic zone. Wellman (1966) examined aerial photographs and identified two sites with evidence of right-lateral displacement along the fault. Treloar and Izatt (1993) noted that minor extrusion might have occurred on the Andarab fault within the Tajik platform due to the Indian plate collision with the Afghan block. In 1956, a massive and destructive earthquake (Mw 7.4) occurred northeast of Bamyan (35.55°N and 67.81°E) between the Andarab and Herat faults (Fig. 3.16). The earthquake created a 50-100 km long surface rupture with 1-2 m slip (Ambraseys and Bilham, 2014). However, there is no mapped fault between Andarab and Herat faults on which this earthquake could have occurred. Both the surface ruptures and geomorphic evidence show that the Andarab fault is tectonically active, like the Darvaz fault.

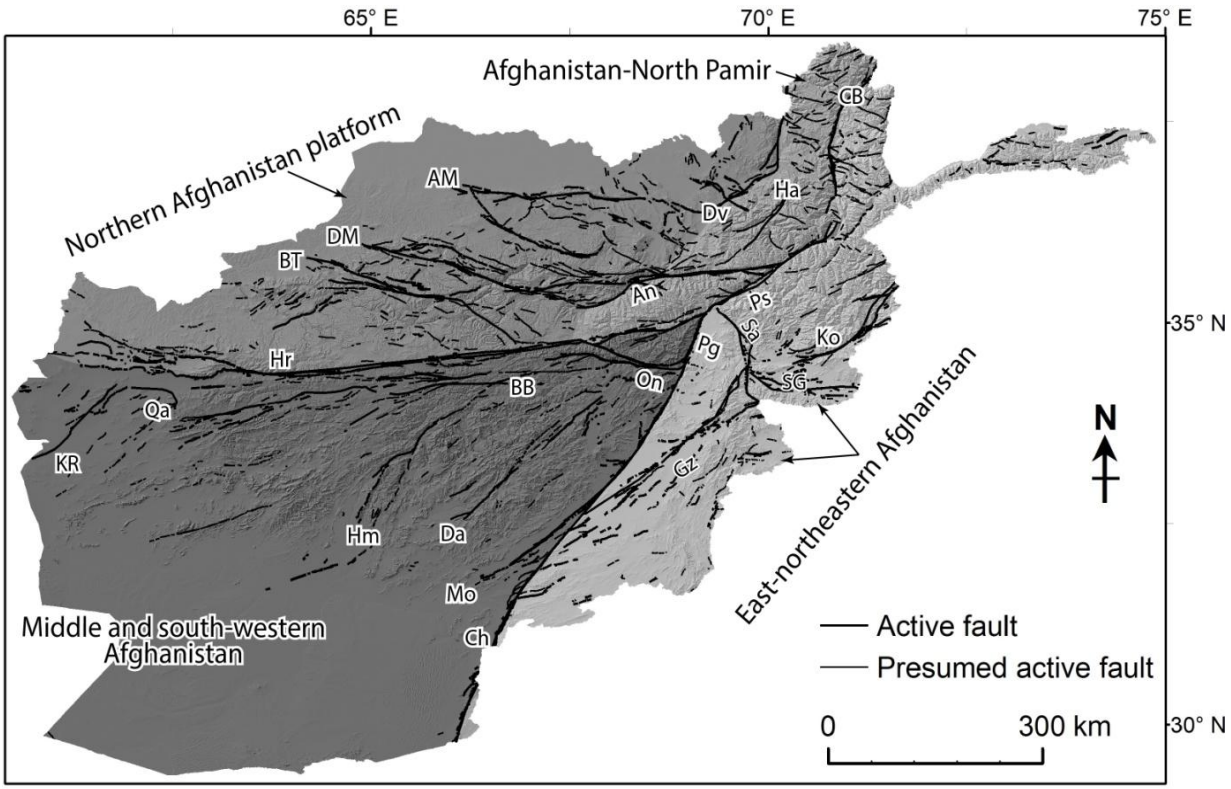

Figure 3.17: Seismic source zones of Afghanistan; 1) East-northeastern Afghanistan, 2) Afghanistan-North Pamir, 3) Northern Afghanistan Platform, and 4) Midlle and south-western Afghanistan.

In the Northern Afghanistan platform seismic source zone, the Alburz Marmul, Dosi Mirza-Valang, and Band-e Turkestan faults are located. Shareq (1981, 1993) suggested that the Alburz Marmul fault is active according to microearthquake studies and earthquake concentrations. Earthquakes are generally associated with the Alburz Marmul fault (Wheeler et al., 2005). This zone has high levels of seismicity next to the Afghanistan-North Pamir seismic source zone within the Eurasian plate. On the east side of the zone, a belt of shallow earthquakes delineates the active northwesterly directed thrust, which carries the northwestern Pamir over the marginal depression (Abers et al., 1988; Brookfield and Hashmat, 2001).

The middle and southwestern Afghanistan seismic zone extends from south of the Herat fault and west of the Chaman fault to the border region with Iran. The seismic zone is sliced by steeply dipping faults trending from southwest to east and northeast. Among the eight known faults (Fig. 3.17), the Herat fault is seismically most active. A damaging earthquake (Mw 7.0) in AD 849 was reported near the western section of the fault close to Herat province (Fig. 3.16). Another event occurred in 1874 north of the capital Kabul near or on the eastern extension of the fault (Quittmeyer and Jacob, 1979). In both historical and recent times, no earthquake has been recorded for most of the fault length. Ambraseys and Bilham (2003) suggested that the slip on the fault would be insignificant in accommodating the north-south convergence. Wellman (1966) classified the fault as being active citing evidence of right-lateral offset of two stream channels >10,000 years old, at two sites approximately 200 km east and 500 km west of Kabul. Also in this zone, the Darafshan fault has evidence for microearthquakes in a stable part of the country. The Makur, Helmand, Onay, Band-e Bayan, Qarghanaw, and Kaj Rod faults are also in this zone, but no evidence is given yet to confirm their seismic potentials.

Chapter 4

Late Pleistocene slip rate of the Chaman fault based on ^{10}Be exposure dating of offset geomorphic surfaces near Kabul, Afghanistan

4.1. Study area

4.1.1. Geomorphic analysis

The active Chaman fault was mapped by visual image analysis with the help of previous literatures. For mapping of the fault, high resolution 3D CORONA and ALOS PRISM images were used (Fig. 4.1). Stereographic pairs of ~1:125,000 scale CORONA images for the whole length of the Chaman fault in Afghanistan and Pakistan were interpreted (Figs. 4.1a). The images represent depth perception and allow an intensive landscape assessment to be made in the area. Moreover, for a small area digitalization of local information and offset measurements were not realized. Thus, by using of ALOS PRISM along with the CORONA satellite images, a more detailed mapping of the Chaman fault is attempted (Fig. 4.1b).

The Chaman fault extends from the Makran Range, northeastward across Baluchistan and to Afghanistan (Fig. 1.1). The fault runs just to the west of Kabul City to the Herat right-lateral strike-slip fault. It is ~650 km long in Afghanistan and terminates near the northern margin of the Kabul block (Fig. 1.2). The fault trace ranges from linear zones less than 1 km wide to zones of several fault strands (Ruleman et al., 2007). In Kandahar and Zabul provinces, east-dipping active thrust faults on the western side of the main fault were mapped, which are more than 20 km long and 10 km wide from the main fault trace. These second-order thrust faults were formed as a result of transpression on the left-lateral motion on the main fault. Some of these thrust faults (Fig. 3.4a).

The Chaman fault typically offsets Pleistocene and Holocene deposits and landforms and is generally marked by continuous fault scarps (Fig. 2.3). These old and young alluvial and fluvial terraces and landforms are differentiated by levels of dissection and surface morphology. The old and young surfaces contain geomorphic evidence for the fault activity for an extended past. The deposits from old alluvial fans have been offset considerable distances from their original sources particularly along the main left-lateral Chaman fault. Younger landforms and stream channels are commonly displaced for short distance. This is a clear evidence of repeated seismic activity of the fault during the Quaternary.

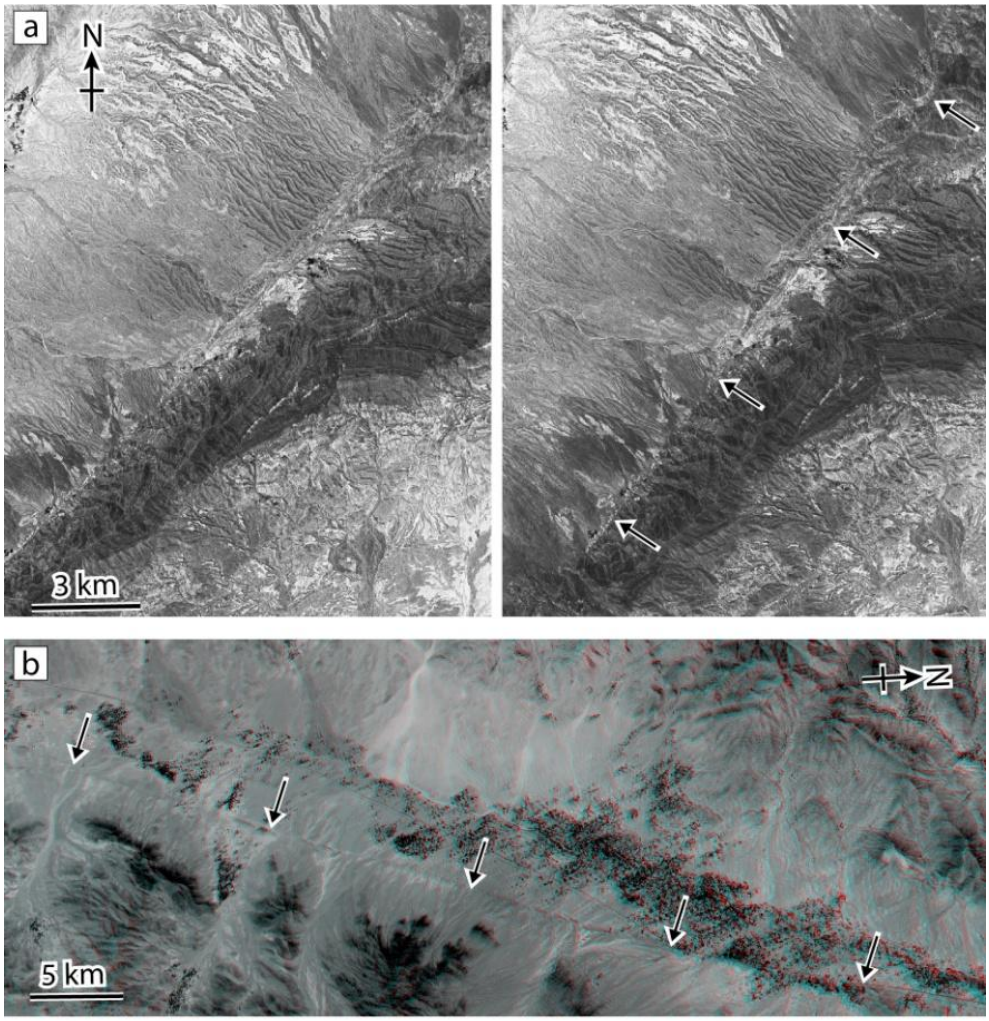

Figure 4.1: Stereo photos showing distribution of the Chaman active fault traces in Afghanistan. a) The top two images are the examples of stereo-paired CORONA satellite images from central section of the fault (Zabul province). b) Anaglyph georeferenced ALOS PRISM satellite image from northern section of the Chaman fault (Wardak province). Arrows denote active fault trace.

Along the fault, tectonic geomorphic features such as offset and beheaded stream channels, offset alluvial fans, shutter ridges, bulges and grabens, fault scarps, and tilted surfaces are commonly observed. The geomorphic expression of the Chaman fault system varies along the whole fault trace. To better differentiate different styles of Quaternary deformations, the Chaman fault system can be divided into four subsidiary fault segments, each with different characteristics and a different degree of earthquake hazard: (1) Chaman fault, (2) Mokur fault, (3) Gardez fault and (4) Paghman fault (e.g., Ruleman et al., 2007) (Fig. 1.1, 3.2). The Gardez and Mokur are northeast-trending left-lateral splay faults, which have linear fault scarps on alluvium, and cut most geologic deposits and bedrock.

Three large and destructive earthquakes recorded on the fault trace (Figs. 1.2, 3.16). An earthquake (M 7.3) took place along the northern end of the fault about 3 km south of the Kabul City on July 5, 1505 (Quittmeyer and Jacob, 1979). An earthquake (M 7.0) on 20 December, 1892, struck the town of Chaman, which formed 60 km surface rupture, and created 60-75 cm left-lateral slip and dropped the west side of the fault down 20-30 cm (Quittmeyer and Jacob, 1979; Wheeler et al., 2005). A third surface rupture was in 1935, 31 May in Baluchistan. The Mw 7.7 Baluchistan earthquake along the Chaman fault system killed to 35,000 people (Ambraseys and Bilham, 2003b) (Fig. 1.2). A forth earthquake with Mw 6.4 occurred in 1978 in the same area as the 1892 earthquake. The earthquake produced about 4 cm left-lateral offset, 5- km-long ground cracking, and dropped the east side of the fault (Yeats et al., 1979) (Fig. 3.16). The last May 13, 2016 earthquake (M 5.5) occurred along the Chaman fault in Qila Abdullah (ISC, 2020; Funning and Garcia 2019) (Fig. 1.2).

4.1.2. Site description

The Sayed Abad valley is a tectonically active region on the western margin of the Kabul block (Fig. 1.2). The Sayed Abad valley is an asymmetrical alluvial basin fed by a moderate to highly-incised and discontinues ephemeral streams network. The basin is approximately 65 km long and as wide as ~8 km. The area includes the watershed boundary of subbasins, which are separated by prominent bedrock outcrops (Fig. 4.2a, white dashed

lines). The central plain of the valley is a depositional center for local deposits derived from the surrounding mountains and surficial sediments. The valley is flat in the center and gently slopes up to the adjacent mountains to form piedmonts. Physical weathering has produced breaks in slope at the edges of the subbasins, and caused rugged terrain.

The topography of the area is strongly influenced by regional and local tectonic activity and fluvial processes. The Sayed Abad valley is formed between Hindu Kush Mountain Ranges (Gorbat, Khwaja Ibrahim, Badam) to the west and the Suleiman Mountain Ranges (Khwaja Ghramban, Abdara, and Syah Topa) to the east (Figs. 1.1, 4.2a). The highest ranges of the mountains reach 3,100 m in elevation (Fig. 4.3). Several ephemeral and perennial streams flow from the surrounding mountains and have dissected the valley-filled sediments extensively. Active streams are generally narrow and shallow, rarely exceeding 50 m in width and 10 m in depth. Major streams have incised alluvial fans and isolated the fan surfaces from active stream erosion and deposition. Shneez River is a north-flowing tributary of Chak River and originates in some of the higher peaks of the west mountain massif (Fig. 4.2a).

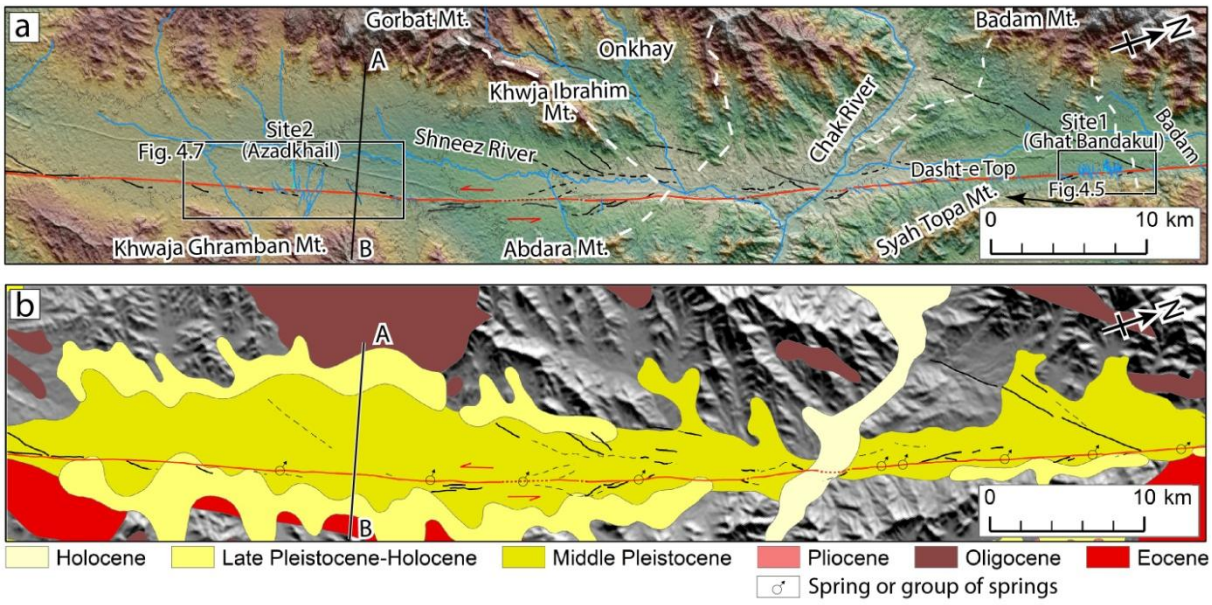

Figure 4.2: Topography and geology of the study area. a) Location and topography of the Sayed Abad valley on the western margin of the Kabul block. The red arrow indicates the left-lateral motion on the Chaman fault. The black line A-B is the transect line shown in Figure 4.3. b) The contact between

alluvium and colluviums (Late Pleistocene-Holocene) filled the valley, and the outcrops of the mountains are Eocene ultramafic intrusions. The Quaternary geologic map modified from Doebrich et al. (2006).

In this area, the Chaman fault has continuous fault scarps in piedmont alluvium at the bottom of the mountains (Fig. 4.2a, 4.4a). The Sayed Abad valley is composed of Tertiary and Quaternary deposits, and the surrounding uplifted ranges are composed of crystalline and sedimentary rocks (e.g., Doebrich et al., 2006) (Fig. 4.2b). The Quaternary valley deposits can be divided into young and old deposits. The underlying sediments are much thicker in the central valley. Based on the geologic map (Doebrich et al., 2006), middle Pleistocene strata are in the center of the valley, grading Middle Pleistocene conglomerates and sandstones and late Pleistocene-Holocene shingly and detrital sediments, gravel, sand, and clay toward the bedrock outcrops. The contact between alluvium and colluviums filled the valley, and the mountains (e.g., Khwaja Ghramban, Abdara) are composed of Eocene ultramafic intrusions (Figs, 4.2b, 4.3). The Gorbat Mountains are primarily composed of Oligocene granodiorite.

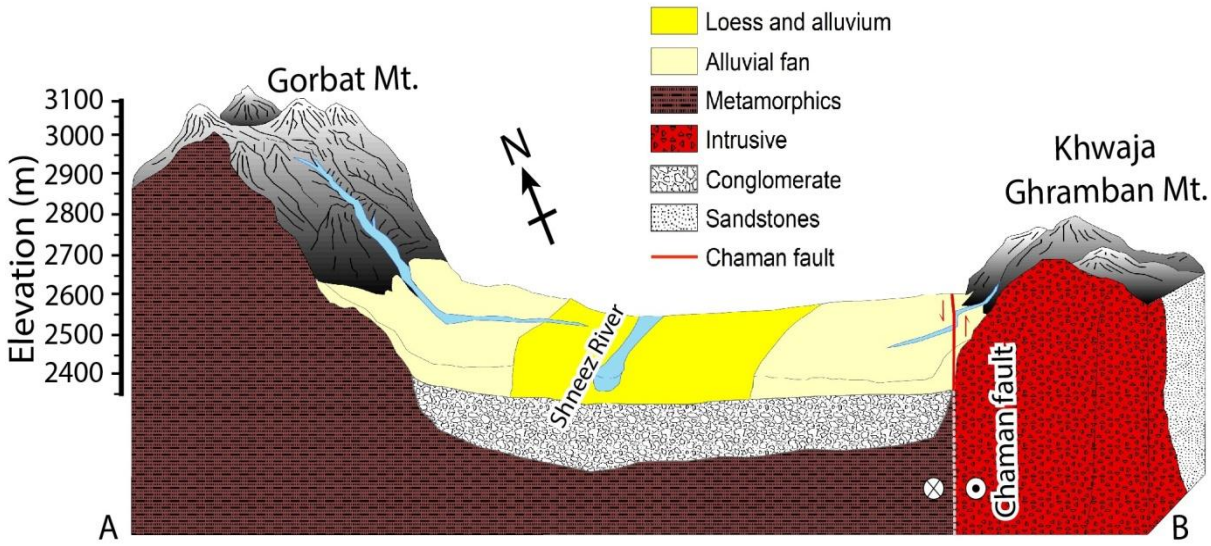

Figure 4.3: Planar view of the Sayed Abad valley. The highest ranges of the mountains reach 3,100 m in elevation.

The fault beheads a series of alluvial fans along the western margin of the mountains. I concentrated my effort on two sites where abandoned alluvial fans are offset left-laterally by

the Chaman fault (Fig. 4.2a). The two sites are located within the easternmost of the Sayed Abad valley near the villages of Dawlatabad (Badam) and Azadkhail, respectively. On each site, faulted alluvial surfaces have been mapped using ALOS PRISM satellite images (Fig. 4.1b). This portion of the fault is characterized by numerous left-lateral steam offsets ranging from tens to hundreds of meters.

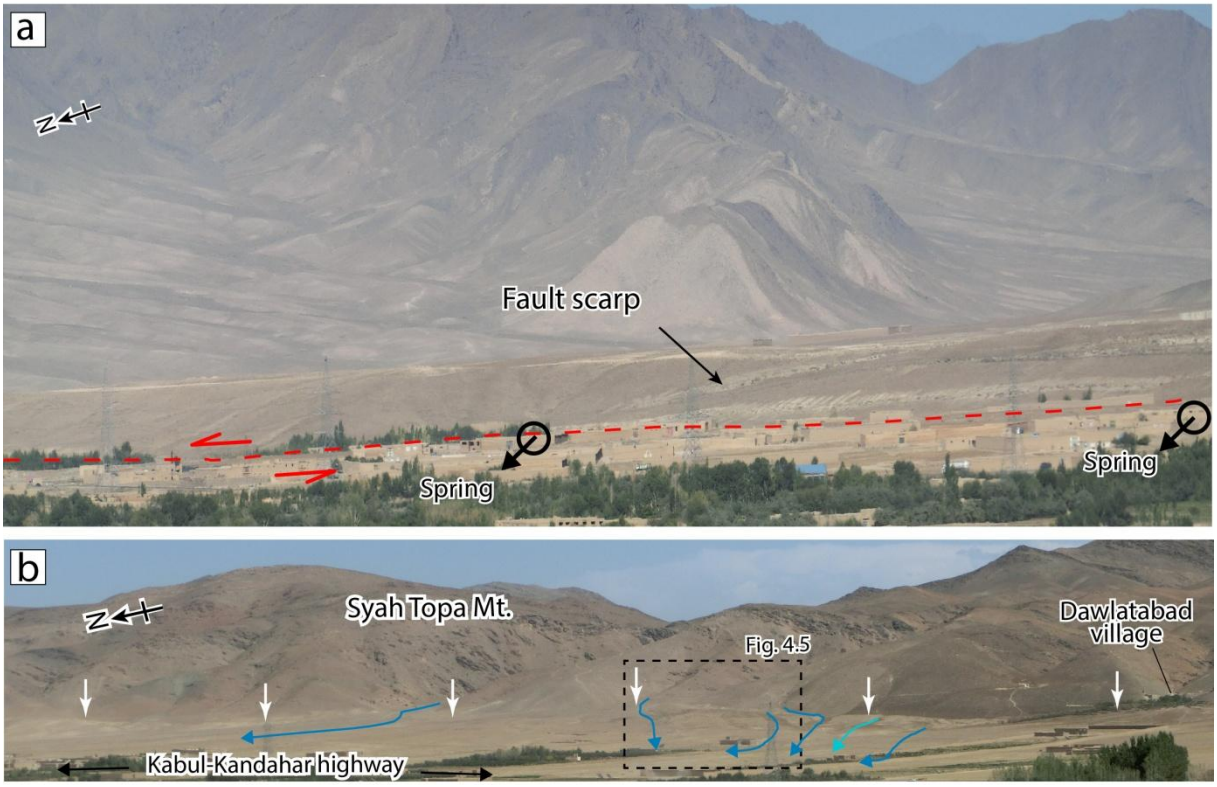

Figure 4.4: Field photos of the Chaman fault at the Sayed Abad valley. a) West-facing fault scarp. b) Field photograph from the top of the hill (34°13'2.00"N, 68°47'56.29"E) looking east toward the Chaman fault and Syah Topa Mountain. The fault follows the base of the range front and white arrows point to the fault trace.

4.1.2.1. Site-1 (Ghat Bandakul alluvial fan)

This area is located near the village of Dawlatabad or Habib China (spring) (34° 12′ 57″ N, 68° 49′ 48″ E at 2300 m asl) at Narkh district, Wardak Province. The site is located approximately 50 km southwest of Kabul City. The Ghat Bandakul fan overlies the rocks of the Syah Topa Mountains to the east and terminates to the west near the Kabul-Kandahar highway (Fig. 4.4b). The fan slopes 3-5° westward for ~1 km from the mountain front. To the

northeast, the fan has an erosional contact with the young alluvial fan. Five sets of well-defined alluvial terraces were formed since the abandonment and breaching of the deposition (Fig. 4.5). The younger set of terraces exists on both sides of the fault trace. Younger terrace (T5) surface is more uniform, unconsolidated, and undeformed that has little stream incision. In comparison, the older surfaces are dissected by networks of incised streams. The older fan (T1- T3) is marked by soil development and lithification lack of sediment piles (T4) present north of the fan (Figs. 4.5, 4.6a). The intermediate age fans (T4) are more extensively developed, well preserved, and not deformed.

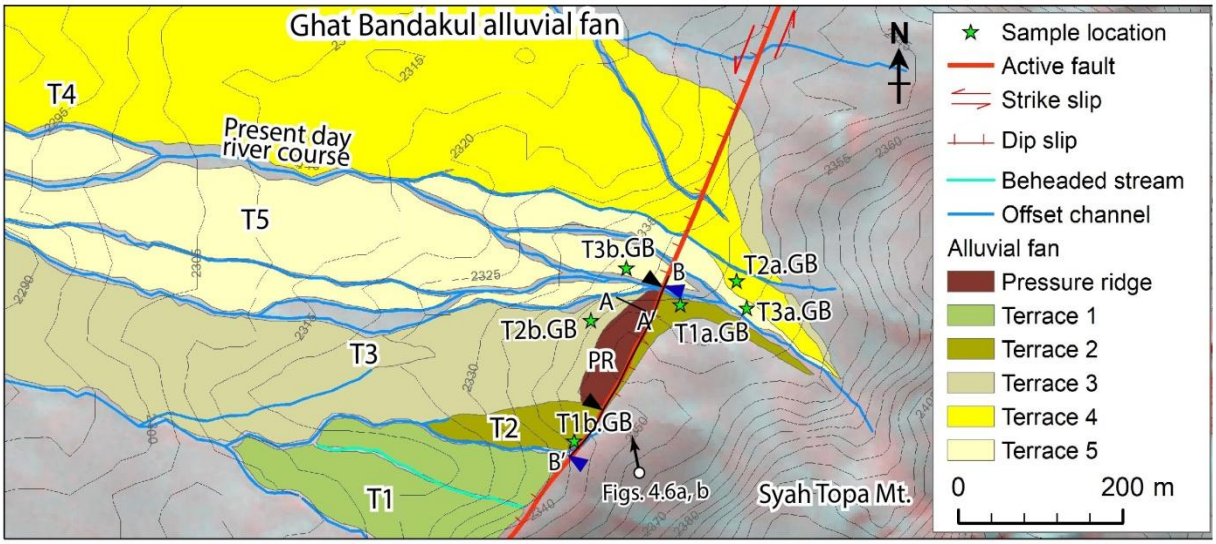

Figure 4.5: Ghat Bandakul alluvial fan surfaces showing apparent left-lateral offsets of two channels. Analysis of satellite images and fieldwork indicate that middle terrace and older terrace is left-laterally offset along the fault 165 m and 235 m, respectively (black and dark-blue triangles). The black lines AA′ and BB′ are the profile lines shown in Figs. 4.10a and 4.10b.

The displaced alluvial fan made a small valley that stands 0.5 – 1.8 m above the T2, making only east-facing fault scarp in the study area (Fig. 4.6a). However, in general, along the Dasht-e Top (Sayed Abad district) and Narkh district, the displaced alluvial fans generally make the west-facing fault scarp (Fig. 4.2a). In this area, more than ten springs were observed along the fault trace. Along with the offset fan, the fault scarp stands high up to 0.5 – 2.1 m above the T3 surface (Figs. 4.6a, 4.10a). The scarp is well preserved where the fault offsets alluvial fans. The alluvial surfaces vary in the ratio of fine sediments and stony pavement. The

fan surface is characterized by shallow (~1 m deep) stream channels that are partially filled by clay, sandstone and granitic clasts originating from Syah Topa bedrock. The desert pavement develops weakly to moderately (Fig. 4.6b). The surface sediments sourced from Ghat Bandakul granitic bedrock. Thus the deposits of displaced fans are rich in quartz. In the fan surfaces (T1-T5), carbonate coatings on cobbles and boulders increase toward Syah Topa Mountain. Most of the fan surfaces are active, and the youngest surface in the north represents little incision by the active channels.

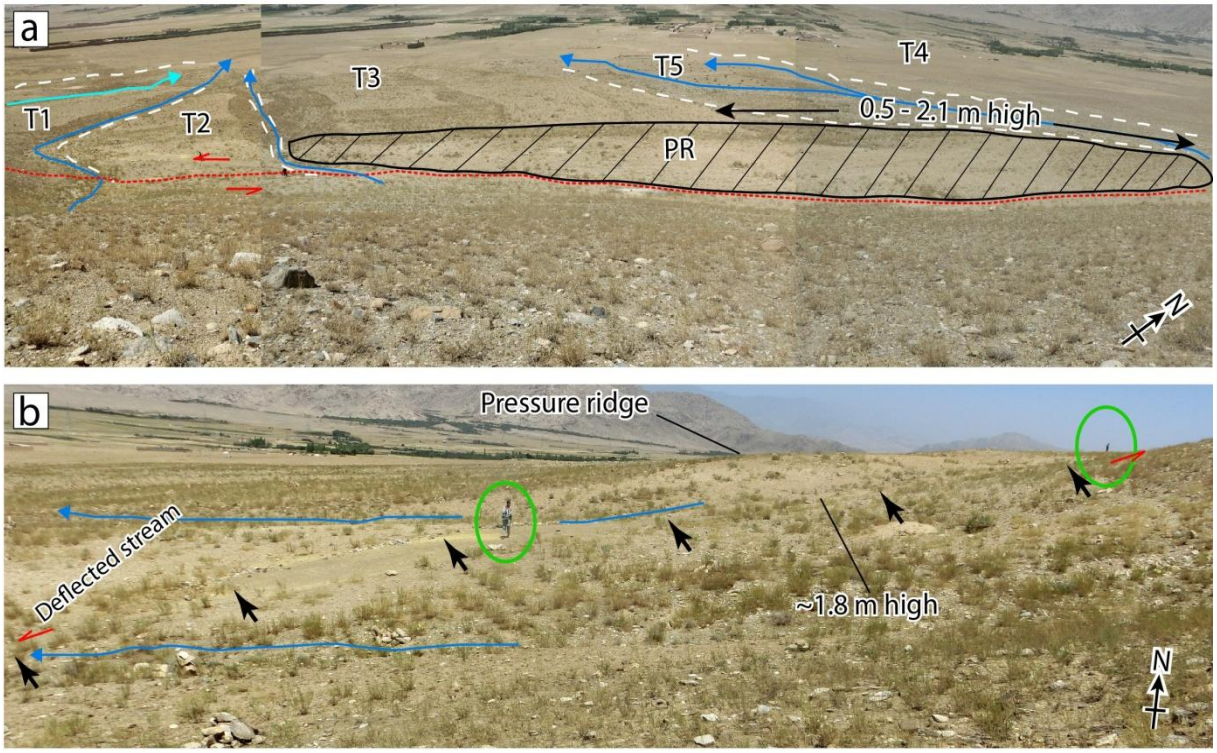

Figure 4.6: View of the Ghat Bandakul alluvial fan offset by the Chaman fault. a) Photo of the terraces displaced left-laterally by the fault. The fault has formed a west-facing ~2 m high scarp. The ephemeral streams are flowing from east to west. The red line shows fault trace, blue lines show offset stream channels and cyan color shows beheaded steam. T and PR stand for terrace and pressure ridge, respectively. b) Looking toward north, fault trace shown by black arrows. The two people stood on displaced alluvial fans showing the piercing point.

4.1.2.2. Site-2 (Azadkhail alluvial fan)

The Azadkhail fan is among the oldest preserved alluvial fans offset by the Chaman fault along the Sayed Abad valley (Fig. 4.2). The fault trace is well characterized by the fault-parallel bulge and depression (Fig. 4.7a). Toward the south and north, the central part of the fan merges with another displaced alluvial fan of approximately the same age. There are visible cuts throughout the distal part of alluvial fans deposited in the Azadkhail area (Fig. 4.7b). The fan slopes ~5° westward for approximately 4 km from the foot of the hill to the center of the valley (Fig. 4.3). At the western side of the alluvial fan, steps in the fault trace to the west produced pull-apart basin filled by recent sediments that appear in white color on the CORONA image (Fig. 4.7a). On the fan surface, broader and deeper ephemeral stream channels are preserved (Figs. 4.2a, 4.10c).

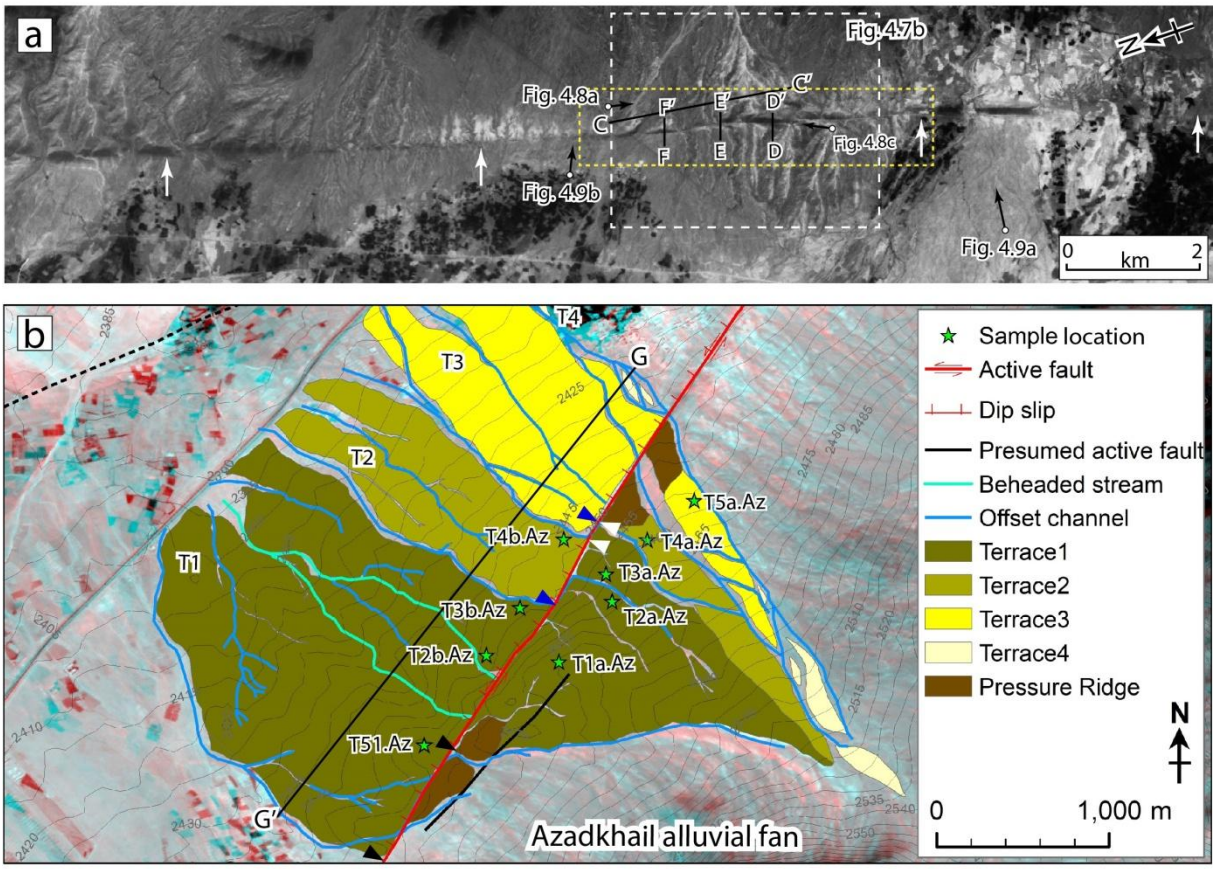

Figure 4.7: Location and geomorphic map of the Azadkhail alluvial fan. a) Corona satellite imagery of the study area showing left-laterally offset channels as they cross the Chaman fault. The black bullet-tailed arrows with figure number show capture location and look direction of the field photographs.

Yellow rectangle shows location of Figure 4.11. Black lines CC′ - FF′ are the profile lines in Figure 4.10c-4.10f. b) Alluvial fan surfaces (T1 – T4) placed over the ALOS Prism anaglyph image with the locations of dated samples. The fan is dissected by stream channels and clearly shows left-lateral offset along the Chaman fault during different geologic time scales. The white, black and dark-blue triangles are piercing points for 130 m, 500 m and 800 m offset, respectively.

The Azadkhail alluvial fan is divided into four distinct terrace surfaces (T1-T4) (Figs. 4.7b, 4.8a). The T1 terrace is topographically higher than T2, and T2 is higher than the rest of the alluvial fan (Figs. 4.8a, 4.10c). The risers between T1 and T2, T2 and T3, and T3 surfaces preserve left lateral displacement along the fault (Fig. 4.7b). The northernmost surface (T4) is the least preserved patch of the fan. The active riverbed has entrenched the younger fans (T3 and T4). Downstream from the Chaman fault trace, the lower surfaces stand ~1.5 m above the active stream beds, which are differentiated by a very light surface color and shallow incision. The alluvial fans are typically composed of granitic clasts originated from Cenozoic bedrock drained by the ephemeral Azadkhail River (Fig. 4.3). The younger deposits are reworked boulders, gravels, sands, and clay (Fig. 4.8b). Non-cohesive to granular deposits are observed on the T3 and T4 surface to a depth of ~1-2 m showing unlithified succession and devoid of any soil development. Also, the younger surfaces suffer little erosion, as suggested by the heavy desert varnish coating on the top of the exposed boulders (Fig. 4.8b, c). The T3 is consolidated and compacted but not well lithified. The oldest deposits (T1 and T2) show a very well-lithified succession and contain very few types of gravel and pebbles. Moreover, the oldest fan has relatively good lithification and deep erosion, and in highly leached areas, the soils are more cohesive. The boulder and cobbles are less developed near the ground suggesting wind deflation in the study area (Fig. 4.8b).

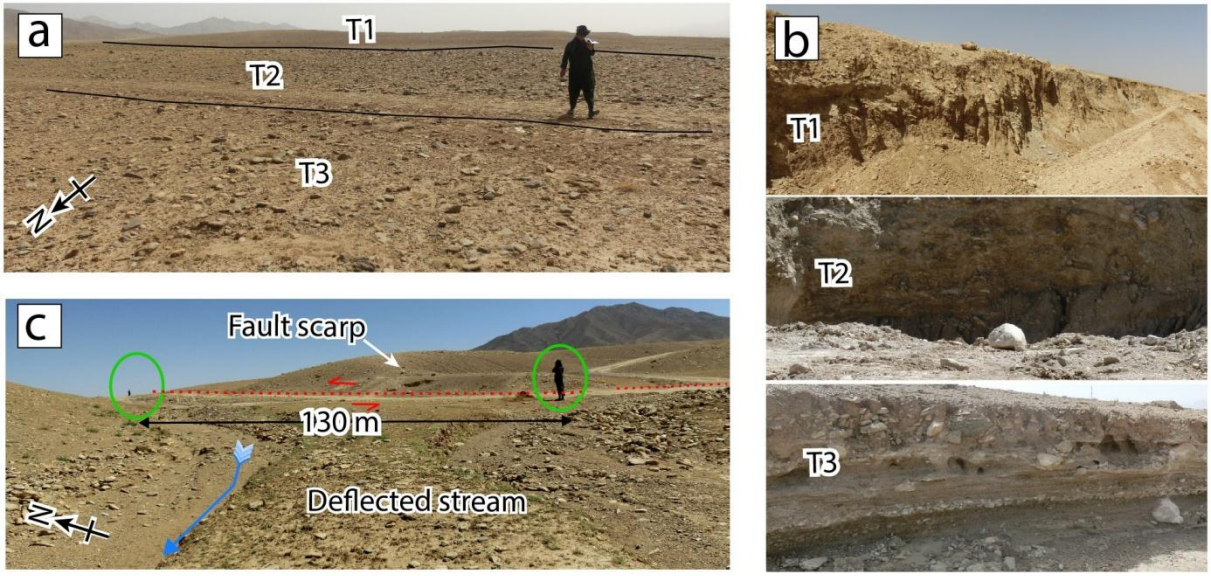

Figure 4.8: Field photos of the Azadkhail alluvial fan. See Figure 4.7a for location. a) View of the T1-T3 surfaces and typically the most considerable elevation difference between younger and older terraces. Older terrace occurred high on the fan ranging measurably by tens of meters (Fig. 4.10c). b) A close-up view of vertical sections of T1, T2 and T3 surfaces exposed in stream channels. c) The two persons stood between the most recently offset stream channels.

Along the fault trace, a clear fault scarp is preserved across this fan (Fig. 4.7a). The fault has formed a west-facing scarp ~2–25 m high (Figs. 4.9, 4.10d - 4.10f). The fault scarps are also cut by stream channels and eroded. The very high scarp in the study area could be due to several earthquakes, as the scarp is high on the older terrace and lower on the younger terrace (Figs. 4.8c, 4.10f). To observe vertical fault offset, topographic profiles were made in the field using a Laser Rangefinder and based on 1-arcsecond Advanced Spaceborne Thermal Emission and Reflection Radiometer (ASTER) digital elevation model (DEM) across the fault trace (Fig. 4.10). Fault movement made pressure and shutter ridges (Figs. 4.7b, 4.9a, 4.10f). There are many mounds lined along a straight line northeast-southwest marking a west-facing fault scarp (Fig. 4.9b). Toward the north, many springs occurred along the Chaman fault, possibly due to vertical enhancement of groundwater flow (Fig. 4.2b). The fault movement also caused a linear valley in alluvial fans, where the older alluvial fan is displaced and bends to the north (Fig. 4.7a). This created a sharp diversion in the stream channels flowing from east to west.

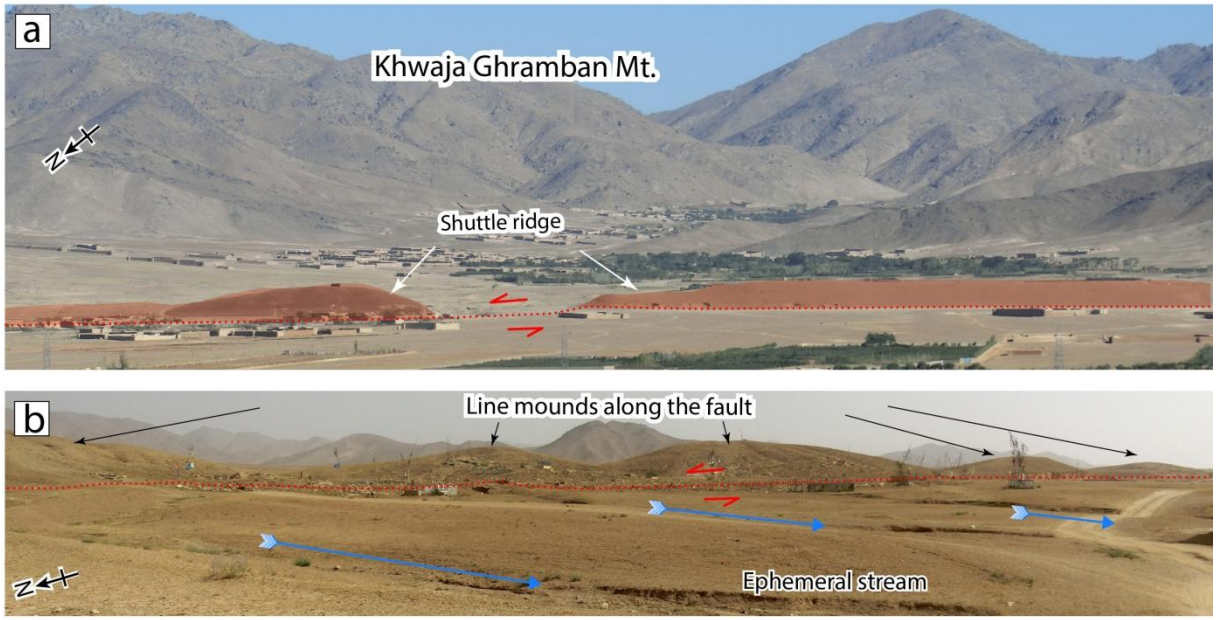

Figure 4.9: Field photographs looking across the Chaman fault at the Azadkhail area. See Figure 4.7a for location. a) Two shuttle ridges south of the displaced Azadkhail alluvial fan. b) Mounds lined-up along eastern side of the Chaman fault.

4.2. Offset measurements

Displacement along the fault in the study area was measured based on geomorphic observation in the field as well as using CORONA and ALOS 3D anaglyph images. Offset of alluvial fans by the Chaman fault is determined by measuring the distance between the northeastern most of each fan and piercing points (black and dark-blue triangles in Fig. 4.5). Most of the northeastern point of each fan was the closest to the active stream at the time of deposition.

Site-1: Within the Ghat Bandakul alluvial fan, incised and abandoned fan surfaces have been offset left-laterally by the Chaman fault from the catchment outlets that fed them (Figs. 4.4b, 4.5). A small pressure ridge forms at the precise location of the northeastern margin of the middle terrace on the western side of the fault (Figs. 4.6a, 4.10b). The fan also shows apparent left-lateral offsets of two channels and a beheaded stream (Fig. 4.4b, 4.5). The fault cuts across the T3 and T2 surfaces. It is estimated the amount of offset of T3 at 165 ± 15

m and that of T2 at 235 ± 24 m (Figs. 4.6b). On the northernmost fan, some younger displacements for less than 20 m were observed.

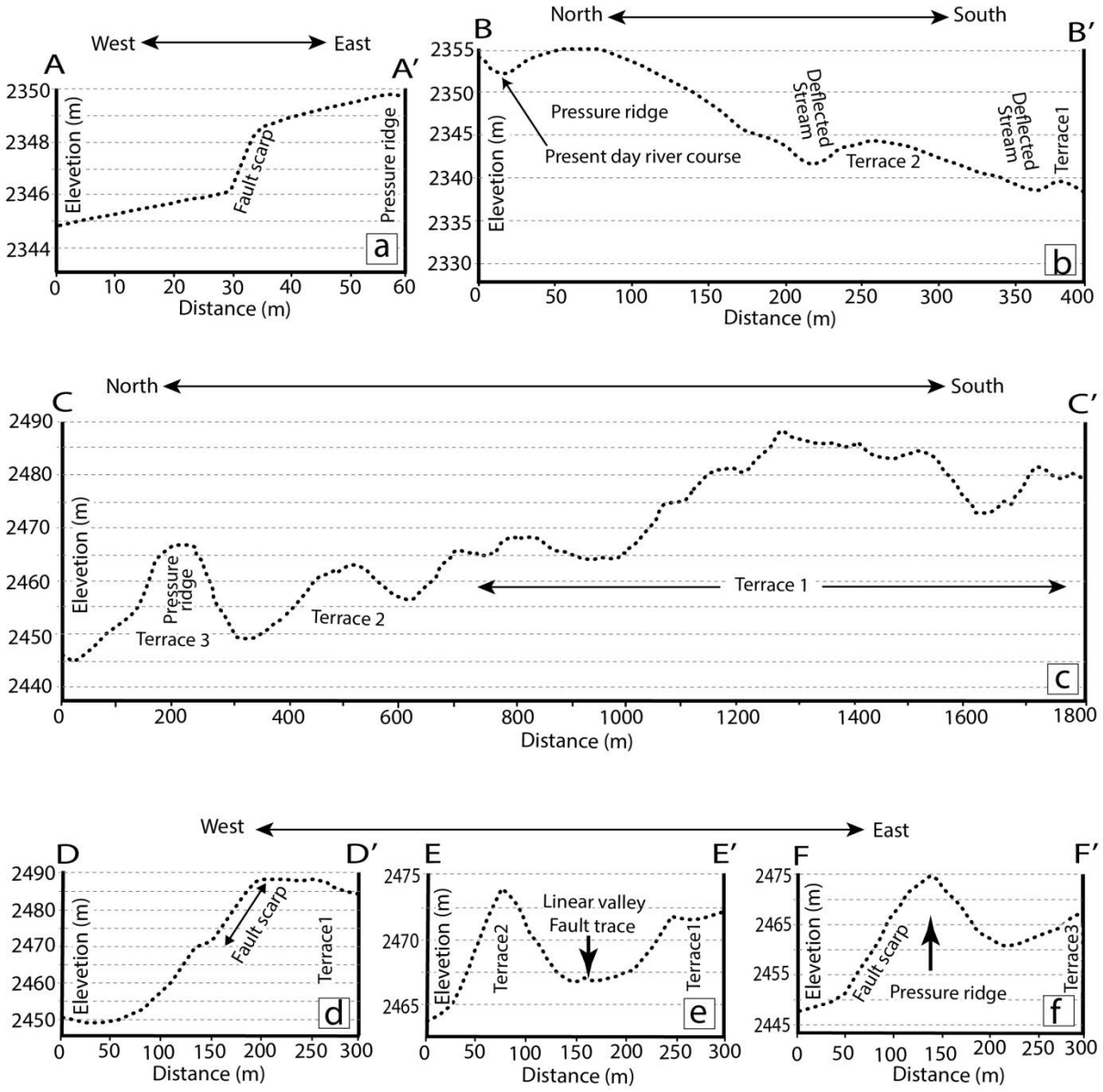

Figure 4.10: Fault scarp profiles at the Ghat Bandakul and Azadkhail sites. a) About 2 m fault scarp measured in the site. b) Fault-parallel topographic profile of the displaced part of the Ghat Bandakul alluvial fan from ASTER 1-arcsecond DEM. The fan is associated with T4, which lies approximately 10 m below the pressure ridge ~2345 m ASL. c) Longitudinal profile along eastern side of the Azadkhail alluvial fan showing T1-T3 surfaces. d) Topographic profile of the fault scarp on the oldest alluvial fan (T1). e) The fault is marked by the linear valley between T1 and T3. f) Northern scarp at Azadkhail alluvial fan over pressure ridge.

Site-2: In Azadkhail fan, three offset stream channels were measured (Fig. 4.7b). The present-day course of the river follows the northern margin of the fan originating from the Khwaja Ghramban Mountains. The incised stream channels pass through the fan surface and trends parallel to the fan apex until the Chaman fault offsets them. Offset stream channels were measured directly by a tape measure in the field as well as from the CORONA and ALOS satellite images using the thalweg of each channel as a piercing point (Fig. 4.8c). The stream channels are >2 m deep and up to 50 m wide. In the Azadkhail site, older deposits are displaced by increasingly larger amounts compared to younger fans, which is clear evidence of repeated faulting over past geologic time. The oldest terrace (T1) extends about 800 ± 70 m to the south on the downthrown side of the fault trace. This was used as the first piercing point to measure the total displacement of the Azadkhail fan along the fault.

To reconstruct the initial Azadkhail alluvial fan surface before the start of left-lateral displacement and move in front of its original place, I need to shift the fan terraces back to its total lateral offset. The high-resolution of the ESRI base map image allows us to build the morphostratigraphy and correctly reconstruct the displaced alluvial fan to its previous position for offset measurement (Fig. 4.11a). Offset reconstructions were done for three different terraces independently for which I decided the age of samples in the direct calculation of the Chaman fault slip rate. Three of the offsets are for the T3, T2, and T1 (Fig. 4.7b). Restoration of the northern margin (T3) produced an offset of 130 ± 14 m from the source channel (Fig. 4.11b). I then obtained a maximum offset of 500 ± 50 m for the terrace2 (T2) (Fig. 4.11c). The geometry and shape of each terrace apex are used to measure their total displacement. The oldest terrace (T1) is offset 800 ± 70 m from the source channel, which is considered an actual offset for the Azadkhail fan (Fig. 4.11d). I observe the T1 surface offset by restoring the western fan surface to its initial location at the front of the displaced channel. The offset is consistent with the contemporaneous deposition of all surfaces. The surficial stream channels and the reasonably straight northern edge of the fan confirm to an erosive relationship between T1 and T2. The T1, T2, and T3 are also vertically offset as much as 30 ± 5 m. Hence,

I plotted several topographic profiles showing several offset channels (Figs. 4.10d-f). The geometry and incision of the fan show that the younger edges have been preserved.

4.3. Surface exposure dating

4.3.1. ^{10}Be TCN method and nuclide measurement

A variety of geochronologic methods, including terrestrial cosmogenic nuclides (TCN) such as ^{10}Be in quartz, are used to estimate the ages of Quaternary deposits and landforms. ^{10}Be is produced at the earth's surface primarily by spallation reactions between high-energy secondary cosmic ray derived particles and oxygen in quartz (Dunai, 2010). The concentration of ^{10}Be is related to (1) the production rate of it at specific latitude and elevation, (2) the half-life, and (3) the length of exposure on earth's surface. ^{10}Be has a half-life of 1.39 Ma (Dunai, 2010; Gold et al., 2015). It is possible to estimate the time since the sample was first exposed to cosmic rays by measuring ^{10}Be concentration in quartz-bearing samples. I present here the first surface exposure ages with ^{10}Be on displaced alluvial fans (Ghat Bandakul and Azadkhail) along the northern end of the Chaman fault in Afghanistan to provide late Pleistocene slip rates of the fault (Figs. 4.5, 4.7b).

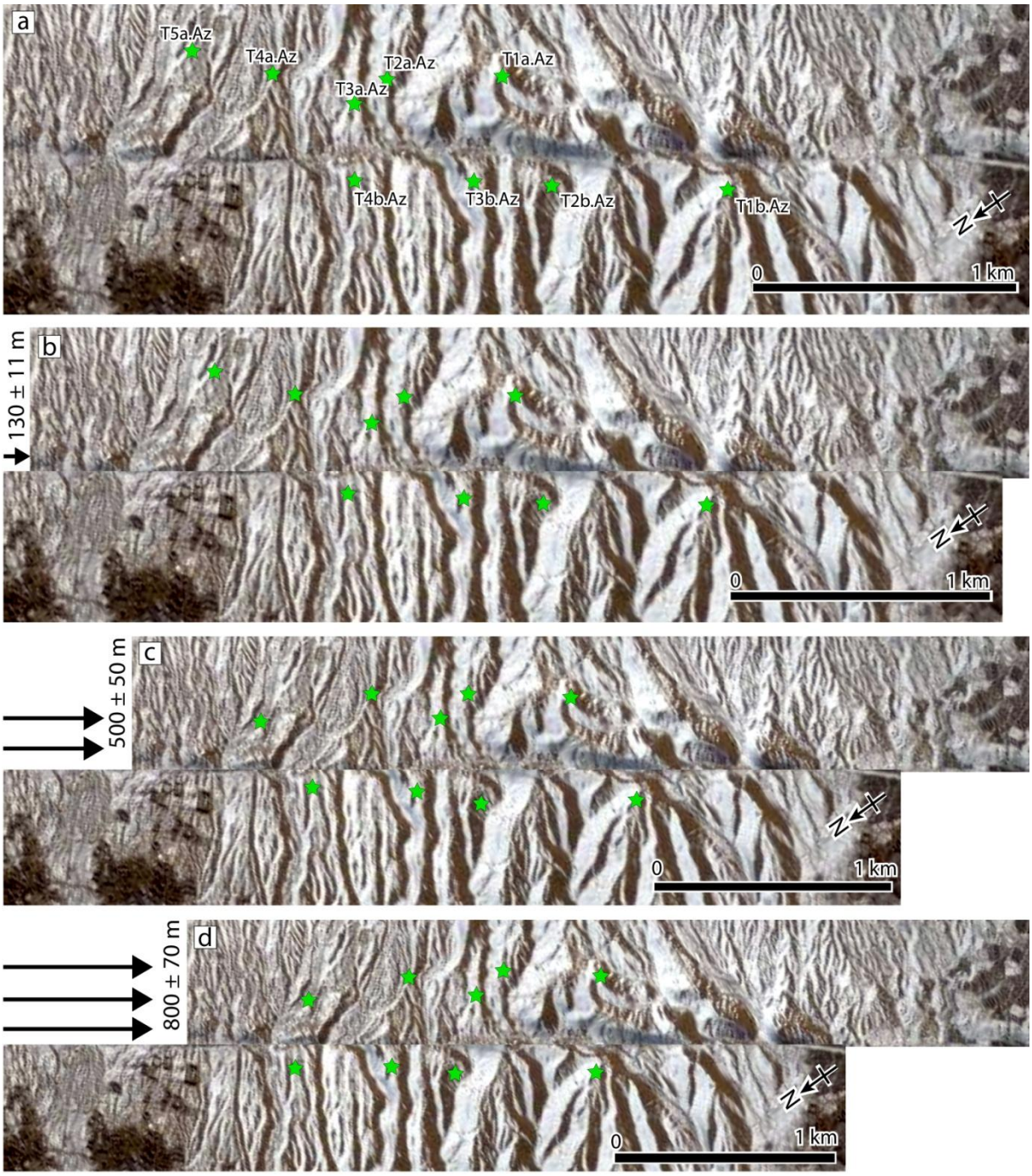

Figure 4.11: Slip restoration of the Azadkhail alluvial fan. The green stars with T letter and number show location and name of the samples collected for ^{10}Be terrestrial cosmogenic nuclides exposure dating. a) Satellite image of the fan from the ESRI base map (2016). b) The Azadkhail fan restored 130 ± 14 m to its pre-faulting position. c) Restoration of the fan with an offset of 500 ± 50 m. d) Restored alluvial fan with an offset of 800 ± 70 m.

Appropriate rock samples were collected using a handheld hammer and chisel from well-embedded sandstone boulders and cobbles, mostly quartzite which yields ^{10}Be (Fig.

4.12). The samples I collected showed minimum evidence for surface weathering, and were in a stable position, have not rolled or slipped downslope. As cosmic rays become attenuated with depth in rocks, about 650-1000 g of the surface block was taken from each of the desired boulder/cobble. Fifteen samples were collected; six from Ghat Bandakul and nine from Azadkhail alluvial fans surfaces (Figs. 4.5, 4.11).

The topmost part of the samples with a thickness of 2-4 cm was cut to be crushed and sieved to separate quartz grains from the 0.25-1.0 mm particle size fraction. Other mineral phases (e.g., Fe-oxide, Mn-oxide, carbonates and organics) were eliminated by selective etching and heavy liquid separation (SPT) according to the procedure of Kohl and Nishiizumi (1992) and Matsushi (2016), in the laboratories of DPRI (Disaster Prevention Research Institute) Kyoto University and MALT (Micro Analysis Laboratory, Tandem Accelerator) the University of Tokyo. The samples were purified chemically by etching 18% HCl for ~16 hours in a heated (~90°C) ultrasonic tank. Then the samples were leached three times for >9 hours in ~1% HF/HNO_3 mixture in a heated (95°C) ultrasonic tank.

I added a known amount of ^{9}Be carrier (~0.25 mg) to the purified quartz samples (~40 g) and then the samples were completely dissolved in a mixture of concentrated HF, HNO_3, and $HClO_4$. After evaporation, Be was separated using anion and cation exchange chromatography (DOWEX 1x8, then 50Wx8 200-400 mesh resin). After the isolation, $Be(OH)_2$ was precipitated in a centrifuge and oxidized in quartz crucibles at a temperature of >400°C. Beryllium oxide (BeO) was then mixed with Niobium (Nb) metal before the determination of the ^{10}Be/^{9}Be ratio by accelerator mass spectrometry (AMS) at MALT (Matsuzaki et al., 2004).

The ratios were normalized by the ^{10}Be AMS measurement standards in the KNB5-1 standard series that was defined and distributed by Nishiizumi et al. (2007). The AMS measurement calculation repeatedly measured to correct for drift. Finally, the rates of production of ^{10}Be were calculated at the Ghat Bandakul and Azadkhail sites using Stone's (2000) polynomials (Table 4.1). The production rates were scaled to latitude and elevation of each sampling area. Then the ^{10}Be concentrations were converted to zero-erosion using SLHL

(seal level high latitude) ^{10}Be production rate of 4.7 ± 0.3 atms/g qtz/yr and a half-life of 1.39 Myr for age calculation (cf. Stone, 2000). The impacts of topography and depth correction were done by numeric integration of the flux corrected for dip and topography (e.g., Nishiizumi et al., 1989).

4.3.2. Berillium-10 model age

The ^{10}Be cosmogenic ages were calculated for all samples by applying the time-independent model of Stone (2000). The exposure ages for each sample are listed in Table 4.1 and shown graphically in Figure 4.13. The ages show the increase of 10Be concentrations that occurred in rocks as a function of time that is exposed to cosmic rays. At both sites, there seems to be a minimal systematic relationship between 10Be concentrations and the samples position, although the Azadkhail alluvial fan is the oldest and located ~50 km away from Ghat Bandakul site to the south along the fault.

Ghat Bandakul alluvial fan: The Ghat Bandakul ages are shown according to the respective samples that were collected from the alluvial fan. The surface ages range from 32.0 kyr to 66.6 kyr (Fig. 4.13a). The two samples (T1b.GB and T2a.GB) show a large amount of scattering at the fan surface. The cosmogonic nuclide analysis shows that the T2a.GB is much younger (1.8 kyr) than expected. ^{10}Be concentrations in the T2a.GB is very low (4.28 ± 1.19×10^4 atoms/g), indicating that sample from the northern fan (terrace4) could be from more rapid erosion of the fan surface than the other terraces and/or this younger sample may have been brought on T4 during recent flood events.

Figure 4.12: View of all sampled boulders for ^{10}Be dating the Ghat Bandakul and Azadkhail alluvial fans. The close-up view of the boulders shows desert varnishing and no weathering effects.

Table 4.1: Sample description and ^{10}Be terrestrial cosmogenic nuclide (TCN) ages for alluvial fan surfaces in the Ghat Bandakul and Azadkhail areas.

Site	Sample[1]	Location		Elev (m)	Size LWH[2] (cm)	Qurtz wt.[3] (g)	Be Carrier (μg)	$^{10/9}$Be [4] ($\times10^{-12}$)	Produ-ction rate (atms/g/ yr)	Nuclide concentr-ateion ($\times10^{4}$ atom/g)	^{10}Be model Age[5] (kyr)
		Lat (°)	Log (°)								
Ghat Bandakul	T1a.GB	34.218	68.834	2349	90×70×60	34.80	398.6	2.03± 0.06	22.71 ± 1.52	148.63 ± 4.52	66.6 ± 4.9
	T1b.GB	34.217	68.832	2330	50×35×40	40.24	399.2	5.01± 0.14	22.43 ± 1.50	326.67 ± 9.42	151.2 ± 11.4
	T2a.GB	34.218	68.834	2350	110×80×92	40.23	397.8	0.15 ± 0.02	22.72 ± 1.52	4.28 ± 1.19	1.9 ± 0.5
	T2b.GB	34.218	68.833	2336	60×40×45	40.18	398.2	1.67 ± 0.05	22.52 ± 1.51	104.47 ± 3.32	46.9 ± 3.5
	T3a.GB	34.218	68.835	2352	55×50×33	35.40	397.0	1.10 ± 0.04	22.75 ± 1.53	75.81 ± 2.62	33.6 ± 2.6
	T3b.GB	34.218	68.833	2338	60×55×30	40.24	367.2	1.27 ± 0.05	22.55 ± 1.51	71.61 ± 2.71	32.0 ± 2.5
Azadkhail	T5a.Az	33.813	68.611	2461	40×40×30	40.10	250 ± 2.0	6.00 ± 0.16	23.38 ± 2.05	241.53 ± 6.47	106.1 ± 10.0
	T4a.Az	33.813	68.609	2458	50×40×35	39.97	250 ± 2.0	6.25 ± 0.16	23.34 ± 2.05	252.34 ± 6.64	111.2 ± 10.5
	T4b.Az	33.812	68.606	2449	70×45×45	40.09	250 ± 2.0	8.13 ± 0.21	23.2 ± 2.04	327.91 ± 8.54	146.6 ± 13.9
	T3a.Az	33.811	68.608	2465	50×45×40	40.02	250 ± 2.0	11.54 ± 0.29	23.44 ± 2.06	485.72 ± 12.29	218.7 ± 21.1
	T3b.Az	33.812	68.606	2459	45×45×30	40.11	250 ± 2.0	9.62 ± 0.24	23.35 ± 2.05	403.81 ± 9.96	180.9 ± 17.2
	T2a.Az	33.810	68.608	2469	40×35×30	40.03	250 ± 2.0	9.49 ± 0.35	23.5 ± 2.06	399.17 ± 14.76	177.5 ± 17.7
	T2b.Az	33.810	68.604	2451	70×65×43	40.30	250 ± 2.0	3.80 ± 0.12	23.23 ± 2.04	158.21 ± 5.01	69.3 ± 6.6
	T1a.Az	33.810	68.605	2467	50×40×20	40.00	250 ± 2.0	6.19 ± 0.16	23.47 ± 2.06	259.80 ± 6.90	113.9 ±10.7
	T1b.Az	33.802	68.600	2467	70×60×50	40.09	250 ± 2.0	9.21 ± 0.23	23.47 ± 2.06	386.83 ± 9.80	172.0 ± 16.4

Note [1] A depth of 2 cm was used for Ghat Bandakul surface samples and 4 cm for Azadkhail samples. Thickness of the samples ranges from 7 – 12 cm.

[2] Topographic slope of the Ghat Bandakul area is 5°, and 0° for Azadkhail site.

[3] The rocks density of 2.6 g/cm^3 was used for all samples.

[4] Isotope ratios were normalized to ^{10}Be standard with a value of $2.79 \pm 0.03 \times 10^{-11}$ (Nishiizumi et al., 2007).

[5] Ages calculated using Stone (2000) time-independent scaling model with half-life correction ^{10}Be 1.51 to 1.387 Myr.

The T1b.GB sample contains substantially more ^{10}Be nuclides than other samples that were collected. The old age (151.2 ± 11.4 kyr) with highest ^{10}Be concentration (326.67 ± 9.42×10^4 atoms/g) most closely indicates that the sample slipped down from the steep hill, probably >40°. The average age for all fans, considering all the 4 samples and ^{10}Be production rates, is 44.8 ± 3.4 kyr. The Ghat Bandakul alluvial fan ages correspond to the stratigraphic sequence of terraces (Table 4.1, Fig. 4.5, 4.10b). The T1a.GB sample collected from terrace2 shows that nuclide activity and terrace height are correlated and showing longer subaerial exposure age (66.6 ± 4.9 kyr) of the terrace surface. The terrace3 ^{10}Be age, excluding the one outlier (T2a.GB), is well clustered and defined the 46.9 ± 3.5 kyr age of displaced alluvial fan (Fig. 4.13a).

Azadkhail alluvial fan: The Azadkhail fan surfaces experienced little erosion, as shown by the heavy desert varnish coatings on top of the rocks. I determined average ^{10}Be nuclide concentrations of 323.9 ± 8.9 ×10^4 atoms/g for all 9 samples. The abandonment of fan surfaces weighted mean age 144 ± 13.8 kyr was calculated. Exposure ages of 9 quartzite samples range from 69.3 ± 6.6 kyr to 218.7 ± 21.1 kyr with individual 1σ total uncertainties of ~20%. The modeled ages correspond to the stratigraphic sequence of terraces, but I also found significant uncertainty of ^{10}Be nuclides for some samples (Table 4.1; Figs. 4.7b, .4.10c). The TCN ^{10}Be result shows considerable scatter from each of the samples. However, the ages suggest that the alluvial fan developed in three stages, even though some samples are affected by inheritance and erosion. The age (172 kyr, 177 kyr and 180 kyr) of three samples (T1b.Az, T2a.Az and T3b.Az) are almost the same, which most closely approaches with the deposition age of the T1 surface (Figs. 4.7b, 4.13b). The T1a.Az, T4a.Az and T5a.Az sampled rocks have almost the same age ranging from 106 kyr to 113 kyr (Table 4.1). The young age (69.3 ± 6.6 kyr) of the sample T2b.Az from the old terrace (T1) could be from more rapid erosion of the fan surface than the other fan. The sampled rocks (T3a.Az and T4b.Az) from T1 and T2 surfaces show a high concentration of nuclides, which reflects nuclide inherited from prior periods of exposure in the Azadkhail catchment area. The determined production rates of ^{10}Be are subject to uncertainty in the exposure age of the Azadkhail sampled rocks. It cannot be

explicitly determined the source of high inheritance but could be from (1) the residence time of sediments in the headwaters, and the catchment may cause the amount; (2) the exposure during transport in the active channel, (3) incision and erosion of older surface that cause high inheritance clasts to sediments in active channel (Bierman et al., 2002; Dühnforth et al., 2017; Grew, 2002). The Azadkhail drainage area is less than 9 km^2 at both sides of the Chaman fault, which is an indication of a rapid transport before the emplacement of the fans (e.g., Le Dortz et al., 2009) (Figs. 4.7-4.9). Most likely, the above three components all contributed to the total inherited nuclides in sampled rocks.

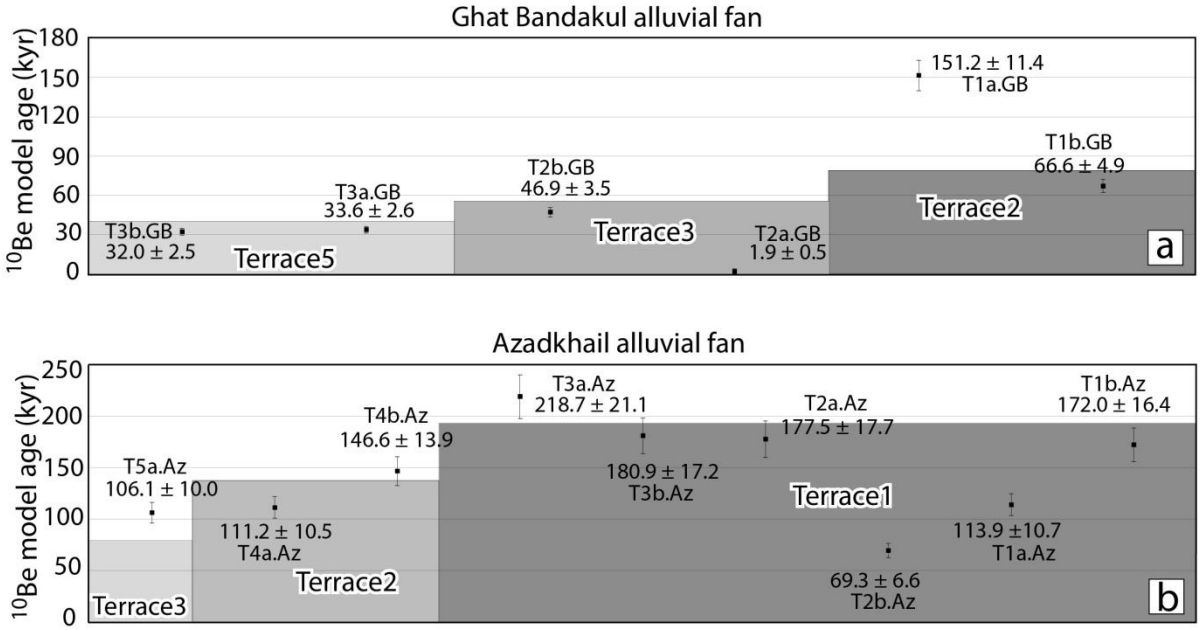

Figure 4.13: Weighted mean of the ^{10}Be model ages. a) The ^{10}Be model ages of the Ghat Bandakul alluvial fan. b) The weighted mean of ^{10}Be model ages of the Azadkhail fan.

To evaluate the importance of nuclide inheritance, I consider the analysis of the samples based on the degree of dissections and estimated abandonment ages of analyzed alluvial surfaces (e.g., Le Dortz et al., 2012). In the Azadkhail fan surface, inheritance refers to nuclide concentrations that are already in the sampled rocks before they were deposited. These caused high concentrations of the ^{10}Be nuclides and led to exposure ages that are older than the time since the deposition of the alluvial fan. Rock fragments should also have been exposed through storage in terraces before final deposition on the fan (Ivy-Ochs et al., 2013).

Reworking of the deposits because of incision of older fans at a higher elevation to younger depositions downstream may be another cause for inheritance in sampled rocks.

The obtained exposure ages also rely on the assumption that the effect of erosion on the most preserved part of the fan surfaces and ^{10}Be nuclides inheritance from exposure prior to the deposition of clasts are negligible (e.g., Farbod et al., 2016) (Table 4.1). The Azadkhail fan is deeply incised by streams and contains loosely cemented clasts, which makes the surfaces erodible (Figs. 4.7b, 4.11a). Therefore, it is essential to estimate the erosion rate for the alluvial fan to correct the exposure ages for the weathering of boulder surfaces. Assuming the age for the younger samples (T1a.Az, T4a.Az, and T5a.Az) allows estimating a maximum erosion rate of 0.116 m/kyr for the fan surface based on ^{10}Be nuclides concentrations measured on the Azadkhail surface along the Chaman fault using the CRONUS-Earth online calculator, version 3 (Balco et al., 2008) (Table 4.1). These samples reflect the erosion rate on the fan surface after the formation, and the erosion rates decrease as fan ages increase. This maximum erosion rate allows us to determine the upper and lower bound of surface abandonment ages. I, therefore, reconstructed the original surface of the Azadkhail fan and then compared it with dissected erosion of the area (Fig. 4.13). The total thickness of the fan is ~20 m that has been removed by the erosion (0.116 m/kyr) compared to the T1 surface (172 kyr). The T1 surface may be in erosional equilibrium because the ^{10}Be exposure age is high for T1 (e.g., Nishiizumi et al., 1993) (Fig. 4.14). As a result, the ^{10}Be exposure age is in proper stratigraphic order, inherited samples with age of 146 kyr and 106 kyr were not considered. Therefore, the obtained age for T2 and T3 surfaces approaches the maximum exposure age. The age of T4b.Az suggests that it has been redeposited from older deposits, which is defined as an outlier. Discarding the outliers (T3a.Az, T4b.Az), the older samples (T1b.Az, T2a.Az, and T3b.Az) do not provide maximum denudation rate higher than 3.5 mm/kyr. The erosion rate indicates an overall exponential decrease of ^{10}Be concentration with increasing elevation (Fig. 4.14b). The obtained exposure ages rely on the assumption that the effect of erosion on the most preserved part of the Azadkhail fan surfaces and ^{10}Be nuclides inheritance from exposure before the deposition of clasts are negligible (Table 4.1).

The discordance of the Azadkhail fan ages represents that some sampled rocks have a complex exposure history compared to the Ghat Bandakul site. The nuclide activity is 2-5 times higher in the Azadkhail fan compared to the exposure age of the surface in the Ghat Bandakul site. This result fits that the oldest samples could be reworked boulders from nearby mountains. I cannot determine the exact timing of the Azadkhail fan activity. Therefore at present, I can only focus on the period of fan deposition for the terrace1 and terrace2 to roughly correlate their ages with the geomorphic classification based on the degree of dissections (Fig. 4.7b). If I exclude the largely inherited ages, including the T2a.Az, I obtained an average age of 176.8 ± 17.1 kyr for terrace1 and 111.2 ± 10.5 kyr for terrace2. The ^{10}Be ages are used as the maximum limiting age of the offset terraces surface because these ages are likely to have only a small amount of inheritance.

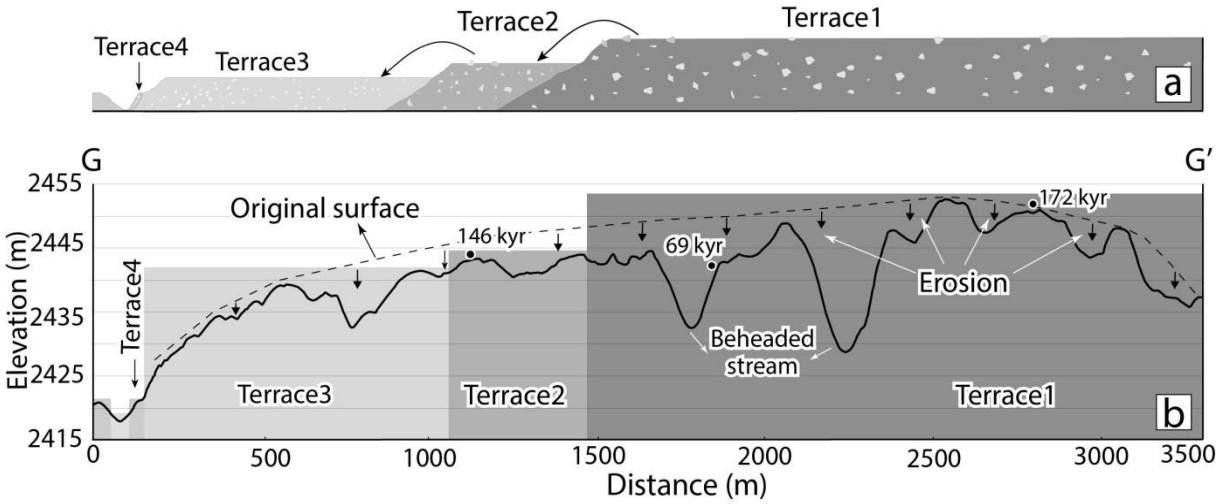

Figure 4.14: Schematic model and longitudinal profile along the Azadkhail alluvial fan. a) Schematic model for the four offset terraces of Azadkhail alluvial fan. The older terrace could have reworded to the younger terrace during the incision of the upper surface. b) Longitudinal profile along the downside of Azadkhail fan showing with the original reconstructed surface of the alluvial fan. Location of the profile is shown in Figure 4.7b.

4.4. Long-term slip rate

I was able to obtain two independent time-integrated slip rates on the Chaman fault in Wardak Province. Based on the TCN dating, I can assertively conclude that the T3 and T2

surfaces of Ghat Bandakul alluvial fan were emplaced 46.9 ± 3.5 and 66.6 ± 4.9 kyr ago, respectively (Table 4.1; Fig. 4.13a). After that date of deposition, the two surfaces have been offset 165 ± 15 m and 235 ± 24 m, respectively. Dividing these offsets by these ages yields an average slip rate of 3.5 ± 0.4 mm/yr at the Ghat Bandakul site. This slip rate calculated here is considered a minimum bound so far along the Chaman fault.

At the Azadkhail site, the abandonment age (111.2 ± 10.5 kyr) of terrace2 determined from one sample of the offset surface (500 ± 50 m) yields a 4.5 ± 0.6 mm/yr slip rate. The 800 ± 70 m total offsets were determined for the oldest surface (terrace1) in which the alluvial fan is restored to its initial geometry (Fig. 4.11d). The terrace1 total left-lateral offset matching with an average age of 176.8 ± 17.1 kyr for the fan yields a slip-rate of 4.5 ± 0.6 mm/yr, same as for terrace2 (Table 4.1; Fig. 4.13b). Combining this slip rate with an average age of terrace2 (111.2 ± 10.5 kyr) yields approximately the same slip rate. Considering this analysis, the 800 ± 70 m and 500 ± 50 m horizontal offsets recorded by the fault constrains the left-lateral slip rate on the Azadkhail fan is 4.5 ± 0.6 mm/yr. In any case, it is the only direct estimate of the slip rate of the Chaman fault across the Azadkhail alluvial fan. Although the ages of all samples are not well consistent, I propose the intermediate slip rate of 4.5 mm/yr is the most reliable estimation at the Azadkhail site. This rate is in agreement with the slip rate determined at the Ghat Bandakul site.

Chapter 5

Active Faults and Seismic Hazard in the Kabul basin, Afghanistan

5.1. Data and Methods

Tectonic geomorphology of the Kabul basin was analyzed using several satellite images covering the area 34.03°-35.25°N and 68.71°-69.82°E. I firstly prepared 3D anaglyph images from the 2.5-m-resolution ALOS PRISM satellite images using Adobe Photoshop. Anaglyph images have a stereoscopic 3D effect by encoding each eye's image using filters of different colors. For regions that are not covered by the ALOS images, I prepared shaded relief maps constructed from the DEM (digital elevation model) of 1-arcsecond SRTM together with the ESRI base map. I also imported the SRTM DEM to Simple DEM Viewer software (Katayanagi, 2019), to produce anaglyph images. Large scale images were constructed from 2.0-m-resolution SPOT earth observation satellite, which is freely available from ESRI as a base map. All these images were imported to ArcMap for geo-referencing into a global framework and manipulated to highlight the scenes to map the critical geomorphic elements of the Kabul basin. I also conducted fieldwork in the broader area, particularly along the Paghman and Chaman faults, to examine the details of the tectonic geomorphic features.

Active and presumed active faults were mapped based on geomorphic criteria commonly used in Japan (The Research Group for Active Faults of Japan, 1992; Tsutsumi and Perez, 2013). The first criterion for the identification of an active fault is the evidence of movement in recent geologic time, i.e., late Pleistocene. I paid close attention to the presence of young offset landforms and deposits along the foot of the mountain ranges. In places where young (Quaternary) strata and landforms are scarce or absent, active and presumed active faults were identified based on systematic offsets of stream channels. Geomorphic surfaces within the basin were classified based on morphology and degree of dissection.

5.2. Geomorphology of the Kabul basin

The Kabul basin is located in the northern part of the Kabul block that is approximately 300 km long and up to 70 km wide (Fig. 1.2). The Kabul block is bounded on the east and west by major active strike-slip faults. The Chaman and Paghman faults bound the western margin and separate the Kabul block from the Helmand block and middle Afghanistan (Fig. 5.1). The northeastern margin is bounded by the Sarobi fault that separates the Kabul block from the Nuristan fault block. The left-lateral Gardez fault defines the southeastern margin of the Kabul block against the Katawaz basin. The northern end of the Kabul block extends to the central Hindu Kush Mountains and is bounded by the Herat-Panjshir Suture Zone (Collett et al., 2015) (Fig. 2.2).

The Kabul basin is bordered on its four sides by mountain ranges (Figs. 5.2, 5.3). The Paghman Mountains on the west reach the maximum elevation of 4400 m and are the primary source of sediments deposited within the basin. In the east, the basin is bordered by the Koh-e Safi Mountains ~2900 m high. The northern margin of the basin is bounded by the Hindu Kush Mountains, while the Koh-e Quragh Mountains bound the southern margin of the basin (Fig. 5.2).

The Kabul basin can be divided into six geomorphological subbasins separated by prominent bedrock outcrops (Mack et al., 2010): the Panjshir, Shomali, Dehsabz, Upper Kabul, Logar and Lower Kabul subbasins (Figs. 5.2, 5.4). These subbasins are the depositional centers of sediments shed from the surrounding surficial deposits and bedrock outcrops. The Kabul basin is fed primarily by the Panjshir, Ghurband, Paghman and Logar Rivers, which flow eastward from the Hindu Kush and Paghman Mountains (Fig. 5.2).

The ridges within the basin are 200-500 m higher than the adjacent valley floors. The central parts of the subbasins are generally flat and rise gradually towards the surrounding mountains (Fig. 5.2). Elevation of the central plains varies from 1800 m to 2200 m. Perennial and ephemeral stream channels have dissected the central plains, but they rarely exceed 20 m in width and 8 m in depth. Some isolated topographic depressions in the Logar and Lower Kabul subbasins act as catchments for surface water runoff and are the sites of playa lakes or

ephemeral marshes (Houben et al., 2009).

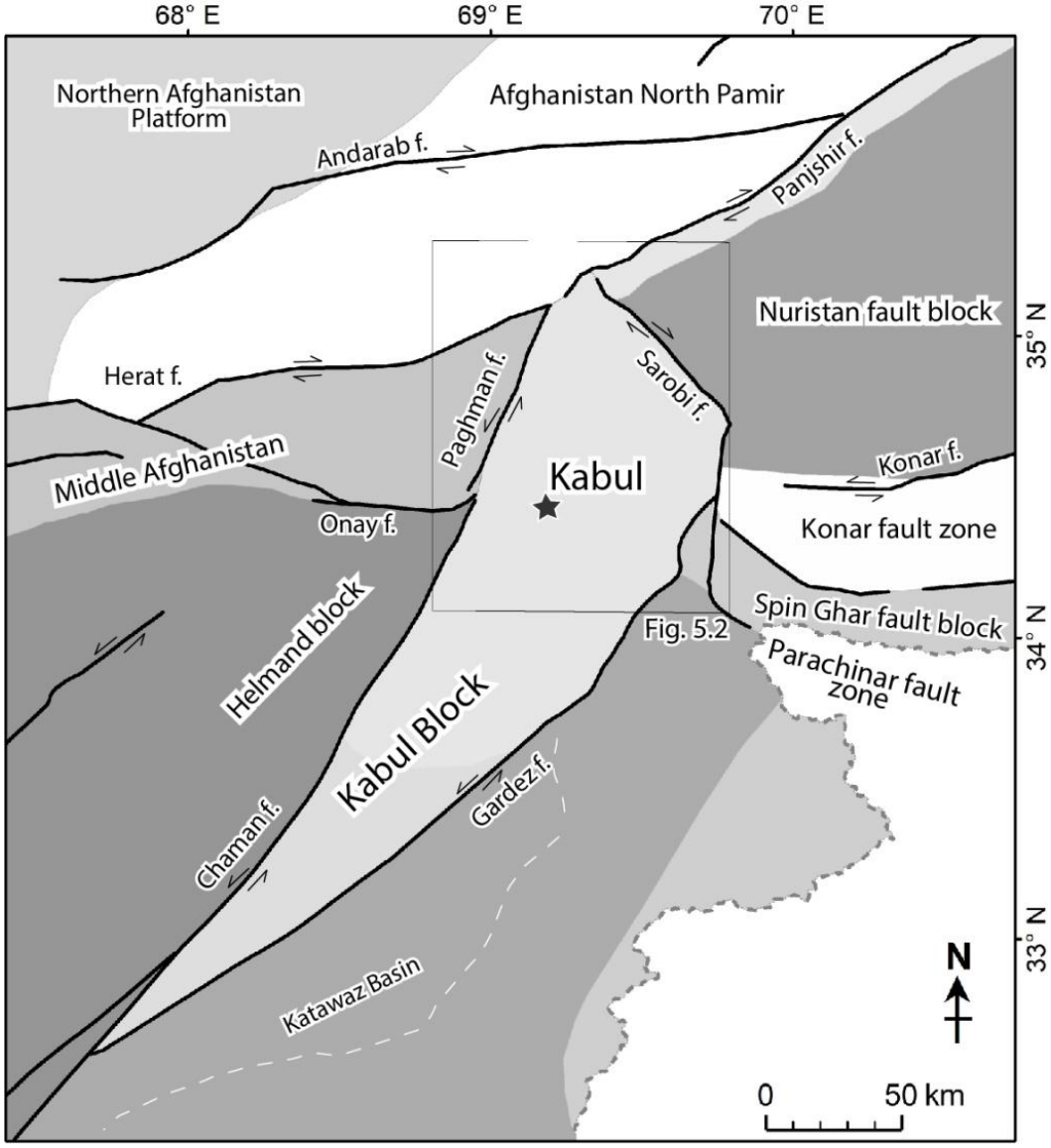

Figure 5.1: Tectonic setting and location of the study area in the northern part of the Kabul block. The rectangle shows the location of Fig. 5.2.

The surrounding mountain ranges consist of Paleoproterozoic gneiss and Late Permian through Late Triassic strata. The Koh-e Safi interbasin ridges (between Dehsabz and Shomali or Dehsabz and Lower Kabul subbasins) are composed of Paleoproterozoic migmatite and gneiss. The basement rocks in the Koh-e Safi Mountains, to the east of the Kabul basin, are overlain by Permian to Jurassic shelf or platform carbonate rocks (Bohannon, 2010). Early Cretaceous gabbro and monzonite intrusions are exposed in the Paghman Mountains (Figs. 5.3, 5.4).

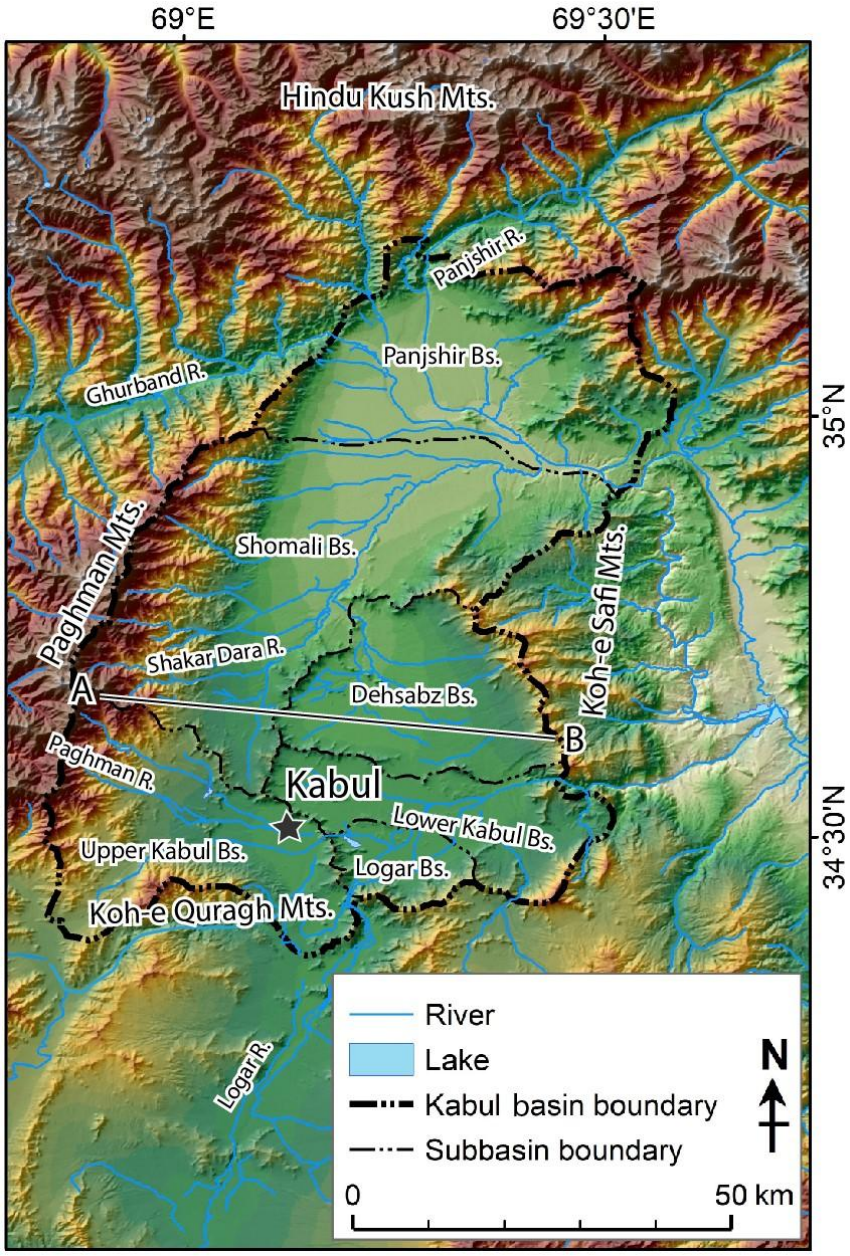

Figure 5.2: Topography of the Kabul basin. The black line (A-B) indicates the location of the geologic cross-section shown in Fig. 5.4.

The basin is filled by less than 80 m thick Quaternary deposits (Böckh, 1971), that overly approximately 800-m-thick Tertiary strata in Kabul City (Broshears et al., 2005; JICA, 2007). Surficial deposits are alluvial fan deposits of various ages and are differentiated by the degree of dissection and morphology. River deposits are present in the active floodplains of the Panjshir and Logar Rivers (Fig. 5.2). Eolian Loess deposits accumulated in the Paghman and Koh-e Safi Mountains. Terrace deposits are well exposed along the major rivers and mountain fronts (Fig. 5.5).

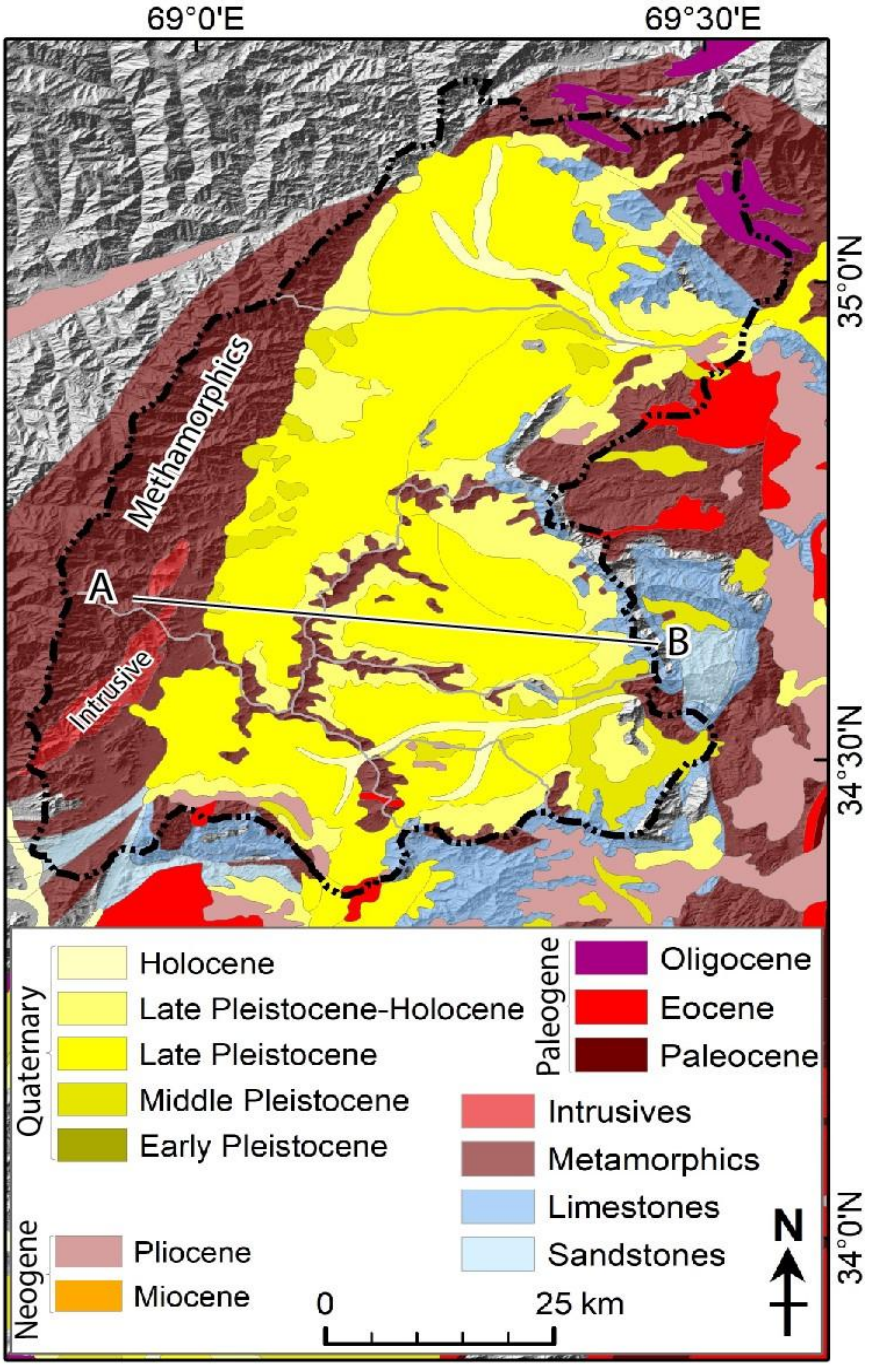

Figure 5.3: Geologic map of the Kabul basin. The map is simplified from Doebrich et al. (2006).

In the study area, terrace deposits are present on flat-lying areas around the drainage systems and their second-order branches (Fig. 5.5). They are up to 70 m higher than the current drainage system (Fig. 5.6a). The Paghman fault displaces a sequence of terraces along the Paghman and Koh-e Quragh Mountains (Figs. 5.5, 5.6b). The terraces overlie the steeply tilted and folded rocks with angular unconformity. The lower section of the terrace deposits is relatively well lithified, whereas the upper section is weakly lithified, altered, and loose. The

fault strands cut them, but the tectonic geomorphic features are rapidly erased by erosion or deposition on active fan surfaces (Fig. 5.6b).

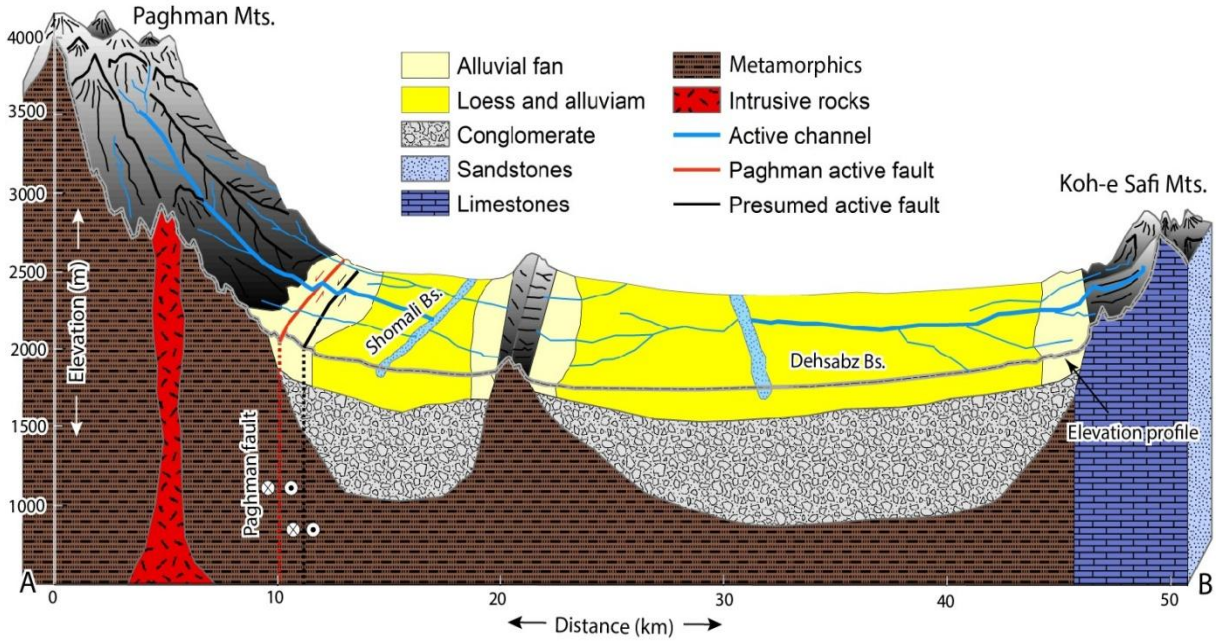

Figure 5.4: Schematic geologic cross-section and topographic profile across the Kabul basin.

5.3. Active deformation

Tectonically, the Kabul basin can be divided into two zones: 1) Kabul highland and 2) Shomali lowland (Fig. 5.5). The Kabul highland is bounded by large active faults. Several small faults, such as the Onay fault, separate the highland from the Helmand block located to the west (Figs. 5.1, 5.5). Within the Kabul highland, the lower Kabul basin is ~250 m lower than the upper Kabul basin (Fig. 5.2).

The Shomali lowland is a gently inclined surface that occupies the lowest part (~1500 m) of the Kabul basin. The Shakar Dara River incises the southern part of the lowland (Fig. 5.2). The north, west, and east edges of the area are characterized by a series of alluvial fans from the surrounding mountains. The western margin of the lowland is bound by the steep Paghman Mountains. In the north and northeast, the lowland is bounded by the Hindu Kush Mountains, which are cut by the east to northeast-trending right-lateral Herat, Andarab and Panjshir faults (e.g, Ruleman et al., 2007) (Figs. 5.1, 2.2) The Hindu Kush Mountains are seismically active and have been uplifting at a rate as much as 10 mm/yr based on recent

GNSS measurements (Dhakal, 2015). The eastern side of the Shomali lowland is marked by a faulted ridge composed of Neogene-Quaternary deposits, which has been incised by small stream channels (Figs. 5.3, 5.4).

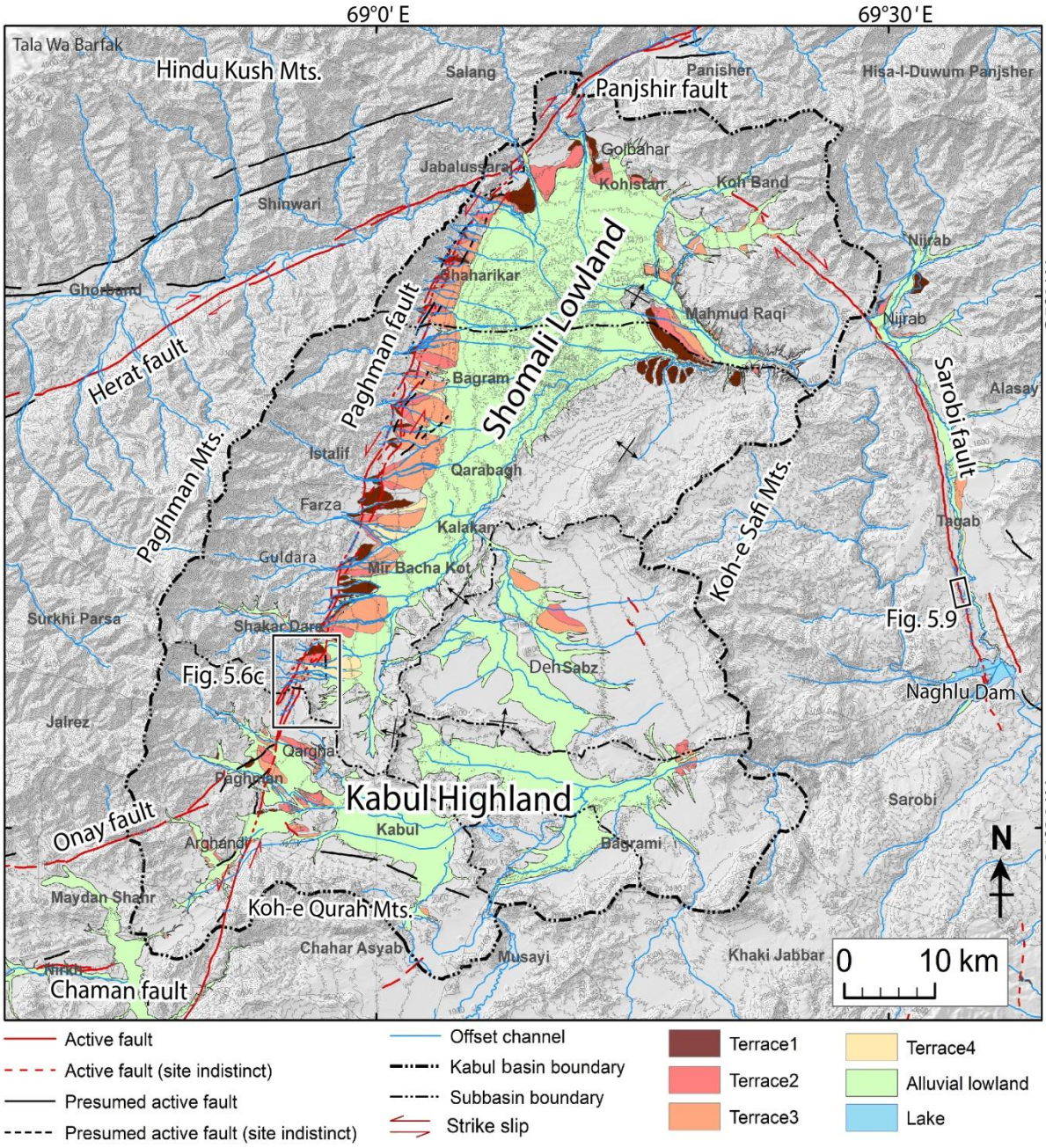

Figure 5.5: Map of active faults and geomorphic features in the Kabul basin based on interpretation of ALOS PRISM and SRTM satellite anaglyph images as well as ESRI base map. Red lines denote active faults and black lines denote presumed active faults. The rectangle shows the location of Fig. 5.6c.

5.3.1. Active faults

5.3.1.1. Paghman fault

The Paghman fault extends for a length of ~80 km. The strike of the fault ranges from N16°E to N35°E (Fig. 5.5). The Paghman fault is the northern extension of the Chaman fault. It extends from Paghman district west of Kabul City northeastward to the northern margin of the Kabul basin. The fault is marked by continuous, linear or arcuate fault scarps on piedmont alluvium at the mountain front. The termination of the recent geologic units (e.g., Quaternary) was also used to delineate the fault strands along the Paghman Mountains.

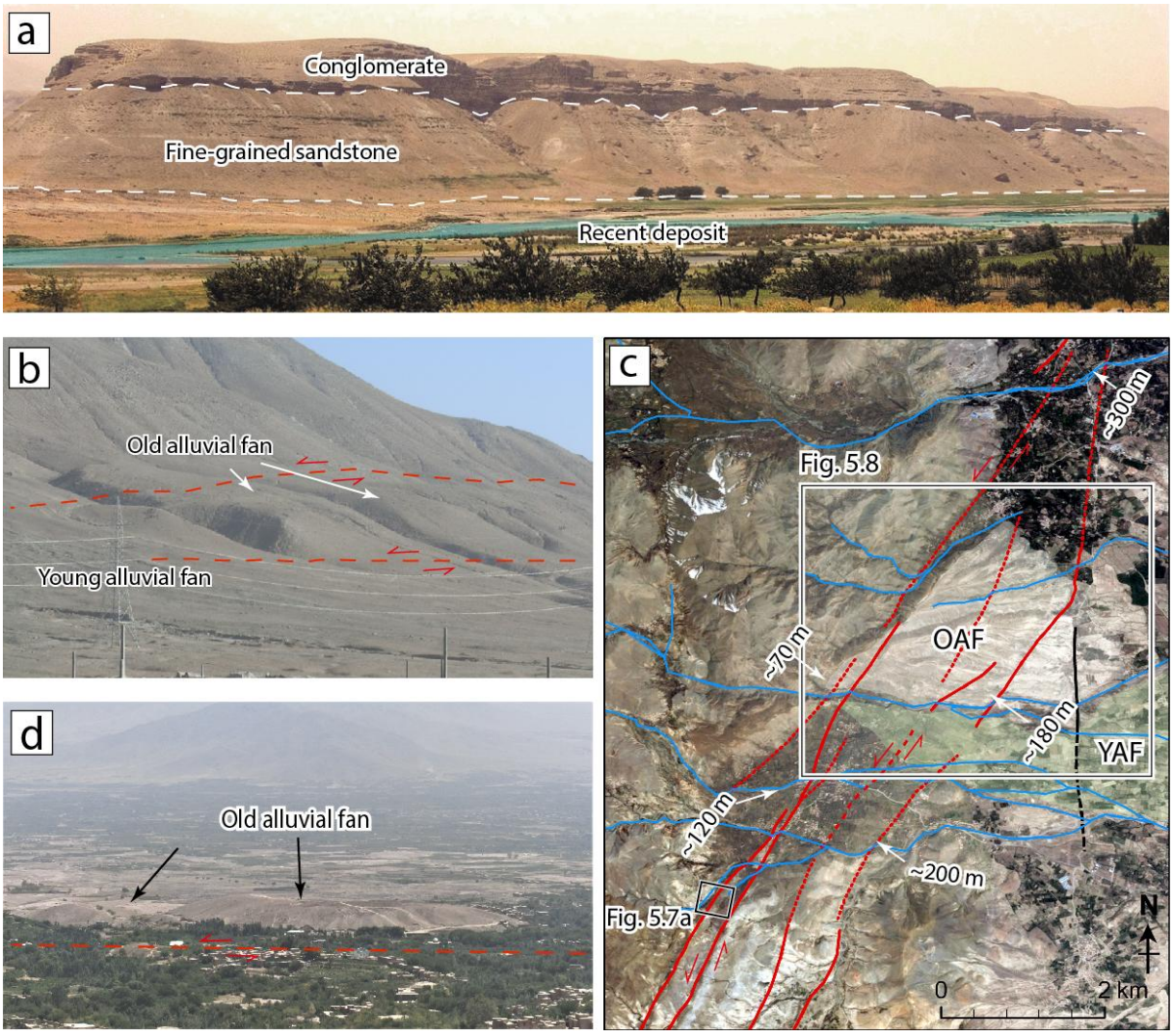

Figure 5.6: Field photos of the Paghman fault and river terraces. a) View of the river terraces along the Panjshir River. The image is modified from Bohannon (2010). b) Photograph of small fault-bounded terraces near Arghandi, Paghman district (34°27'3.04"N, 68°56'34.66"E). c) Young and old alluvial fans (YAF and OAF) as well as fault strands of the Paghman fault on top of the ESRI base map. The

old alluvial fan has moved northward relative to its source drainage. The location of Fig.5.8 is also shown by the box. d) Oblique view looking east across the Paghman fault (34°48'23.46"N, 69° 4'3.27"E). The hill is the old alluvial fan that has been transported left-laterally and made west-facing fault scarp.

The fault typically offsets late Pleistocene and Holocene deposits and is marked by continuous fault scarps (Figs. 5.3, 5.5). The old alluvial fans are preserved as deeply dissected remnants of thick fan deposits that are now isolated at the top of low hills in the southwest part of the basin as well as along the Paghman Mountains' front (Fig. 5.6d). Tectonic geomorphic features such as offset and beheaded stream channels, offset fans, shuttle ridges, fault scarps, and tilted alluvial surfaces are common (Figs. 5.6c, 5.7a). The fault also formed a linear valley between Qargha and Shakar Dara district (Fig. 5.5). It is hard to identify the fault trace along the range front from Arghandi to Qargha because of intensive human modification for farming.

In some places, the mountain ranges are deformed primarily by strike-slip faulting, with minor northeast-striking thrust faults. For example, two strands of the Paghman fault offset gneiss between Farza and Istalif districts, which caused a scarp facing upslope toward the mountain (Fig. 5.7b). Middle-late Pleistocene conglomerate and sandstone rocks in the low hills possibly thrust to the west above the gneiss. Near Chaharikar, the age of the strata of these low hills was reported as Neogene (Bohannon, 2010) (Fig. 5.5).

The fault strands cut across alluvial fans along the piedmonts of the Paghman Mountains (Fig. 5.7a). I was able to measure the amount of left-lateral displacement of stream channels (Figs. 5.5, 5.6c). The old alluvial fans have been displaced let-laterally >200 m from their sources. These fans are now located near small drainages, which cannot be the source of such massive fans (Ruleman et al., 2007) (Fig. 5.7b). In contrast, the young alluvial fan was offset for a smaller amount (~70 m) (Fig. 5.6c). Both glacial and fluvial processes are the primary agents of terrace formation. Sediments were deposited in the mountain ranges during the previous glacial periods, then transported by streams and formed fans. The alluvial fans were disrupted by the fault movement, and fluvial action has caused the formation of several

terrace surfaces (Figs. 5.6c, 5.7).

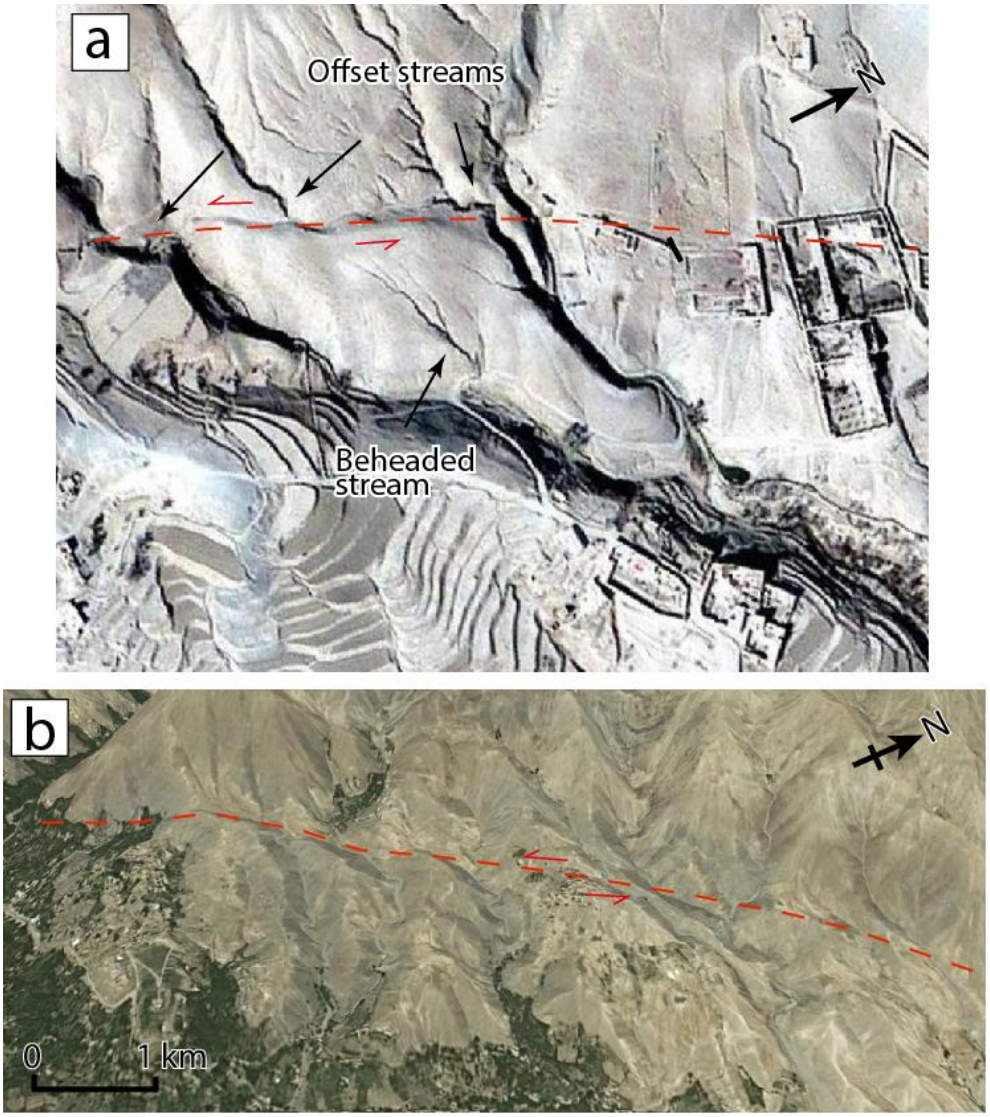

Figure 5.7: Satellite images looking northwest along the central section of the Paghman fault. a) ESRI base map image showing beheaded and offset channels along the fault between Shakar Dara and Paghman districts. b) View of the Paghman Mountains' front, where the Paghman fault offsets metamorphic rocks between Farza and Istalif districts. The fault dips to the northwest and has large reverse and strike-slip components of displacement. The image is modified from Google Earth.

5.3.1.2. Sarobi fault

The 150-km-long Sarobi fault is one of the most noticeable structures northeast of the Kabul basin. The southwestern segment of the fault extends from the Parachinar fault zone, through the Kabul-Logar ophiolite belt to the Sarobi district (Figs. 5.1, 5.5). The northern

segment of the fault extends northward from the Naghlu Dam. The fault runs along the Tagab valley, crosses the Koh-e Safi Mountains, and reaches the north end of the Kabul block. I interpreted the Sarobi fault as a right-lateral strike-slip fault (Fig. 5.9). Based on the high-resolution 3D anaglyph images, I interpret that the fault plane dips steeply to almost vertical, particularly from Naghlu Dam to Tagab district (Fig. 5.5).

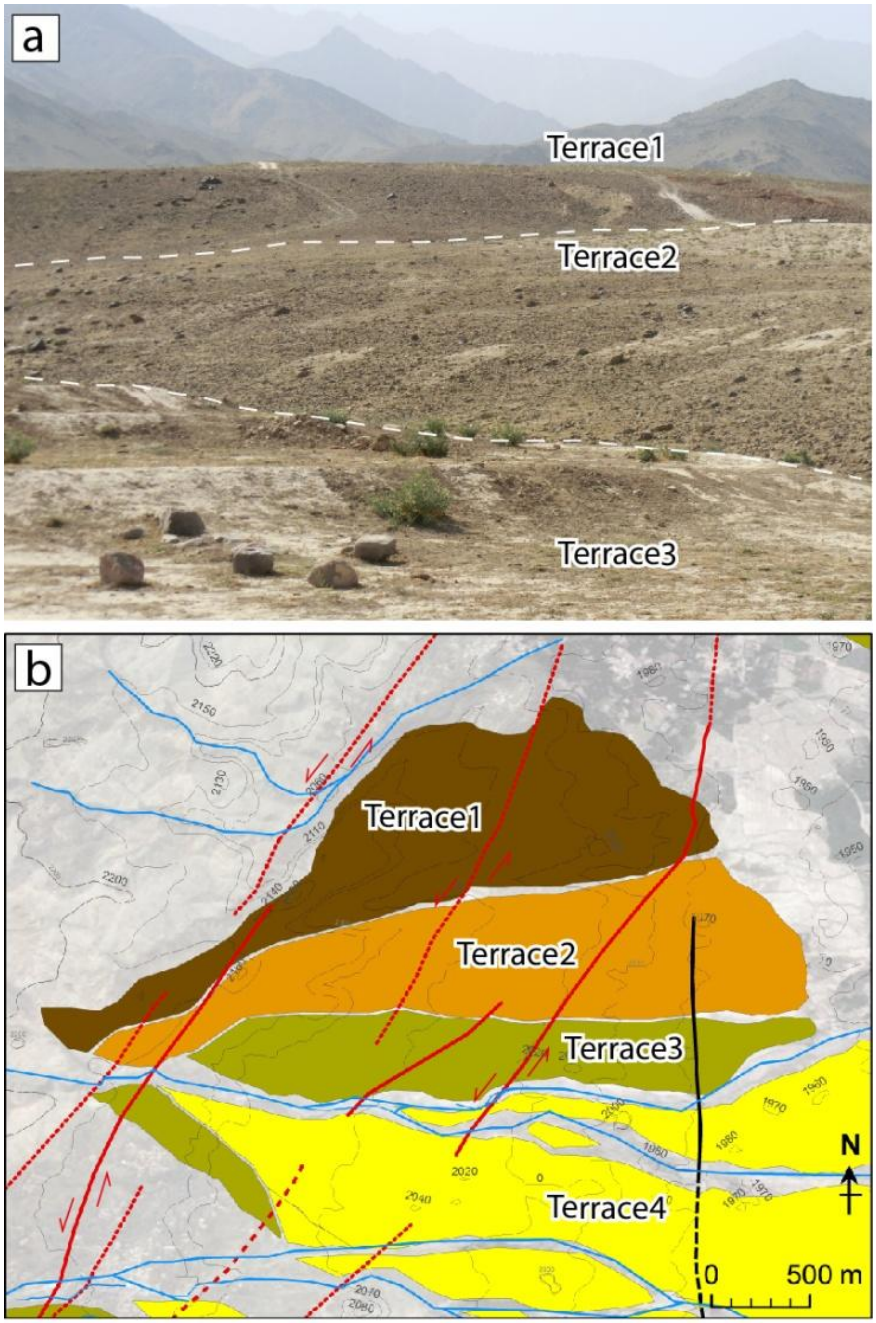

Figure 5.8: The Paghman fault showing left laterally offset of alluvial fan. a) Photo of the offset alluvial fans along the Paghman fault. b) Map of the alluvial fan surfaces showing apparent left-lateral offsets.

The Sarobi fault has a steep, linear, and arcuate range-front scarp south of the Nijrab district (Fig. 5.5). The fault scarp is not distinct on piedmont alluvium further north from Koh-e Malikar to Golbahar, Kapisa Province. Fault scarps are present for a distance of ~40 km north of the Naghlu Dam and faces to the east toward the valley. The Sarobi fault probably has been active in the Quaternary (Fig. 5.9). Late Pleistocene deposits along the piedmont suggest enough activity for the burial of middle Pleistocene and older deposits on the hanging-wall of the main fault trace. The Sarobi fault forms a prominent north-trending fold that deforms recent (Pleistocene) alluvial deposits near the Tagab district.

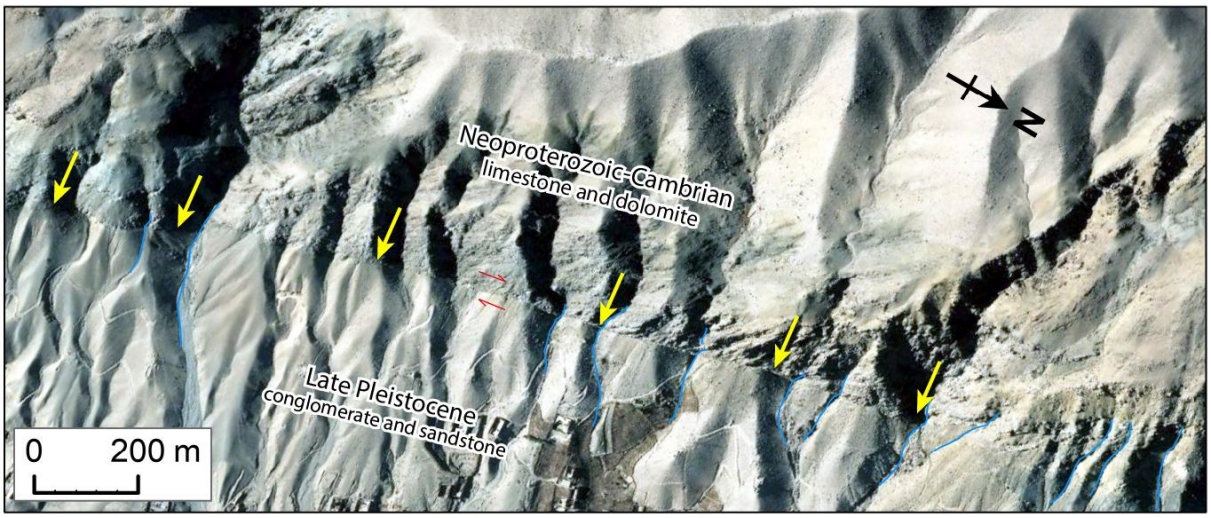

Figure 5.9: Satellite image of the Sarobi fault near the Naghlu Dam. Yellow arrows indicate the fault trace.

5.4. Seismic potential and related hazards in the Kabul basin

Northeastern Afghanistan, including the Kabul basin, has a long history of damaging earthquakes (Figs. 3.13, 5.10). The occurrence of both shallow (<40 km) and deep (>70 km) earthquakes characterizes this region. The intermediate-depth (40-70 km) earthquakes are interpreted to be a result of lithospheric subduction due to the convergence of the Indian and Eurasian plates (Pegler and Das, 1998). Much of the north-south compression is believed to be accommodated by major active faults such as the Chaman, Paghman, Gardez, Sarobi, Konar, Panjshir, Andarab and Herat faults (Fig. 5.1). The Chaman and Sarobi faults have been active during the Quaternary. It is important to accurately estimate the seismic hazard of the

Kabul area to reduce the damages from future earthquakes.

The seismic hazards of the Kabul area can be learnt from the 1505 earthquake on the northern extension of the Chaman fault (Fig. 5.10). The M 7.3 earthquake occurred on the northern end of the Chaman fault near Kabul City (34.53°N, 69.13°E), which produced approximately 60-km-long surface rupture (Ambraseys and Bilham, 2014; Quittmeyer and Jacob, 1979).

The moment magnitude (M_w) of crustal earthquakes has the following relationship to the surface rupture length (SRL).

$$M_w = 5.08 + 1.16 \times \log (SRL)$$

The total length of the Chaman fault is ~860 km. It is ~650 km long in Afghanistan and splays northward into several synthetic strands. South of the Kabul block, the Gardez fault branches northeast from the Chaman fault (Ruleman et al., 2007). The length of the Chaman fault north of the branching point is 240 km, and this portion of the Chaman fault could produce an M_w 7.8 earthquake based on the empirical relation. The length of the Paghman fault (80 km) suggests an M_w 7.3 earthquake. Out of the 150 km length of the Sarobi fault, the northern 40-km-long section shows evidence of active faulting. Judging from the length of the fault (40 km), the size of the resultant earthquake would be M_w 6.9.

In this study, the slip rate of the northern Chaman fault near Kabul has been estimated at 4.6 mm/yr. Since the 1505 earthquake, 1.8-2.6 m of potential slip should be stored on the northern Chaman fault. If I divide the horizontal displacement (2-3 m) during the 1505 earthquake (Quittmeyer and Jacob, 1979) by the geomorphic slip rate, the average recurrence interval of a large earthquake would be ~400-650 yrs. The elapsed time since the last earthquake event on the northern Chaman fault and Paghman fault is close to the calculated recurrence interval, and the likelihood of future big earthquake is high. If a large earthquake similar to the M 7.3 1505 earthquake occurs near Kabul, the human and property losses could be devastating, and vastly more severe than in 1505, when Kabul was a relatively small garrison town. Kabul now has a population of over 4 million, including many refugees living in mud-block houses similar to those that collapsed in the 2002 Nahrin earthquake of

magnitude 6.1 that killed more than 1,200 people (e.g., Ambraseys and Bilham, 2014) (Fig. 1.1).

There are little data on the late Quaternary activity of the right-lateral Herat and Panjshir faults (Fig. 5.1). However, an earthquake of Mw 7.4 (1956) struck a region northeast of Bamyan (35.55°N and 67.81°E) between the Andarab and Herat faults (Fig. 3.14). Another event occurred in 1874 north of Kabul near or on the eastern extension of the Herat fault (Quittmeyer and Jacob, 1979) (Fig. 5.10).

Earthquakes cause liquefaction, ground displacement, landslide and fire. The Kabul metropolitan area is located on water-saturated granular materials, which can lose their frictional strength during severe ground shaking. Several landslide masses are present on the steep slopes in the study area. The 1505 earthquake triggered a landslide in the valley just north of Paghman (Quittmeyer and Jacob, 1979). In the region close to the Sarobi fault, rockslides occur nearly every year, particularly during the rainy season. In the mountainous terrains, such as in northeastern Afghanistan, the high topographic relief is one of the causes of landslides. The Kabul basin presents significant variations in relief from low-lying valleys (~1500 m) to high altitude mountains (>4000 m). Thus, the likelihood of coseismic landslides is very high.

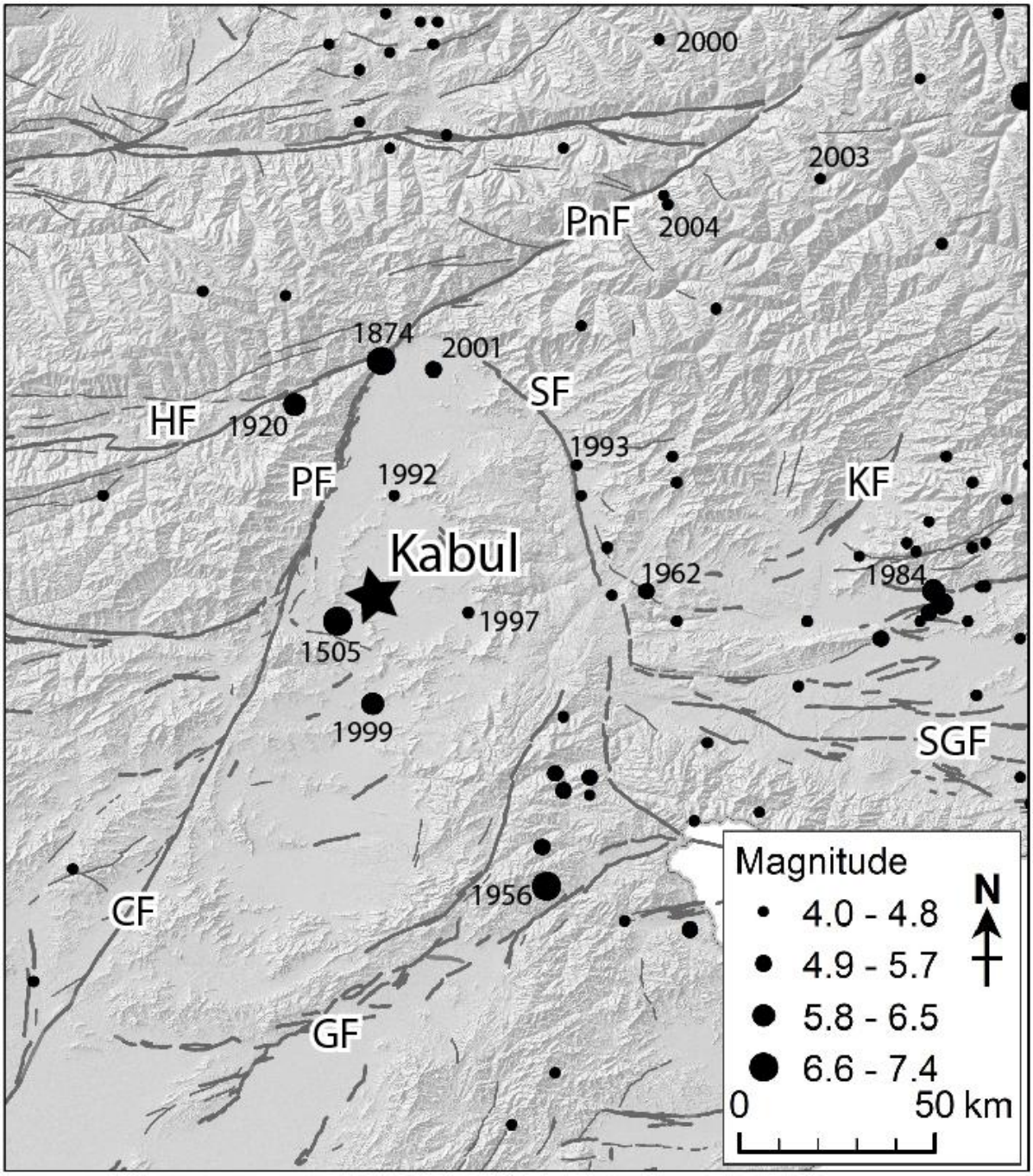

Figure 5.10: Location of all crustal earthquakes (<40 km deep) in the Kabul basin and surrounding regions. The seismicity data is modified from Ambraseys and Bilham, 2003a; and Dewey, 2006.

In this earthquake-prone area, many buildings are built illegally on steep slopes (Fig. 5.11). The houses are cut into the hill and constructed by mud-block mortared together with mud. Although most homes have flat roofs, consisting of 20-50 cm of dried mud supported by wooden beams, the mud-block walls are not braced against horizontal shaking. The 2005 Kashmir earthquake (M_w 7.6) struck the Himalayan region with >87,000 deaths, and most of

the fatalities were due to widespread collapses of buildings and stone barns (Durrani, 2006).

Figure 5.11: Houses on the slop of mountain in Kabul City. a) Homes, seemingly built on top of the next. b) Houses on the south slope of Koh-i-Asmai Mountain (Photos by Mohamad Hamid Hamdard).

Chapter 6

Discussion

Slip-rate of the Chaman fault

Several studies have investigated the slip rate on the Chaman fault using various methods, such as geology, geomorphology, and geodesy. Slip rates based on these methods are generally inconsistent with the slip rates I have calculated based on ^{10}Be cosmogenic dating (Table 4.1; Fig. 6.1). Our left-lateral slip rates of the fault are much lower than the geologically (10^6 years) estimated slip rates of 19-24 mm/yr and 25-35 mm/yr (Beun et al., 1979; Lawrence et al., 1992). In contrast, the slip rate (4.6 mm/yr) is six times less than the geomorphologically estimated rates of 33.3 ± 3.0 mm/yr (Ul-Hadi et al., 2013). Furthermore, the calculated rate (4.5 ± 0.6 mm/yr) is also slower than the GPS observations (18 ± 1 mm/yr) over seven years along the Chaman fault (Mohadjer et al., 2010). The GPS slip rate is approximately three times larger compared to the estimated geomorphic rate at Ghat Bandkul and Azadkhail areas (Figs, 1.1, 6.1). The obtained slip rate (4.5 ± 0.6 mm/yr) is in close agreement with a post-seismic slip rate of ~8 mm/yr, which was estimated by Furuya and Satyabala (2008) from InSAR analysis.

Alternatively, the slip rate along the Chaman fault from 28.25° N, where the arcuate faults of the Makran Range merge parallel to the Ghazaband fault, to the northern end of the Kabul block seems to be inconstant, and a decrease in slip could be envisaged. These observations suggest that the Chaman fault accommodates the majority of the slip in the south in the border region with Baluchistan. The following mechanisms could explain the discrepancies between the slip rates estimated using different methods:

1) I noticed that the Chaman fault becomes less and less clear as it approaches its northeastern termination. Consequently, the actual slip rate of the Chaman fault could reach a value closer to zero. Besides the reason above, the difference between our geomorphic rate

4.5 ± 0.6 mm/yr and the rate of 33.3 ± 3.0 mm/yr obtained by Ul-hadi et al. (2013) could be explained as follow. The two study areas are quite far (~400 km) from each other, and kinematically the slip rate on the Chaman fault should decrease north of the fault.

2) The fault splays into several synthetic strands in the Afghanistan side (e.g., Ruleman et al., 2007), which strikes to the east. Thus, the slip rate on the main fault is locally partitioned, where there are the segment splays. In particular, south of the Kabul block the Chaman fault branches into Gardez and Mokur faults (Fig. 6.1). Because of those, the slip rate on the main trace of the Chaman fault is lower in the Afghanistan side. The Gardez and Mokur active faults have a left-lateral offset of several meters and probably accommodate the internal deformation of the block in the region.

3) A large number of small faults, which do not produce large earthquakes, could absorb a significant part of the shear to south along the Chaman fault (Fig. 6.2).

4) Convergence of thrust faults along with the main fault may cause strain partitioning rates that ranges 3- 6 mm/yr (Bernard et al., 2000; Szeliga et al., 2009), 8 mm/yr (Crupa et al., 2017), and 13 ± 3 m/yr (Ambraseys and Bilham, 2003b). The shortening is accommodated in the northwest to southeast direction by the thrust faults in the Sulaiman Ranges (Fig. 3.4a). Slip on any of these faults should significantly lower the slip rate of the Chaman fault toward the northeast.

Despite the considerable fault length, seismic activity, including instrumental data, shows fever events than expected from the total convergence accommodated by the boundary zone between Indian and Eurasian plates (e.g., Ambraseys and Bilham, 2003a; Dayem, 2010). Most seismic activities along the Chaman fault are predicted in the central part (29°N -31°N) (Ul-Hadi et al., 2013). The interseismic rate of the Chaman fault is 8.0 ± 3.1 mm/yr near Qalat, Afghanistan (Furuya and Satyabala, 2008). In historical and recent times, earthquakes on the Chaman fault south of 33°N has not exceeded Mw 6.8 (Ambraseys and Bilham, 2003b). From 1900 to 2002, the seismic activity is not representative of the long-term slip rate within the area. From 29.5°N to 32.3°N, the 8 mm/yr rate corresponds to 1 m of slip accumulated for more than 124 years since the 1892 earthquake (Fattahi and Amelung, 2016).

This may cause 0.38 m of potential slip available for the next earthquake of Mw7.0, using a locking depth of 10.6 km. Szeliga et al. (2012) clarified that the absence of earthquakes with M > 7 in the last century suggests that the region of the Chaman fault near Qalat may have accumulated enough strain for a massive earthquake. Therefore the creeping segment of the Chaman fault has the potential to generate a big earthquake. Ambraseys and Bilham (2003b) also predicted a slip deficit that could be enough to trigger one or more earthquakes of Mw7.0.

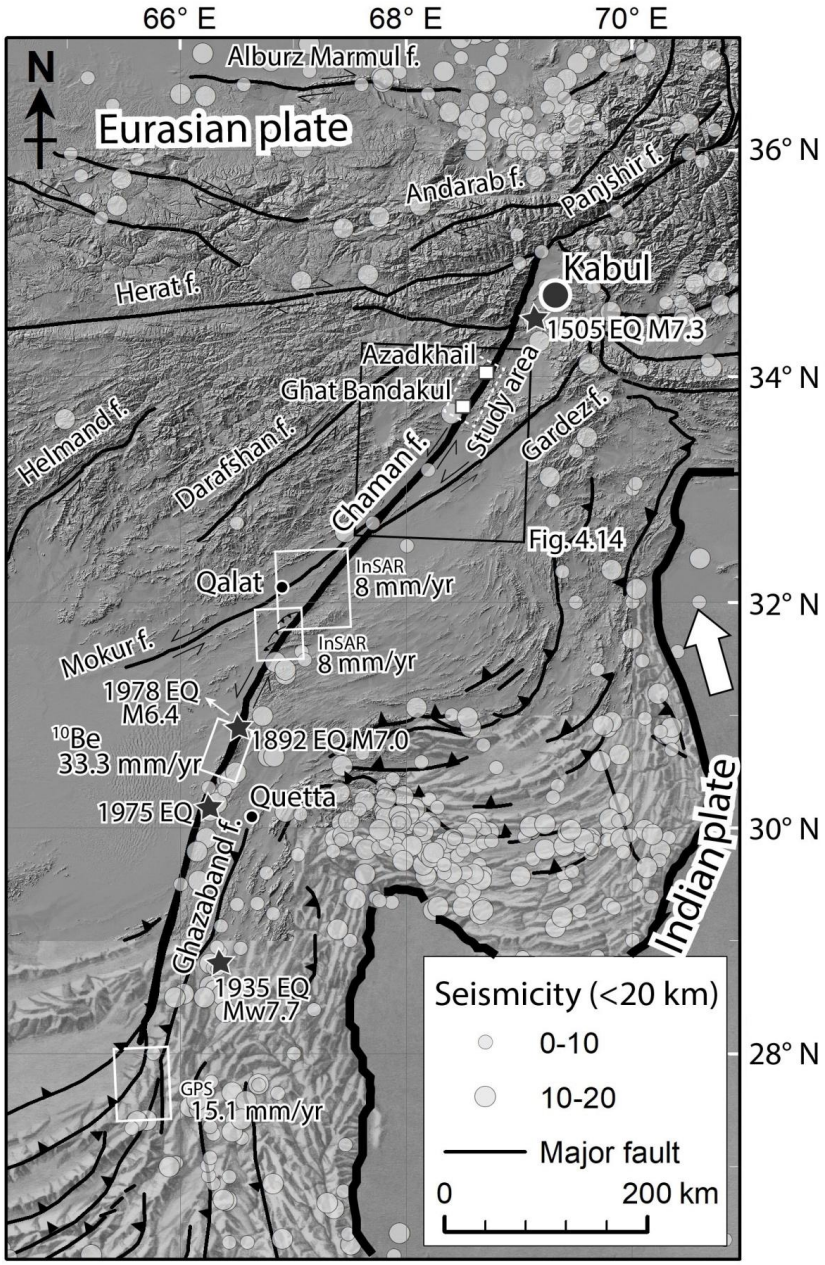

Figure 6.1: The historical earthquakes and the slip rate on the Chaman fault. The earthquake data are compiled from Ambraseys and Bilham, 2003b; Lawrence et al., 1992; Quittmeyer and Jacob, 1979.

Furuya and Satyabala (2008) stated that the 2005 earthquake was followed by slow slip over 50 km of the Chaman fault for at least a year. This may raise the possibility that other parts of the Chaman fault might rupture in slow slip events, reducing the seismic hazard. The southern segment of the fault (32.3°N - 35.0°N) has a slip rate of 16.8 ± 0.51 near Kabul (Szeliga et al., 2012). InSAR does not cover this region, but Fattahi and Amelung (2016) used the slip rate and locking depths inferred farther south. They obtained a slip rate of 8 mm/yr, perhaps close to our study area (4.5 ± 0.6 mm/yr), which is corresponding to the Mw 7.6 earthquake. On July 5, 1505, an earthquake (M 7.3) occurred on the northernmost segment of the Chaman fault 3-km south of the Kabul City (Quittmeyer and Jacob, 1979), close to our first site (Ghat Bandakul). The 3.5 - 4.5 mm/yr calculated geomorphic slip rate near the Kabul, about 1.8-2.6 m of potential slip, should be stored on the Chaman fault since 1505. Since that time, the Kabul should have had an earthquake as massive as the 1505 event by now.

The slip rate on the Chaman fault is high near Kabul, and it is supposed the next earthquake is overdue. A possible reason that the region has not had its earthquake yet is that part of the fault may be experiencing aseismic creep, but there was also a small earthquake south of the Kabul. For example, in 2005, an earthquake of Mw 5.0 at a focal depth of from 2 to 3 km and slip greater than 10 cm was accompanied by surface rupture along 6.5 km of the Chaman fault (Yeats, 2012). If such kind of event happens, the human and property losses could be devastating. Because, Kabul is one of the most rapidly growing cities with a population over 4 million, and the people are living in the buildings of substandard construction or that had been heavily damaged by war, but without provision to make these buildings resistant to earthquakes due to general lack of awareness of the risks. The timing of the earthquake cycle for the Chaman fault is poorly known, and surely it needs a comprehensive dataset to be obtained from future studies.

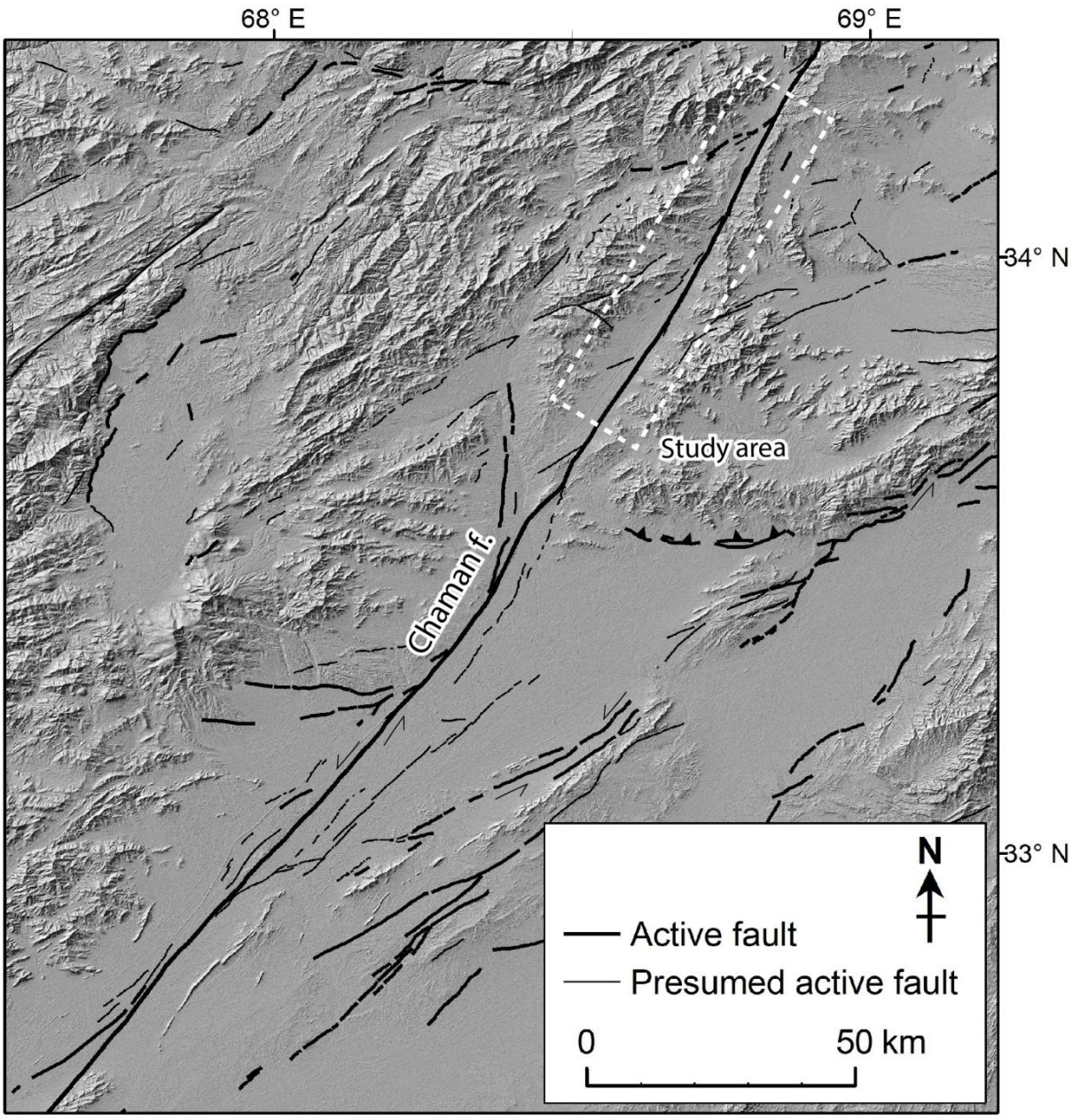

Figure 6.2: A large number of small faults located close to the area of study.

Chapter 7

Conclusions and recommendations

7.1. Conclusions

The objective of this dissertation is to contribute to a better understanding of the active tectonics and the seismic hazard in Afghanistan. Active faults are very useful in hazard assessment to the degree that allows estimation of the slip-rate of fault average over several earthquakes. This is one of the main challenges to mitigate the seismic risk in the country. This study presented a review of the tectonic and geologic setting of Afghanistan and interpreted Bouguer and free-air anomaly data since 1966. Based on the data interpretation, the highest Bouguer and free-air anomalies are associated with the ophiolites belt (including the Kabul-Altimur or Logar, Khost, Waziristan, and Muslim Bagh ophiolites), which represents a high-density zone of transition between northwestern Afghan Block and southeastern plate boundary zone. The Bouguer gravity anomalies decrease westward to the Chaman fault with a low value over the Katawaz basin and high over the eastern Sulaiman foreland. The central and eastern Hindu Kush is characterized by negative free-air gravity anomalies, while in the western Hindu Kush the anomaly is zero. This shows that the western Hindu Kush is in isostatic equilibrium, whereas central and eastern Hindu Kush ranges are not in isostatic equilibrium and therefore this is a seismically active region.

In this study, the first active faults map of Afghanistan was introduced based on 1-arcsecond SRTM data and briefly described the surface trace geometry and geomorphic features. Many active faults cut and deformed the young deposits and landforms. I then analyzed the earthquakes catalog data available for the country (from 800 A.D. to 2004, and ISC from 2005-2016). The earthquake catalog together with tectonic geomorphic mapping provides a general perspective of the past and current distribution of earthquakes in the country. Based on the catalog data, the greater part of the interior of Afghanistan is

seismically less active, but near or northeast of Kabul experiences intense seismicity. Northeastern Afghanistan has been affected by frequent shallow and intermediate-depth earthquakes.

For contributing to the assessment of seismic hazard, a total of four seismic source zones are proposed in the country based on the characteristics of the mapped faults: 1) east-northeastern Afghanistan, 2) Afghanistan-North Pamir, 3) Northern Afghanistan platform, and 4) middle and south-western Afghanistan. East-northeastern seismic source zone is the most seismically active region in Afghanistan that almost half of the earthquakes occurred in this area. Major and young left-lateral strike-slip faults cut this region. Among the faults, the Chaman fault has the most evidence for seismic activity. Movement of the fault has produced five historical surface ruptures. In addition to significant shallow earthquakes, the second seismic source zone has been affected by many intermediate-depth earthquakes. Northern Afghanistan platform appears to have relatively minor seismic activities, and generally earthquakes along this zone have occurred with decreasing frequency toward the west. The rate of earthquake activity in middle-southwestern Afghanistan is lower than other source zones.

Along the Chaman fault, two offset alluvial fans (Ghat Bandakul and Azadkhail) were mapped and used to identify a longer-term slip rate. Mapping and dating of offset alluvial fans by the Chaman fault yield a Quaternary displacement history. The two fans have been associated with tectonics and have a favorite target for study using ^{10}Be cosmogenic dating. The Ghat Banakul alluvial fan shows explicit left-lateral offsets of two terraces 165 ± 15 m and 235 ± 24 m, respectively. Interpretation of the beryllium-10 cosmogenic exposure dating for boulders on the fan surface indicates that they were deposited 46.9 ± 3.5 kyr and 66.6 ± 4.9 kyr (1σ). Finally, a 3.5 ± 0.4 mm/yr slip rate was obtained along the Chaman fault.

The Azadkhail alluvial fan is the oldest geomorphologically preserved alluvial that offset left-laterally for 500 ± 50 m and 800 ± 70 m. The beryllium-10 cosmogenic exposure ages for the two offsets are 111.2 ± 10.5 and 176.8 ± 17.1 kyr, respectively. It was estimated that the average slip rate is 4.5 ± 0.6 mm/yr at this site. This is the first geomorphic based slip

rates derived from actual offset alluvial fans along the Chaman fault in Afghanistan. Comparison of our results of beryllium-10 exposure date with slip rate (3.5 - 4.5 mm/yr) on the Chaman fault suggests that the slip rate does not agree with the present-day slip rate 18 mm/yr measured by GPS. The results show a clear trend of increasing fault slip rate with an increasing distance from the northeast to the southwest. The observations suggest that the southern of the Chaman fault accommodates the majority of a slip than the northern portion in Afghanistan. The estimated slip rates also indicate that shortening and transfer of shear onto Gardez and Mokur left-lateral faults significantly affect the pattern of the fault in Afghanistan.

This study also provides the first detailed description of active faults in the Kabul basin, Afghanistan. Two large active strike-slip faults (the Paghman and Sarobi faults) and several smaller faults were mapped. The regional left-lateral shear is accommodated mainly by the Chaman and Paghman faults. The Sarobi fault is a right-lateral fault northeast of the basin. These faults are clearly expressed in landforms and offset Quaternary deposits. The lengths of these faults imply that they are capable of generating earthquakes larger than Mw 6.9.

I strongly believe this research provides useful information for seismic hazard mitigation, land use planning, urban development from local to national levels. Active faults were particularly focused on, as they are likely to cause major earthquakes in the future. The active fault map can also serve as a base map for future geological and geophysical studies.

7.2. Recommendations

The principal outcomes of this study provide essential information about the active and presumed active faults in Afghanistan, slip-rate estimation along the Chaman fault, and active tectonics and seismic hazard along the Kabul basin. The following recommendations are suggested for conducting further researches in the region.

1) For future studies, it is required to update the map based on new satellite images interpretation and field observations.

2) At the present, our understanding of the active deformation in Afghanistan remains

poorly constrained. In fact, except for the Chaman fault, there is no data of the slip rate on the active faults due to insecurity. However, determining the geologic, geomorphic and geodetic slip rates along the active faults are key points to assess the active deformation pattern. Therefore, performing a dense GPS network, interseismic interferometric and geomorphic studies remain an important study to assess seismic hazard from the faults and understand active tectonics in Afghanistan.

3) For future studies, more work is needed to be done on the northeastern end of the Chaman fault to determine the fault slip-rate and to understand the crustal deformation processes within the Kabul block. I, therefore, plan to use surface exposure and burial dating using in-situ produce beryllium-10 TCNs to date alluvial fan and quantify geomorphological processes.

4) To better assess the seismic hazard of Kabul, trenching investigations along the Paghman fault and northern Chaman fault are needed. We now know the precise location of the faults, but do not know earthquake history along the faults. Through trenching studies, we need to collect data on the recurrence interval of large surface-rupturing earthquakes and the timing of the most recent earthquake events.

References

Abdullah, S., Chmyriov, V.M., Dronov, V.I., 2008. Geology and Mineral Resources of Afghanistan. British Geological Survey, London.

Abers, G., Bryan, C., Roecker, S., McCaffrey, R., 1988. Thrusting of the Hindu Kush over the Southeastern Tadjik Basin, Afghanistan: Evidence from two large earthquakes. Tectonics 7, 41–56. https://doi.org/10.1029/TC007i001p00041

Ambraseys, N., Bilham, R., 2014. The tectonic setting of Bamiyan and seismicity in and near Afghanistan for the past twelve centuries, in: Margottini, C. (Ed.), After the Destruction of Giant Buddha Statues in Bamiyan (Afghanistan) in 2001. Springer, pp. 101–152. https://doi.org/10.1007/978-3-642-30051-6_6

Ambraseys, N., Bilham, R., 2003a. Earthquakes in Afghanistan. Seismol. Res. Lett. 74, 107–123. https://doi.org/10.1785/gssrl.74.2.107

Ambraseys, N., Bilham, R., 2003b. Earthquakes and associated deformation in Northern Baluchistan 1892-2001. Bull. Seismol. Soc. Am. 93, 1573–1605. https://doi.org/10.1785/0120020038

ARG (Presidential Palace), 2015. Afghanistan Earhquake. Accessed April 30, 2020 at: https://twitter.com/ARG_AFG/status/658965482108821504.

Balco, G., Stone, J.O., Lifton, N.A., Dunai, T.J., 2008. A complete and easily accessible means of calculating surface exposure ages or erosion rates from ^{10}Be and ^{26}Al measurements. Quat. Geochronol. 3, 174–195. https://doi.org/10.1016/j.quageo.2007.12.001

Bernard, M., Shen-Tu, B., Holt, W.E., Davis, D.M., 2000. Kinematics of active deformation in the Sulaiman Lobe and Range, Pakistan. J. Geophys. Res. Solid Earth 105, 13253–13279. https://doi.org/10.1029/1999jb900405

Beun, N., Bordet, P., Carbonnel, J.P., 1979. Premières données quantitative relatives au coulissage du décrochement de Chaman (Afghanistan du sud-est). Comptes rendus l'Académie des Sci. 288, 931–934.

Bierman, P.R., Caffee, M.W., Davis, P.T., Marsella, K., Pavich, M., Colgan, P., Mickelson, D., Larsen, J., 2002. Rates and timing of Earth surface processes from In Situ-produced cosmogenic Be-10. Mineral. Petrol. Geochemistry 50, 147–206. https://doi.org/10.2138/rmg.2002.50.4

Böckh, E.G., 1971. Report on the groundwater resources of the city of Kabul, report for Bundesanstalt für Geowissenschaften und Rohstoffe. BGR No. 002101, 43.

Bohannon, R.G., 2010. Geologic and Topographic Maps of the Kabul North 30' × 60' Quadrangle, Afghanistan. U.S. Geol. Surv. Sci. Investig. Map 3120 1–34. https://doi.org/https://doi.org/10.3133/sim3120

Boulin, J., 1990. Neocimmerian events in Central and Western Afghanistan. Tectonophysics 175, 285–315. https://doi.org/10.1016/0040-1951(90)90177-A

Boyd, O.S., Mueller, C.S., Rukstales, K.S., 2007. Preliminary Earthquake Hazard Map of Afghanistan. U.S. Geol. Surv. Open-File Rep. 2007–1137, 1–25. https://doi.org/10.3133/ofr20071137

Brookfield, M.E., Hashmat, A., 2001. The geology and petroleum potential of the North Afghan platform and adjacent areas (northern Afghanistan, with parts of southern Turkmenistan, Uzbekistan and Tajikistan). Earth-Science Rev. 55, 41–71. https://doi.org/10.1016/S0012-8252(01)00036-8

Broshears, R.E., Akbari, M.A., Chornack, M.P., Mueller, D.K., Ruddy, B.C., 2005. Inventory of groundwater resources in the Kabul Basin, Afghanistan. U.S. Geol. Surv. Scietific Investig. Rep. 2005-5090 1–34.

Collett, S., Faryad, S.W., Mosazai, A.M., 2015. Polymetamorphic evolution of the granulite-facies Paleoproterozoic basement of the Kabul Block, Afghanistan. Mineral. Petrol. 109, 463–484. https://doi.org/10.1007/s00710-015-0371-9

Crupa, W.E., Khan, S.D., Huang, J., Khan, A.S., Kasi, A., 2017. Active tectonic deformation of the western Indian plate boundary: A case study from the Chaman Fault System. J. Asian Earth Sci. 147, 452–468. https://doi.org/10.1016/j.jseaes.2017.08.006

Dayem, K.E., 2010. Major intracontinental strike-slip faults and contrasts in lithospheric

strength. Geosphere 6, 444–467. https://doi.org/https://doi.org/10.1130/GES00519.1

Debon, F., Afzali, H., Le Fort, P., Sonet, J., 1987. Major intrusive stages in Afghanistan: Typology, age and geodynamic setting. Geol. Rundschau 76, 245–264. https://doi.org/10.1007/BF01820586

Desio, S.A., Poretti, G., 1991. Gravity anomalies in North-Eastern Afghanistan and on the Pamirs syntaxis. Rend. Lincei 2, 131–144. https://doi.org/10.1007/BF03001417

Dewey, J.W., 2006. Seismicity of Afghanistan and vicinity. Geol Surv Open-File Rep 2006–1185. No.28, 1–55. https://doi.org//10.3133/ofr20061185

Dhakal, S., 2015. Evolution of Geomorphologic Hazards in Hindu Kush Himalaya, in: Shaw, R., Krishna, H.N. (Eds.), Mountain Hazards and Disaster Risk Reduction. Springer, Tokyo, pp. 53–72. https://doi.org/10.1007/978-4-431-55242-0_4

Doebrich, J.L., Wahl, R.R., Ludington, S.D., Chirico, P.G., Wandrey, C.J., Bohannon, R.G., Orris, G.J., Bliss, J.D., Wasy, A., Younusi, M.O., 2006. Geologic and Mineral Resource Map of Afghanistan. 1:850,000. U.S. Geol. Surv. No.2006-10. https://doi.org/https://doi.org/10.3133/ofr20061038

Dühnforth, M., Densmore, A.L., Ivy-Ochs, S., Allen, P., Kubik, P.W., 2017. Early to Late Pleistocene history of debris-flow fan evolution in western Death Valley (California) using cosmogenic ^{10}Be and ^{26}Al. Geomorphology 281, 53–65. https://doi.org/10.1016/j.geomorph.2016.12.020

Dunai, T.J., 2010. Cosmogenic nuclides: Principles, concepts and applications in the earth surface sciences. Cambridge University Press, Cambridge. https://doi.org/10.1017/CBO9780511804519

Durrani, A.J., 2006. The Kashmir Earthquake of October 8 , 2005 : Impacts in Pakistan. EERI Spec. Earthq. Rep. 1–8.

Engdahl, E.R., van der Hilst, R., Buland, R., 1998. Global teleseismic earthquake relocation with improved travel times and procedures for depth determination. Bull. Seismol. Soc. Am. 88, 722–743.

Farbod, Y., Shabanian, E., Bellier, O., Abbassi, M.R., Braucher, R., Benedetti, L., Bourlès,

D., Hessami, K., 2016. Spatial variations in late Quaternary slip rates along the Doruneh Fault System (Central Iran). Tectonics 35, 386–406. https://doi.org/10.1002/2015TC003862

Fattahi, H., Amelung, F., 2016. InSAR observations of strain accumulation and fault creep along the Chaman Fault system, Pakistan and Afghanistan 8399–8406. https://doi.org/10.1002/2016GL070121

Funning, G.J., Garcia, A., 2019. A systematic study of earthquake detectability using Sentinel-1 Interferometric Wide-Swath data. Geophys. J. Int. 216, 332–349. https://doi.org/https://doi.org/10.1093/gji/ggy426

Furuya, M., Satyabala, S.P., 2008. Slow earthquake in Afghanistan detected by InSAR. Geophys. Res. Lett. 35, 1–15. https://doi.org/10.1029/2007GL033049

Gaedicke, C., Prexl, A., Schlüter, H.U., Meyer, H., Roeser, H., Clift, P., 2002. Seismic stratigraphy and correlation of major regional unconformities in the northern Arabian Sea. Geol. Soc. Spec. Publ. 195, 25–36. https://doi.org/10.1144/GSL.SP.2002.195.01.03

Gaina, C., Van Hinsbergen, D.J.J., Spakman, W., 2015. Tectonic interactions between India and Arabia since the Jurassic reconstructed from marine geophysics, ophiolite geology, and seismic tomography. Tectonics 34, 875–906. https://doi.org/10.1002/2014TC003780

Gold, P.O., Behr, W.M., Rood, D., Sharp, W.D., Rockwell, T.K., Kendrick, K., Salin, A., 2015. Holocene geologic slip rate for the Banning strand of the southern San Andreas Fault, southern California. J. Geophys. Res. Solid Earth 120, 5639–5663. https://doi.org/10.1002/2015JB012004

Grew, E.S., 2002. Mineralogy, Petrology and Geochemistry of Beryllium: An Introduction and List of Beryllium Minerals. Rev. Mineral. Geochemistry 50, 1–76. https://doi.org/10.2138/rmg.2202.50.01

Gupta, H.K., 1993. Seismic hazard assessment in the Alpide belt from Iran to Burma. Ann. Geophys. 36, 61–82.

Hayes, G.P., Myers, E.K., Dewey, J.W., Briggs, R.W., Earle, P.S., Benz, H.M., Smoczyk, G.M., Flamme, H.E., Barnhart, W.D., Gold, R.D., Furlong, K.P., 2017. Tectonic

summaries of magnitude 7 and greater earthquakes from 2000 to 2015. U.S. Geol. Surv. Open-File Rep. 2016–1192 148. https://doi.org/https://doi.org/10.3133/ofr20161192

Hinze, W.J., Aiken, C., Brozena, J., Coakley, B., Dater, D., Flanagan, G., Forsberg, R., Hildenbrand, T., Keller, G.R., Kellogg, J., Kucks, R., Li, X., Mainville, A., Morin, R., Pilkington, M., Plouff, D., Ravat, D., Roman, D., Urrutia-Fucugauchi, J., Véronneau, M., Webring, M., Winester, D., 2005. New standards for reducing gravity data: The North American gravity database. Geophysics 70. https://doi.org/10.1190/1.1988183

Houben, G., Niard, N., Tünnermeier, T., Himmelsbach, T., 2009. Hydrogeology of the Kabul Basin (Afghanistan), part I: Aquifers and hydrology. Hydrogeol. J. 17, 665–677. https://doi.org/10.1007/s10040-008-0377-z

ISC, 2020. ISC-EHB dataset. https://doi.org/https://doi.org/10.31905/PY08W6S3

Ischuk, A., Bendick, R., Rybin, A., Molnar, P., Khan, S.F., Kuzikov, S., Mohadjer, S., Saydullaev, U., Ilyasova, Z., Schelochkov, G., Zubovich, A. V, 2013. Kinematics of the Pamir and Hindu Kush regions from GPS geodesy. J. Geophys. Res. Solid Earth 118, 2408–2416. https://doi.org/10.1002/jgrb.50185

Ivy-Ochs, S., Dühnforth, M., Densmore, A.L., Alfimov, V., 2013. Dating Fan Deposits with Cosmogenic Nuclides, in: Advances in Global Change Research. pp. 243–263. https://doi.org/10.1007/978-94-007-4336-6_16

Iwahashi, J., 2010. 1: 25,000-scale Active fault map in urban areas published by GSI. Bull. Geospatial Inf. Auth. Japan 58, 29–37.

Jadoon, I.A.K., Khurshid, A., 1996. Gravity and tectonic model across the Sulaiman fold belt and the Chaman fault zone in western Pakistan and eastern Afghanistan. Tectonophysics 254, 89–109. https://doi.org/https://doi.org/10.1016/0040-1951(95)00078-X

JICA (Japan International Cooperation Agency), 2007. The study on groundwater resources potential in Kabul Basin, in the Islamic Republic of Afghanistan. 3rd Jt. Tech. Committee, Sanyu Consult. Inc., Kabul Afghanistan. 1-20.

Jung, W., Brozena, J., Peters, M., 2013. Predicting gravity and sediment thickness in Afghanistan. Geophys. J. Int. 192, 586–601. https://doi.org/10.1093/gji/ggs038

Katayanagi, Y., 2019. “SimpleDEMViewer” Available at: www.jizoh.jp/english.html.

Kohl, C.P., Nishiizumi, K., 1992. Chemical isolation of quartz for measurement of in-situ -produced cosmogenic nuclides. Geochim. Cosmochim. Acta 56, 3583–3587. https://doi.org/10.1016/0016-7037(92)90401-4

Koulakov, I., Tychkov, S., Bushenkova, N., Vasilevsky, A., 2002. Structure and dynamics of the upper mantle beneath the Alpine-Himalayan orogenic belt, from teleseismic tomography. Tectonophysics 358, 77–96. https://doi.org/10.1016/S0040-1951(02)00418-3

Lawrence, R.D., Khan, S.H., Nakata, T., 1992. Chaman Fault, Pakistan-Afghanistan. Ann. Tectonicae 6, 196–223.

Le Dortz, K., Meyer, B., Sébrier, M., Braucher, R., Bourlès, D., Benedetti, L., Nazari, H., Foroutan, M., 2012. Interpreting scattered in-situ produced cosmogenic nuclide depth-profile data. Quat. Geochronol. 11, 98–115. https://doi.org/10.1016/j.quageo.2012.02.020

Le Dortz, K., Meyer, B., Sébrier, M., Nazari, H., Braucher, R., Fattahi, M., Benedetti, L., Foroutan, M., Siame, L., Bourlès, D., Talebian, M., Bateman, M.D., Ghoraishi, M., 2009. Holocene right-slip rate determined by cosmogenic and OSL dating on the Anar fault, Central Iran. Geophys. J. Int. 179, 700–710. https://doi.org/10.1111/j.1365-246X.2009.04309.x

Lillie, R.J., 1991. Evolution of gravity anomalies across collisional mountain belts: Clues to the amount of continental convergence and underthrusting. Tectonics 10, 672–687. https://doi.org/10.1029/91TC00356

Mack, B.T.J., Akbari, M.A., Ashoor, M.H., Chornack, M.P., Coplen, T.B., Emerson, D.G., Hubbard, B.E., Litke, D.W., Michel, L., Plummer, L.N., Rezai, M.T., Senay, G.B., Verdin, J.P., Verstraeten, I.M., 2010. Conceptual Model of Water Resources in the Kabul Basin, Afghanistan. U.S. Geol. Surv. Sci. Investig. Rep. 2009–5262, 240.

Matsushi, Y., 2016. Chemistry for in-situ 10Be and 26Al measurement for terrestrial quartz by AMS at MALT.

Matsuzaki, H., Nakano, C., Yamashita, H., Maejima, Y., Miyairi, Y., Wakasa, S., Horiuchi, K., 2004. Current status and future direction of MALT, the University of Tokyo. Nucl. Instruments Methods Phys. Res. Sect. B Beam Interact. with Mater. Atoms 223–224, 92–99. https://doi.org/10.1016/j.nimb.2004.04.022

McGinnis, L.D., 1971. Gravity fields and tectonics in the Hindu Kush. J. Geophys. Res. 76, 1894–1904. https://doi.org/10.1029/jb076i008p01894

McNab, F., Sloan, R.A., Walker, R.T., 2019. Simultaneous orthogonal shortening in the Afghan-Tajik Depression. Geology 47, 862–866. https://doi.org/10.1130/G46090.1

Menon, A., Lai, C.G., Macchi, G., 2004. Seismic hazard assessment of the historical site of Jam in Afghanistan and stability analysis of the minaret. J. Earthq. Eng. 8, 251–294. https://doi.org/10.1080/13632460409350527

Mohadjer, S., Bendick, R., Ischuk, A., Kuzikov, S., Kostuk, A., Saydullaev, U., Lodi, S., Kakar, D.M., Wasy, A., Khan, M.A., Molnar, P., Bilham, R., Zubovich, A. V., 2010. Partitioning of India - Eurasia convergence in the Pamir - Hindu Kush from GPS measurements. Geophys. Res. Lett. 37, 1–6. https://doi.org/10.1029/2009GL041737

Mohadjer, S., Ehlers, T.A., Bendick, R., Stübner, K., Strube, T., 2016. A Quaternary fault database for central Asia. Nat. Hazards Earth Syst. Sci. 16, 529–542. https://doi.org/10.5194/nhess-16-529-2016

Molnar, P., Tapponnier, P., 1975. Cenozoic Tectonics of Asia: Effects of a Continental Collision. Science (80-.). 189, 419–426. https://doi.org/10.1126/science.189.4201.419

Nikolaev, V.G., 2002. Afghan–Tajik depression: Architecture of sedimentary cover and evolution. Russ. J. Earth Sci. 4, 399–421. https://doi.org/10.2205/2002ES000106

Nishiizumi, K., Imamura, M., Caffee, M.W., Southon, J.R., Finkel, R.C., McAninch, J., 2007. Absolute calibration of 10Be AMS standards. Nucl. Instruments Methods Phys. Res. Sect. B Beam Interact. with Mater. Atoms 258, 403–413. https://doi.org/10.1016/j.nimb.2007.01.297

Nishiizumi, K., Kohl, C.P., Arnold, J.R., Dorn, R., Klein, I., Fink, D., Middleton, R., Lal, D., 1993. Role of in situ cosmogenic nuclides 10Be and 26Al in the study of diverse

geomorphic processes. Earth Surf. Process. Landforms 18, 407–425. https://doi.org/10.1002/esp.3290180504

Nishiizumi, K., Winterer, E.L., Kohl, C.P., Klein, J., Middleton, R., Lal, D., Arnold, J.R., 1989. Cosmic ray production rates of 10Be and 26Al in quartz from glacially polished rocks. J. Geophys. Res. 94, 17907–17915. https://doi.org/10.1029/JB094iB12p17907

Pegler, G., Das, S., 1998. An enhanced image of the Pamir-Hindu Kush seismic zone from relocated earthquake hypocentres. Geophys. J. Int. 134, 573–595. https://doi.org/10.1046/j.1365-246X.1998.00582.x

Peters, S.G., King, T. V., Mack, T.J., Chornack, M.P., 2011. Summary of the Nalbandon Lead and Zinc Area of Interest, in: Summaries of Important Areas for Mineral Investment and Production Opportunities of Nonfuel Minerals in Afghanistan. pp. 851–895.

Prevot, R., Hatzfeld, D., Roecker, S.W., Molnar, P., 1980. Shallow earthquakes and active tectonics in eastern Afghanistan. J. Geophys. Res. Solid Earth 85, 1347–1357. https://doi.org/10.1029/JB085iB03p01347

Quittmeyer, R.C., Jacob, K.H., 1979. Historical and modern seismicity of Pakistan, Afghanistan, northwestern India, and southeastern Iran. Bull. Seismol. Soc. Am. 69, 773–823.

Robinson, J., Beck, R., Gnos, E., Vincent, R.K., 2000. New structural and stratigraphic insights for northwestern Pakistan from field and Landsat Thematic Mapper data. Bull. Geol. Soc. Am. 112, 364–374. https://doi.org/10.1130/0016-7606(2000)112<364:NSASIF>2.0.CO;2

Roecker, S.W., Soboleva, O. V., Nersesov, I.L., Lukk, A.A., Hatzfeld, D., Chatelain, J.L., Molnar, P., 1980. Seismicity and fault plane solutions of intermediate depth earthquakes in the Pamir- Hindu Kush region. J. Geophys. Res. Solid Earth 85, 1358–1364. https://doi.org/10.1029/JB085iB03p01358

Ruleman, C.A., Crone, A.J., Machette, M.N., Haller, K.M., Rukstales, K.S., 2007. Map and Databse of Probable and possible Quaternary faults in Afghanistan. U.S. Geol. Surv. Open-File Rep. 2007-1103, 1–45. https://doi.org/10.3133/ofr20071103

Schurr, B., Ratschbacher, L., Sippl, C., Gloaguen, R., Yuan, X., Mechie, J., 2014. Seismotectonics of the Pamir 33, 1501–1518. https://doi.org/10.1002/2014TC003576

Sengor, A.M.C., 1984. The cimmeride orogenic system and the tectonics of Eurasia. Spec. Pap. Geol. Soc. Am. 195, 82. https://doi.org/10.1130/SPE195-p1

Shareq, A., 1993. Seismic hazard assessment in the Islamic state of Afghanistan, in: McGuire, R.K. (Ed.), The Practice of Earthquake Hazard Assessment. International Association of Seismology and Physics of the Earth's Interior, pp. 1–6.

Shareq, A., 1981. Geological observations and geophysical investigations carried out in Afghanistan over the period of 1972–1979, in: Geological Evolution of Central Asian Basins and the Western Tien Shan Range. The Geological Society, London, pp. 75–86. https://doi.org/10.1029/gd003p0075

Shroder, J.F., 2014. Overview of the geology and geography of Afghanistan, in: Shroder, J.F. (Ed.), Natural Resources in Afghanistan: Geographic and Geologic Perspectives on Centuries of Conflict. Elsevier, pp. 17–55. https://doi.org/10.1016/C2013-0-14018-4

Siehl, A., 2017. Structural setting and evolution of the Afghan orogenic segment - A review. Geol. Soc. London, Spec. Publ. 427, 57–88. https://doi.org/10.1144/SP427.8

Stone, J.O., 2000. Air pressure and cosmogenic isotope production. J. Geophys. Res. Solid Earth 105, 23753–23759. https://doi.org/10.1029/2000jb900181

Szeliga, W., Bilham, R., Kakar, D.M., Lodi, S.H., 2012. Interseismic strain accumulation along the western boundary of the Indian subcontinent 117, 1–14. https://doi.org/10.1029/2011JB008822

Szeliga, W., Bilham, R., Schelling, D., Kakar, D.M., Lodi, S., 2009. Fold and thrust partitioning in a contracting fold belt: Insights from the 1931 Mach earthquake in Baluchistan. Tectonics 28, 1–13. https://doi.org/10.1029/2008TC002265

Tapponnier, P., Mattauer, M., Proust, F., Cassaigneau, C., 1981. Mesozoic ophiolites, sutures, and large-scale tectonic movements in Afghanistan. Earth Planet. Sci. Lett. 52, 355–371. https://doi.org/10.1016/0012-821X(81)90189-8

Tapponnier, P., Molnar, P., 1979. Active faulting and Cenozoic tectonics of the Tien Shan,

Mongolia, and Baykal regions. J. Geophys. Res. 84, 3425–3459. https://doi.org/10.1029/JB084iB07p03425

Tapponnier, P., Peltzer, G., Le Dain, A.Y., Armijo, R., Cobbold, P., 1982. Propagating extrusion tectonics in Asia: new insights from simple experiments with plasticine. Geol. Soc. Am. 10, 611–616. https://doi.org/10.1130/0091-7613(1982)10<611:PETIAN>2.0.CO;2

The Research Group for Active Faults of Japan, 1992. Maps of Active Faults in Japan with an Explantory Text. University of Tokyo Press, Tokyo.

Treloar, P.J., Izatt, C.N., 1993. Tectonics of the Himalayan collision between the Indian Plate and the Afghan Block: A synthesis. Geol. Soc. London, Spec. Publ. Spec. Publ. 74, 69–87. https://doi.org/10.1144/GSL.SP.1993.074.01.06

Trifonov, V.G., 1978. Late Quaternary tectonic movements of western and central Asia. Bull. Geol. Soc. Am. 89, 1059–1072. https://doi.org/10.1130/0016-7606(1978)89<1059:LQTMOW>2.0.CO;2

Tsutsumi, H., Perez, J.S., 2013. Large-scale active fault map of the Philippine fault based on aerial photograph interpretation. Act. Fault Res. 39, 29–37. https://doi.org/10.11462/afr.2013.39_29

Ul-Hadi, S., Khan, S.D., Owen, L.A., Khan, A.S., Hedrick, K.A., Caffee, M.W., 2013. Slip-rates along the Chaman fault: Implication for transient strain accumulation and strain partitioning along the western Indian plate margin. Tectonophysics 608, 389–400. https://doi.org/10.1016/j.tecto.2013.09.009

USGS, 2020. M 7.4 - Hindu Kush earthquake, Afghanistan. Accessed April 30, 2020 at URL; https://earthquake.usgs.gov/earthquakes/eventpage/usp000azhc/executive.

Waheed, A., Wells, N.A., 1990. Changes in paleocurrents during the development of an obliquely convergent plate boundary (Sulaiman fold-belt, southwestern Himalayas, west-central Pakistan). Sediment. Geol. 67, 237–261. https://doi.org/10.1016/0037-0738(90)90037-T

Walker, R., Jackson, J., 2004. Active tectonics and late Cenozoic strain distribution in central

and eastern Iran. Tectonics 23, 1–24. https://doi.org/10.1029/2003TC001529

Wellman, H.W., 1966. Active wrench faults of Iran, Afghanistan and Pakistan. Int. J. Earth Sci. 55, 716–735. https://doi.org/10.1007/BF02029650

Wheeler, R.L., Bufe, C.G., Johnson, M.L., Dart, R.L., 2005. Seismotectonic Map of Afghanistan, with Annotated Bibliography. US Geol Surv Open-File Rep 2007–1264 31.

Wheeler, R.L., Frankel, A., 2000. Geology in the 1996 USGS seismic-hazard maps, central and eastern United States. Seismol. Res. Lett. 71, 273–282. https://doi.org/10.1785/gssrl.71.2.273

Yeats, R., 2012. Active Faults of the World. Cambridge University Press, Cambridge.

Yeats, R.S., Lawrence, R.D., Jamil-ud-din, S., Khan, S.H., 1979. Surface effects of the 16 March 1978 earthquake, Pakistan-Afghanistan border, in: Farah;, A., DeJong, K.A. (Eds.), Geodynamics of Pakistan. Geological Survey of Pakistan, Quetta, pp. 359–361.

Yeats, R.S., Madden, C., 2003. Damage from the Nahrin, Afghanistan, Earthquake of 25 March 2002. Seismol. Res. Lett. 74, 305–311. https://doi.org/10.1785/gssrl.74.3.305